

ABSTRACT

KHAN, MOHAMMAD, RASHED. Characterizing, Rupturing, and Removing Surface Oxide to Manipulate Liquid Metals. (Under the direction of Michael David Dickey).

Liquid metals offer new opportunities for soft, stretchable, and shape-reconfigurable electronic and electromagnetic components. Mercury is a common liquid metal, but its toxicity limits its use. Gallium and its alloys are the best alternatives to mercury. However, gallium forms a surface oxide layer (skin) that has historically been considered a nuisance because of its tendency to stick to surfaces and impede flow. This dissertation describes new ways to control the shape of a room temperature liquid metal alloy, eutectic gallium indium (EGaIn), by manipulating the skin. The skin provides mechanical stability to the liquid metal such that it can be molded into non-spherical shapes such as wires. It is also possible to flow the liquid metal on demand for shaping it into functional components in microsystems (e.g., antennas, switches, sensors, electronic filters). This thesis describes shape shifting antennas and electronic filters that change their electrical length, and therefore, frequency in response to pressure. The application of positive pressure ruptures the oxide and advances the metal further into microchannels. Once inside the channels, the adhesion of the oxide to the walls prevents the metal from being removed easily without leaving metallic residue on the walls of the channel. Electrochemical reduction, however, can remove the oxide in a controlled way in the presence of electrolyte. Removal of the oxide induces capillary behavior; this process is termed 'recapillarity'. Recapillarity can turn on and off capillary behavior using applied voltage to withdraw the metal cleanly and controllably from microchannels. Current density is the key factor dictating the velocity of withdrawal since current reduces the oxide on the leading interface of the metal as well as the oxide sandwiched between the wall of the

microchannel and the liquid metal. Spectroscopic measurements through silicon nitride windows confirm the presence of the oxide on the metal at the walls of the microchannels. In addition, the composition of the channel walls affects the morphology of the oxide on the walls of the channel. Outside of microchannels, recapillarity also enables the patterning of films of liquid metal. It is also possible for the metal to flow smoothly through capillaries and across surfaces without sticking by using an interfacial slip layer of water between EGaIn and the surface. The presence of water also changes the chemical composition of the oxide skin from gallium oxide to gallium oxide-mono-hydroxide, which weakens its modulus by an order of magnitude and yield stress by a factor of five. The slip layer provides new opportunities to control and actuate liquid metal plugs in microchannels – including the use of continuous electrowetting—enabling new possibilities for shape reconfigurable electronics, sensors, actuators and antennas. Combinations of the techniques described in this dissertation are capable of producing reversibly tunable metallic components that can be harnessed as antennas and sensors for microsystems.

© Copyright 2015 by Mohammad Rashed Khan

All Rights Reserved

Characterizing, Rupturing, and Removing Surface Oxide to Manipulate Liquid Metals

by
Mohammad Rashed Khan

A dissertation submitted to the Graduate Faculty of
North Carolina State University
in partial fulfillment of the
requirements for the degree of
Doctor of Philosophy

Chemical Engineering

Raleigh, North Carolina

2015

APPROVED BY:

Dr. Michael D. Dickey
Committee Chair

Dr. Saad Khan

Dr. Edmond F. Bowden

Dr. Glenn Walker

DEDICATION

This dissertation is dedicated to my family for their lifelong support and encouragement.

BIOGRAPHY

Mohammad Rashed Khan was born on August 23, 1983, in Dhaka, Bangladesh. He grew up in Dhaka, Bangladesh as well. After graduating from Dhaka Residential Model College in August, 2000, he entered into Bangladesh University of Engineering and Technology (BUET) for his undergraduate degree in Chemical Engineering. In 2007, he graduated with his Bachelor of Science in Chemical Engineering from BUET. He worked as a Lecturer in the same department of BUET for two years. In fall 2009, he joined in the Department of Chemical and Biomolecular engineering at NC State University as a graduate student. Under the guidance of Professor Michael D. Dickey, he pursued multidisciplinary research on gallium alloys, unconventional micro and nano fabrication, microfluidics, thin oxide films, metal/oxide interfaces, rheology, electrochemistry, and interfacial studies.

ACKNOWLEDGMENTS

First and foremost, I would like to thank my advisor and my mentor Dr. Michael Dickey, for his constant guidance, support, encouragement, and patience. I am grateful to him for giving me the opportunity to be a part of his research team and carry out all of the published, unpublished or pending works during last five years. It has been truly an honor and privilege. I would also like to take my time to say thanks to Dr. Saad Khan, Dr. Edmond Bowden, and Dr. Glenn Walker to be a part of my committee members.

I am thankful to Dr. Bowden for all of his suggestions and collaborations. We appreciate that he let us borrow some equipment and chemicals from his lab that helped to finish and publish some of the important works. Dr. Khan and Dr. Walker also deserve special thanks for their suggestions on rheology and microfluidics.

My special appreciation goes to Dr. Ju-Hee So; without her guidance I think I won't be able to be a good lab citizen. She took her time to train me on EGaIn, taught me soft lithography, replica molding and many other things that played a vital role to my success. Dr. Dhana Shavitri, Dr. Shavirl Desai, Dr. Etienne Palleau deserve special thanks for their constant support.

I am thankful to all my lab members, grads, undergrads, visiting scholars, exchange students, high school kids who worked with me on many different occasions. My very special thanks to Collin Eaker. We collaborated on majority of my work on electrochemistry. Chris Trlica, a person who deserves many special thanks from me. We worked together on so many projects, so many experiments, spent so many hours near the stereoscope and tried so many things with

EGaIn. He is one of the leading contributors to many of my works in this dissertation. My special thanks to Dr. Gerard Hayes, and Silu Zhang as well for their work on shape shifting devices.

I mentored many undergraduate students during my graduate study. It has been a pleasure to train them and work in collaboration with them. I may have forgotten some of their names but Jacob, Michael Valeri, Justin Chew, Steven, Stephen, John, Jennifer, Nathan, Jarret, Andrew deserve special mention. Joh Bell, a high school kid, amazed me so much when I mentored him in 2013. He showed his excellent computer skills which helped us finish in-plane patterning work.

I am thankful to most of my friends in Raleigh, especially my soccer buddies; you guys are awesome. Finally, I would like to thank my parents, uncle, sister and specially Taliman, my wife, for their constant love and support in every single moment of my life. I won't be able to finish the touch line without them. I would also like to thank almighty Allah for everything else.

TABLE OF CONTENTS

LIST OF TABLES	-	-	-	-	-	-	-	-	ix
LIST OF FIGURES	-	-	-	-	-	-	-	-	x
CHAPTER 1: INTRODUCTION	-	-	-	-	-	-	-	-	01
1.1 Overview	-	-	-	-	-	-	-	-	02
1.2 Motivation	-	-	-	-	-	-	-	-	04
1.3 Liquid Metals	-	-	-	-	-	-	-	-	05
1.3.1 Physical Properties	-	-	-	-	-	-	-	-	07
1.3.2 Rheology	-	-	-	-	-	-	-	-	09
1.3.3 Wetting and Adhesion	-	-	-	-	-	-	-	-	11
1.3.4 Electrochemistry	-	-	-	-	-	-	-	-	13
1.4 Applications of Liquid metal	-	-	-	-	-	-	-	-	16
1.4.1 Patterning	-	-	-	-	-	-	-	-	16
1.4.2 Reconfigurable Devices	-	-	-	-	-	-	-	-	24
1.5 Thesis Outline	-	-	-	-	-	-	-	-	29
1.6 References	-	-	-	-	-	-	-	-	32
CHAPTER 2: FREQUENCY SHIFTING LIQUID METAL ANTENNA	-	-	-	-	-	-	-	-	52
2.1 Introduction	-	-	-	-	-	-	-	-	53
2.2 Results	-	-	-	-	-	-	-	-	54
2.3 Conclusion	-	-	-	-	-	-	-	-	60
2.4 References	-	-	-	-	-	-	-	-	62
CHAPTER 3: FREQUENCSY SHIFTING LIQUID METAL FILTER	-	-	-	-	-	-	-	-	66

3.1 Abstract	-	-	-	-	-	-	-	-	-	67
3.2 Introduction	-	-	-	-	-	-	-	-	-	67
3.3 Design	-	-	-	-	-	-	-	-	-	68
3.4 Measurement and Simulation	-	-	-	-	-	-	-	-	-	70
3.5 Conclusion	-	-	-	-	-	-	-	-	-	75
3.6 Reference	-	-	-	-	-	-	-	-	-	76
CHAPTER 4: INVESTIGATION OF LIQUID METAL INTERFACE	-	-	-	-	-	-	-	-	-	78
4.1 Abstract	-	-	-	-	-	-	-	-	-	79
4.2 Introduction	-	-	-	-	-	-	-	-	-	80
4.3 Experimental Design	-	-	-	-	-	-	-	-	-	81
4.4 Results and Discussion	-	-	-	-	-	-	-	-	-	85
4.5 Conclusion	-	-	-	-	-	-	-	-	-	92
4.6 References-	-	-	-	-	-	-	-	-	-	93
CHAPTER 5: RECAPILLARITY DRIVEN WITHDRAWAL	-	-	-	-	-	-	-	-	-	97
5.1 Abstract	-	-	-	-	-	-	-	-	-	98
5.2 Introduction	-	-	-	-	-	-	-	-	-	99
5.3 Results and Discussion	-	-	-	-	-	-	-	-	-	103
5.4 Conclusions	-	-	-	-	-	-	-	-	-	115
5.5 References-	-	-	-	-	-	-	-	-	-	117
CHAPTER 6: IN-PLANE PATTERNING OF LIQUID METAL	-	-	-	-	-	-	-	-	-	124
6.1 Abstract	-	-	-	-	-	-	-	-	-	125
6.2 Introduction	-	-	-	-	-	-	-	-	-	126

6.3 Results and Discussions	-	-	-	-	-	-	-	-	128
6.4 Conclusion	-	-	-	-	-	-	-	-	136
6.5 References	-	-	-	-	-	-	-	-	138
CHAPTER 7: INFLUENCE OF WATER ON LIQUID METAL	-	-							143
7.1 Abstract	-	-	-	-	-	-	-	-	144
7.2 Introduction	-	-	-	-	-	-	-	-	145
7.3 Experimental Section	-	-	-	-	-	-	-	-	147
7.4 Result and Discussion	-	-	-	-	-	-	-	-	147
7.5 Conclusion	-	-	-	-	-	-	-	-	161
7.6 References	-	-	-	-	-	-	-	-	163
APPENDIX	-	-	-	-	-	-	-	-	170

LIST OF TABLES

Table 1: List of technologies till date	-	-	-	-	-	-	17
---	---	---	---	---	---	---	----

LIST OF FIGURES

CHAPTER 1: INTRODUCTION

Figure 1	Brief overview of challenges associated with flexible devices	-	-	
-	-	-	-	05
Figure 2	Comparison of EGaIn and Mercury in microchannel.			
-	-	-	-	07
Figure 3	Removal of oxide from liquid metal droplet	-	-	-
-	-	-	-	09
Figure 4	Rheological characterization of liquid metal in a rheometer	-	-	
-	-	-	-	10
Figure 5	Wetting behavior of an oxide coated metal drop	-	-	-
-	-	-	-	12
Figure 6	Giant and switchable surface activity of liquid metals using oxide as surfactant in an electrochemical environment.	-	-	-
				14
Figure 7	Oxide skin can be removed or grown depending upon the direction of bias.	-	-	
-	-	-	-	15
Figure 8	Soft lithographic approach to make microfluidic channels filled with liquid metals	-	-	-
				18
Figure 9	Different ways of producing shapes and patterns	-	-	-
-	-	-	-	19
Figure 10	3D printing of free-standing liquid metal structures	-	-	-
-	-	-	-	21

Figure 11	Soft and stretchable liquid metal embedded polymers-	-	-	-
-	-	-	-	23
Figure 12	Stretchable radio frequency liquid metal antennas from polymers other than PDMS.-	-	-	25
Figure 13	Liquid metal filled capacitive sensors for normal force detection and measurement.	-	-	26
Figure 14	Schematic depiction of a reversible vacuum pressure actuated liquid metal device in the presence of acid vapor to remove the oxide	-	-	27

CHAPTER 2: FREQUENCY SHIFTING LIQUID METAL ANTENNA

Figure 1	A depiction of an antenna that reconfigures its shape in response to pressure (not to scale)	-	-	-	-	-	-	-	-	55
Figure 2	Photographs of a shape reconfigurable antenna in three different states.	-	-	-	-	-	-	-	-	56
Figure 3	Three distinct frequency responses illustrating the frequency shifting nature of the antenna.	-	-	-	-	-	-	-	-	57
Figure 4	Sequential micrographs of the process of merging liquid metal segments.	-	-	-	-	-	-	-	-	59

CHAPTER 3: FREQUENCYSY SHIFTING LIQUID METAL FILTER

Figure 1	Geometry of bandstop filter with a 50 Ω microstrip transmission line from Port 1 to Port 2 and open stub section.-	-	-	-	-	-	-	-	-	69
-----------------	---	---	---	---	---	---	---	---	---	----

Figure 2	Cross section of a 50 Ω microstrip transmission line	-	-	-	-	-	-	-	-	69
Figure 3	Geometry of bandstop filter: (a) State 1, (b) State 2, and (c) State 3.	-	-	-	-	-	-	-	-	71
Figure 4	Photographs (left) and micrographs (right) of the microstrip filter in three different states	-	-	-	-	-	-	-	-	72
Figure 5	Measured reflection coefficient for each state of the filter.	-	-	-	-	-	-	-	-	73
Figure 6	Measured and simulated transmission coefficient response for each state of the microstrip filter.	-	-	-	-	-	-	-	-	73
Figure 7	Measured transmission coefficient of a prototype with an open stub shortened from 22.7 mm to 0.5 mm.	-	--	-	-	-	-	-	-	74

CHAPTER 4: INVESTIGATION OF LIQUID METAL INTERFACE

Figure 1	Experimental procedure for detecting the presence of oxide at the interface with an air-impermeable wall.	-	-	-	-	-	-	-	-	84
Figure 2	A schematic diagram of the assembly of EGaIn and the nitride window for EDS measurement	-	-	-	-	-	-	-	-	87
Figure 3	Atomic percentage of gallium and oxygen from EDS measurements on EGaIn-silicon nitride interfaces prepared by placing the droplet of EGaIn on the nitride substrate or injecting EGaIn into a channel with the nitride wall.	-	-	-	-	-	-	-	-	88

Figure 4	Interfacial morphology of EGaIn with pristine (a), oxygen plasma treated (b), or plasma treated and acid-treated (c) PDMS substrates.	-	-	-	-	89
Figure 5	Interfacial morphology of EGaIn with pristine (a), oxygen-plasma treated (b), acid-treated (c) glass substrates.	-	-	-	-	91

CHAPTER 5: RECAPILLARITY DRIVEN WITHDRAWAL

Figure 1	An example of reduction-driven liquid metal withdrawal in a PDMS microchannel.	-	-	-	-	102
Figure 2	Effect of meniscus shape, and shape of the metal in the reservoir on withdrawal velocity.	-	-	-	-	105
Figure 3	Effect of electrical length on the liquid metal withdrawal.	-	-	-	-	108
Figure 4	The shape of the meniscus during withdrawal provides mechanistic insight into recapillarity.	-	-	-	-	113
Figure 5	Two demonstrations of shape-reconfigurability of liquid metal microstructures by recapillarity.	-	-	-	-	114

CHAPTER 6: IN-PLANE PATTERNING OF LIQUID METAL

Figure 1	Cartoon depiction of in-plane recapillarity.	-	-	-	-	129
Figure 2	Photograph of the (a) EGaIn spreader that can create a $\approx 120\mu\text{m}$ thin film. (ii) 10 mM NaF solution covers the majority of the film, except for (iii) only a small					

portion which serves as a contact point for a Cu wire. The film itself is the cathode and another piece of Cu wire touches the electrolyte to serve as an anode. (b) Four frames from a typical withdrawal experiment at regular time intervals. Initial (i) raw frames are processed in ImageJ for analysis. (ii) Corresponding plot of radius (of the hole) vs. time, and (iii) Plots of velocity of withdrawal vs. time for different applied currents. - -

- - - - - 131

Figure 3 a) Plots of velocity of withdrawal (i.e., radial rate of expansion) vs. current density for different applied currents and applied voltages, showing linear correlation. b) A sample frame from the video of withdrawal, showing an extreme case of withdrawal irregularities. c) Scanning-electron microscope (SEM) image of the leading edge of the EGaIn film after a partial withdrawal. - - - - -

- - - - - 133

CHAPTER 7: INFLUENCE OF WATER ON LIQUID METAL

Figure 1 Contrasting the behavior of EGaIn in (a) a dry capillary, and (b) a capillary pre-filled with water. - - - - - 148

Figure 2 The effect of water exposure on the mechanical properties of the oxide skin that forms on EGaIn. - - - - - 152

Figure 3 The presence of a thin slip layer of aqueous electrolyte between the capillary wall and a plug of liquid metal enables continuous electrowetting of the plug. - -

- - - - - 154

Figure 4	Evidence of a water slip layer in an open system. - - - -	156
Figure 5	‘Wet’ to ‘dry’ transition of a glass substrate. - - - -	158
Figure 6	Demonstration of a reconfigurable antenna that can be injected and withdrawn from microchannels due to a water slip layer. - - - -	160

APPENDIX A

Figure S1	(a) Isometric view of the acrylic substrate used to perform recapillarity experiments in glass capillaries. (b) Side view of a typical setup using an acrylic substrate and a glass capillary. Reservoirs measure 4 mm x 4 mm x 2 mm. - - - -	172
------------------	---	-----

Figure S2	Effect of electrolyte concentration on withdrawal speed of EGaIn. For a given voltage, more concentrated electrolytes enable faster withdrawal due to increased current. - - - -	173
------------------	--	-----

Figure S3	Effect of interfacial ion gradients on the withdrawal velocity. (a) After 11 sec of withdrawal, the voltage was turned off and a syringe needle was inserted into the capillary to flush the interface with fresh electrolyte before withdrawal was resumed. (b) The withdrawal velocity does not show any velocity increase after flushing the interface and turning the voltage back on after the 11 sec mark on the plot. A plot of current (not shown) also indicates insignificant changes after flushing. - - - -	174
------------------	---	-----

Figure S4	Effect of electrical length on withdrawal velocity. A copper wire (anode) was inserted into the capillary to shorten the electrical distance between the anode and the metal interface. Shortening the distance increases the velocity for a given voltage. - - -	
------------------	---	--

Figure S5 A plot of current vs. time as EGaIn is injected into a capillary toward the counter electrode. The pump injected EGaIn at $t=5$ sec and continued until $t=40$ sec. As EGaIn displaces electrolyte, current increases.-

CHAPTER 1
INTRODUCTION

1.1 OVERVIEW

This dissertation seeks to understand and manipulate the native oxide that forms on eutectic gallium indium (EGaIn) to control the shape of the metal. EGaIn is a liquid metal at room temperature. The aim of this dissertation is to elucidate the properties of a passivating¹ oxide layer (skin) that forms spontaneously on a room temperature liquid metal alloy, eutectic gallium indium² (EGaIn), and manipulate it to control the shape of the metal. In the absence of the oxide, EGaIn is a high surface tension^{3,4}, low viscosity⁵ Newtonian liquid metal at room temperature. In the presence of the oxide, the rheological properties change such that it can be molded into useful, non-spherical shapes (e.g., antennas⁶⁻¹⁰, interconnects^{11,12}, electrodes^{13,14,15}). Application of stress beyond a critical value can rupture the oxide, allowing the metal to flow (e.g., into microfluidic channels) and providing a method to elongate or move conductive structures. Removing the skin chemically or electrochemically allows the metal to flow freely in response to capillary forces, which offers a route to change the shape of the metal. In this dissertation, we seek to understand these properties to better control the shape of the metal by accomplishing the following:

- I. **Demonstration and characterization of shape shifting devices** by using engineered microfluidic channels that harness the rheological and yield properties of the oxide-coated EGaIn to control the way it flows into microchannels in response to pressure. Chapter 2 and 3 demonstrates and characterizes pressure responsive shape shifting devices.
- II. **Interfacial studies of EGaIn**. We focus on understanding the interface of the liquid metal in contact with different surfaces (e.g, hydrophobic and hydrophilic, air

permeable and air impermeable). Chapter 4 reports on spectroscopy to probe this interface and optical microscopy to investigate the morphology. These studies suggest that injecting metal into capillaries results in an oxide layer between the metal and the walls of microchannels. a.

III. **Investigation and characterization of electrochemistry to** reduce the oxide skin to induce capillary behavior, which can cause the metal to withdraw from microchannels on demand (Chapter 5). Chapter 6 shows that this principle can also locally destabilize films of liquid metal and create different patterns. These studies underscore the importance of electrical current for controlling the capillary-driven movement of the metal.

IV. **Demonstration of a slip layer to enable reconfigurable liquid metal components.** The presence of the oxide skin on the surface of the liquid metal causes it to stick to most surfaces, which limits the ability to easily reconfigure its shape on demand. Chapter 7 shows that water can provide an interfacial slip layer between EGaIn and many surfaces, which allows the metal to flow smoothly through capillaries and across surfaces without sticking. The slip layer provides new opportunities to control and actuate liquid metal plugs in microchannels – including the use of continuous electrowetting—enabling new possibilities for shape reconfigurable electronics, sensors, actuators and antennas.

1.2 MOTIVATION

Electronic devices consist of multiple types of materials, including semiconductors, insulators, and conductors. This thesis focuses only on conductors, which are vital in nearly all electronic devices. Conventional electronic devices typically contain rigid metals (e.g., copper, aluminum, and gold). There is great interest in making electronics flexible (and stretchable) because of the new applications that emerge¹⁶. Examples include conductive textiles^{17,18}, paper like flexible displays^{19–22}, conducting skin²³, RFID tags^{24,25}, solar cells²⁶, non-volatile memory^{27,28} and photovoltaics²⁹. Typically, flexible electronics are fabricated by making conventional materials thin (cf. Figure 1). Aluminum foil is an everyday example of a material rendered flexible simply by being thin. However, thin film geometries on flexible substrates cannot be stretched significantly because of induced fracture upon strain^{30,31}. Several groups have addressed this problem by using buckled or out-of-plane geometries that deform like an accordion and therefore offer greater flexibility^{32–34}. **Figure 1** summarizes these approaches.

Liquids do not fracture and therefore are appealing materials for stretchable electronic devices. However, familiar liquids—like salt water—often have low electrical conductivity and high vapor pressure, which restricts their applicability in flexible electronic devices. Moreover, most of the liquids cannot be micro-molded into useful shapes such as wires since surface tension causes fluids to adopt a shape that minimizes the free surface energy. All of these aforementioned challenges can be addressed by harnessing the properties of room temperature liquid metals based on gallium. The following section will introduce gallium

alloys along with some of the important properties will also be discussed in successive sections.

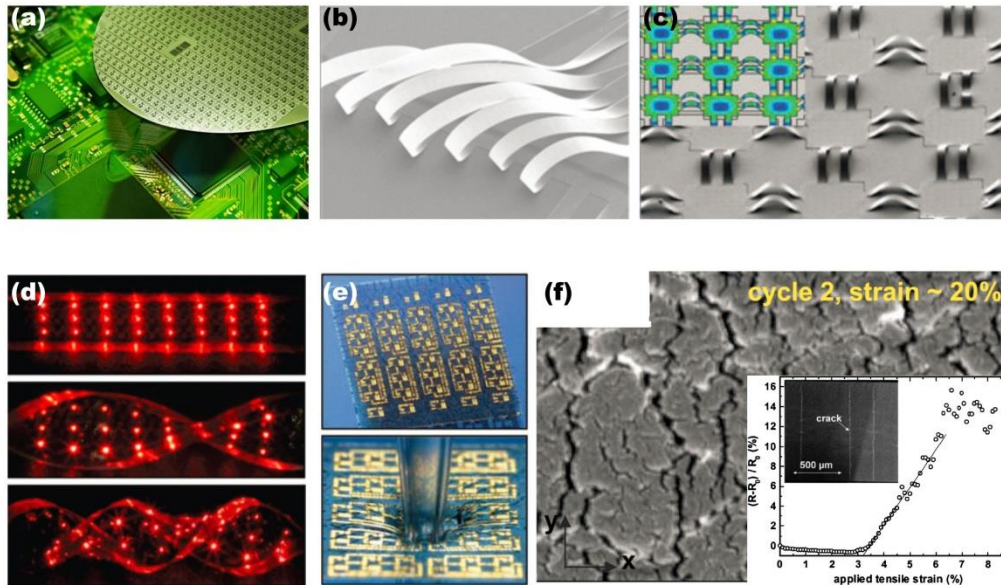


Figure 1. Brief overview of challenges associated with flexible devices. (a) A silicon wafer can be sliced into (b) ribbons or (c) wavy sheets and embedded into (d-e) elastomeric substrate³². f) These devices can crack or develop fracture upon repeated applied strain^{33,34}.

1.3 LIQUID METALS

There are five known elements that are liquid at (or near room temperature): mercury, gallium, cesium, rubidium and francium. Rubidium and cesium are explosively reactive and francium is radioactive, so these metals are not practical. Mercury is the most common room

temperature liquid metal but its high surface energy, its toxicity, and its density makes it unfavorable for microfluidic applications^{5,35}. Gallium is a compelling liquid metal because it has a low bulk viscosity (like mercury)³⁶, but forms a surface oxide¹ that dominates its fluid behavior⁵. **Figure 2** compares the behavior of mercury and EGaIn (one of the alloys of gallium) in microchannels.

Gallium melts at 30 °C³⁷ and is therefore technically a solid at room temperature (although it is known to super cool readily)^{38,39}. Other low melting metals (e.g., indium, zinc and tin) form alloys that depress the melting point of gallium below room temperature³⁷. We focus on eutectic gallium indium because it is the simplest of these alloys (i.e., it is binary) and much is known about its properties. EGaIn melts at 15.7 °C⁵ and has an extremely low vapor pressure at ambient temperature^{40,41}. The surface of EGaIn oxidizes readily to form a passivating layer¹ (i.e., it does not grow thicker with time in dry conditions) which we call a ‘skin’. The skin consists of oxides of gallium⁵, similar to the oxide that forms on pure gallium. This oxide can be removed by using acid or base (cf. Figure 3) and in the absence of the skin these alloys behaves like other high surface tension fluids. Most experimental conclusions from EGaIn (regarding its skin) are most likely to be applicable for other alloys of gallium too, like, GaInSn (Galinstan). Furthermore, studies on gallium and its surface oxide are typically relevant to EGaIn since gallium dominates the important interfacial properties.

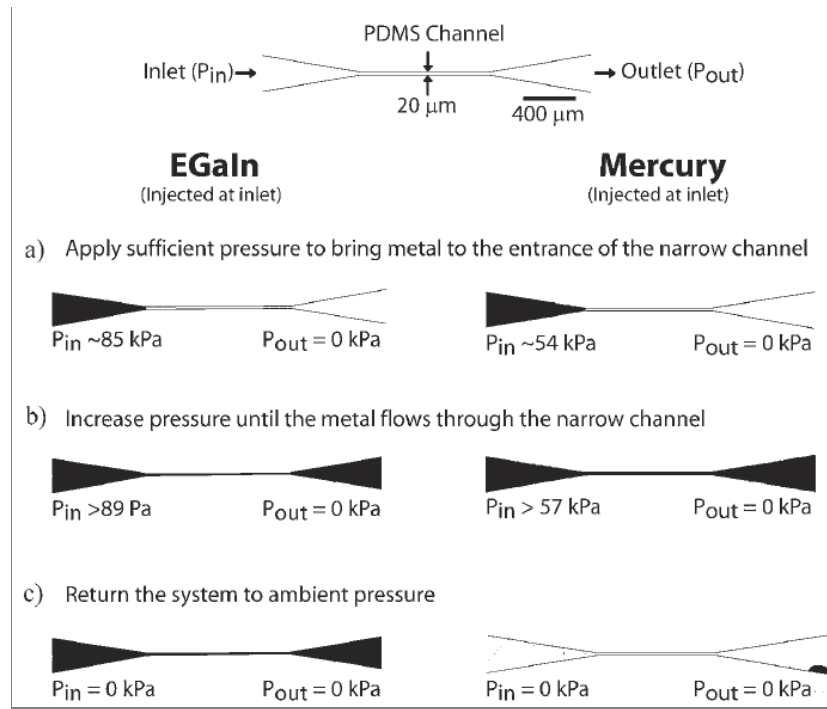


Figure 2: Comparison of EGaIn and Hg in a tapered microchannel. (a-b) Both of these metals can be injected into a 20 μm channel by applied pressure. Higher applied pressure is required for EGaIn due to the presence and yield properties of the oxide skin. (c) EGaIn structure is mechanically stabilized by the oxide; however, Hg retracts from the microchannel due to higher surface tension and absence of the skin. This image is adapted from reference⁵.

1.3.1 PHYSICAL PROPERTIES

Pure gallium is an odorless soft, grey white metal having a rhombic face centered crystal lattice in the solid form^{36,42} ($a = 4.517$, $b = 4.511$, and $c = 7.645$); in liquid form it closely resembles mercury³⁶. Gallium and its alloys are liquids over a wide range of

temperatures^{36,39,43,44}. Of all the elements, gallium has one of the largest ranges between its normal melting point (30 °C) and its normal boiling point (~2200 °C).

Gallium has several interesting properties that occur during freezing: a) It can super cool to a temperature below its melting point up to -40 °C³⁹ (i.e., 70 °C below its freezing point). b) The density of gallium in the liquid state (6.095 g/cm³) is larger than the solid state (5.904 g/cm³), resulting in 3.2% increase in volume when it solidifies^{36,45}, c) Electrical conductivity of liquid gallium is higher than solid gallium because of the increase in co-ordination number in the molten state^{36,45}. Electrical resistance and thermal expansion of solid gallium are different along the three crystallographic planes^{36,45}.

The surface of gallium and its alloys oxidize rapidly in air to form oxides of gallium (reported, but not proven to be amorphous¹). It forms on gallium and other forms of gallium alloys (i.e., GaIn or GaInSn) even at ppm levels of oxygen concentration^{1,47}. Among all the polymorphs^{48,49} of gallium oxide, β -Ga₂O₃⁵⁰⁻⁵³ is chemically⁵⁴ and thermally the most stable^{48,55}. This form is a wide band gap^{56,57} transparent n-type semiconductor with amorphous structure. It has been widely used as a gas sensor^{56,58-60}, luminescent phosphor⁶¹, transparent oxide⁵⁴, catalyst^{59,62,63}, insulator^{52,53,64} for gallium based semiconductors, nanowires and nano ribbons, in laser lithography, solar cells, and optoelectronic devices⁶⁵⁻⁷⁰.

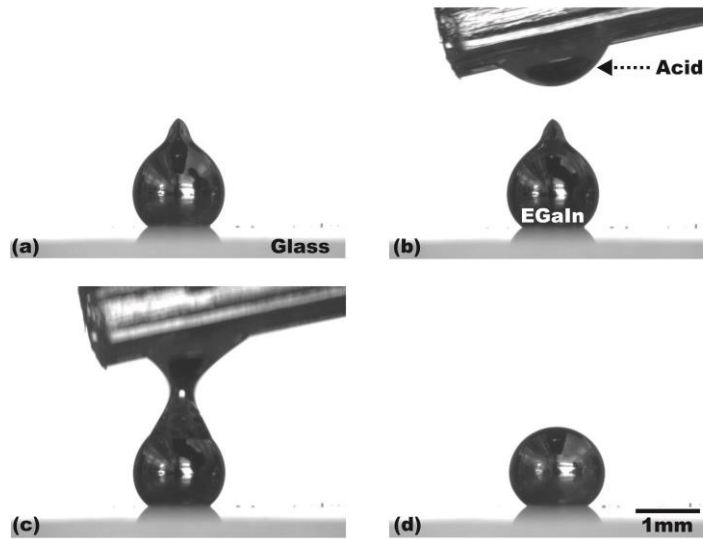


Figure 3: (a) Non-spherical shape of a liquid metal drop is stabilized by the presence of the oxide, even though the bulk metal has a very high surface tension. (b-c) Addition of acid ($\text{pH} < 3$) or base ($\text{pH} > 10$) can remove the oxide and (d) the metal drop beads up due to high surface tension. This image has been adapted from reference ⁴⁶.

The oxide skin forms quickly in air (within microseconds⁷¹) and is passivating (i.e., does not grow thicker with time in dry air)¹. The following section highlights some of the key properties of the oxide which have been harnessed in this dissertation to accomplish some of the key objectives.

1.3.2 RHEOLOGY

The ability to flow or stabilize the metal on demand is important for shaping it into useful, and in some cases, responsive structures (i.e., those that change shape by flowing in response

to some stimuli)^{6,8,72}. When the skin ruptures, the underlying metal gets exposed and is prone to oxidation in the presence of oxygen. Sandwiching the metal in a parallel plate rheometer offers one route to characterize the yield stress of the oxide coated metal.^{5,73}

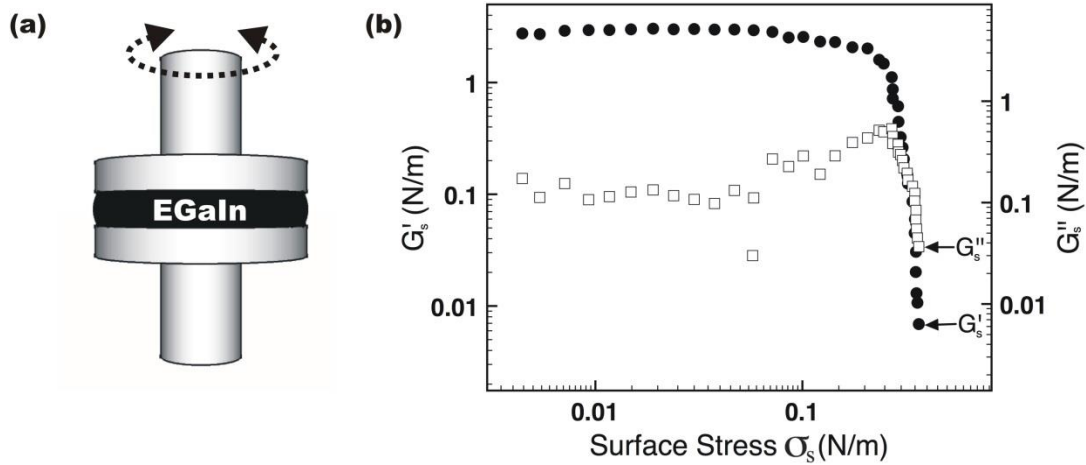


Figure 4: Rheological characterization of liquid metal in air using (a) a parallel plate rheometer. In a typical experiment, the metal is sandwiched in between the oscillatory-top plate and stationary-bottom plate. The sample is about ~ 1 mm thick. Once the top plate is rotated at an angular velocity, any resistance to deform the liquid metal is essentially coming from the surface oxide. Therefore this test is usually considered as an interfacial characterization. (b) The oxide ruptures ~ 0.5 N/m applied stress, where the elastic modulus drops instantaneously and the viscous modulus takes over. Beyond this applied stress, the skin acts like an elastic membrane and gives the metal mechanical stability. This image is adapted from reference⁵⁰.

The oxide is strong enough to support the material below its critical limit but it ruptures in response to external stimuli once the applied stress is higher than $\sim 0.5\text{-}0.6\text{ N/m}$, as shown in **Figure 4**. This property affects the pressure required to inject the metal into microchannels⁶. Different micro-components can be designed, fabricated and analyzed by harnessing the geometry of the microchannels, yield stress of the oxide and viscosity of the liquid metal. Several studies have already explored this for the formation of 3-D⁷⁴ and 2-D⁷⁵ structures and to form stretchable interconnects¹¹, wires⁷⁶, antennas^{77,6}, sensors^{78,79}, and plasmonic structures⁸⁰ fabricated by injecting the metal into microchannels.

1.3.3 ADHESION AND WETTING

The oxide adheres to most surfaces^{5,75,81–83} (with some notable exceptions^{84,85}). The interaction of metal/oxide interface with substrates affects the mechanical stability of the metal in the channels, the behavior of the metal during injection and withdrawal, and the electrical characteristics of the interface between the metal and the walls of microchannels⁸⁶. The mechanical properties of the oxide, its adhesion to surfaces, and its ability to break and reform complicate the interpretation of conventional interfacial measurements (e.g. pendant drop, sessile drop, contact angle). Specifically, the shape and contact angle of the oxide-coated metal depends very much on how the metal is handled (i.e., it is hysteretic). Thus, the most reliable methods of characterization are those that dispense the metal in the same manner, such as measurements of the advancing and receding contact angle. The adhesion of the liquid metal has been attributed to the formation and mechanical history of the metal/oxide interface.⁸¹ **Figure 5** briefly summarizes the wetting nature of the oxide skin.

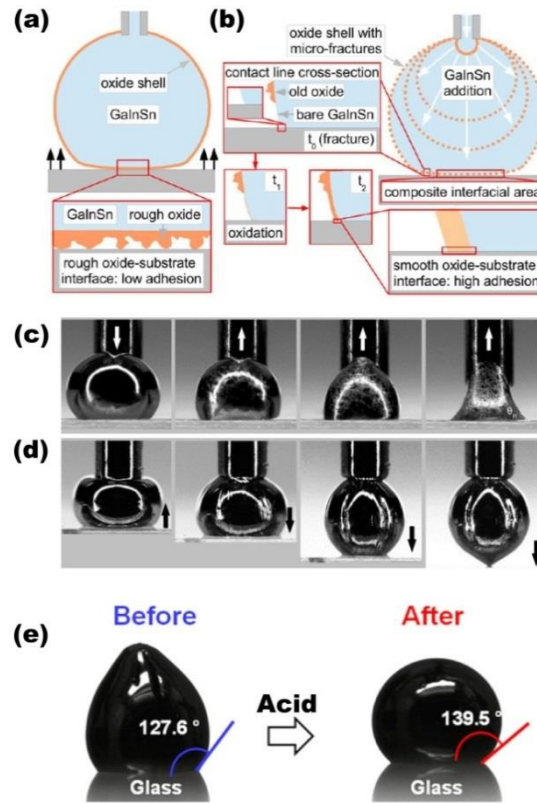


Figure 5: A droplet of liquid metal can be brought in contact or pulled away from surface in many different ways. Two of these approaches are illustrated in (a) and (b). (a) Schematic illustration of (old) rough oxide – surface interface, where the droplet is brought in contact by changing the height of the stage. (b) Schematic illustration of (new) smooth oxide –surface interface, where the droplet barely touches the surface initially and then the volume of the drop increases. (c) Optical images from advancing-receding experiments that utilize the concept of (b). (d) Optical images from the same experiment that utilizes the concept in (a). Freshly grown oxide tends to stick to surfaces more than the old oxide. (e-f) Freshly grown or old oxide can be dissolved by using acid, acid vapor or by using acid impregnated surface. (a-d) are adapted from reference ⁸¹ and (e) is adapted from ⁸⁷.

Actuating the metal in microchannels necessitates either removing the oxide or preventing it from adhering to surfaces. It is possible to remove it using acid, acid vapor, base, or acid impregnated surfaces^{82,84,88} which are hazardous and corrosive materials⁸⁹. It is possible to use Teflon-like surfaces or roughened surfaces^{81,90,91} to reduce the adhesion of the metal oxide. In the case of microsystems, these approaches limit the materials of construction and increase the complexity of fabrication. For these reasons, most studies involving the actuation of liquid metals in microchannels focus on Hg despite its toxicity⁹²⁻⁹⁴.

1.3.4 ELECTROCHEMISTRY

It is possible to utilize electrochemical reactions to deposit or remove the oxide using low voltages (<1 V)⁹⁵. In the absence of the oxide, the metal has a large surface tension. Depositing the oxide by electrochemical oxidation in electrolyte lowers the surface tension of gallium alloys by two orders of magnitude⁹⁵. Electrical control of surface oxidation is simple, requires minimal energy, and provides rapid and reversible control of interfacial tension over an enormous range. This approach avoids the use of toxic mercury, and provides a new opportunity for shape reconfigurable, reversible microfluidic electronics featuring gallium alloys as the conductive elements. **Figure 6** briefly illustrates this concept.

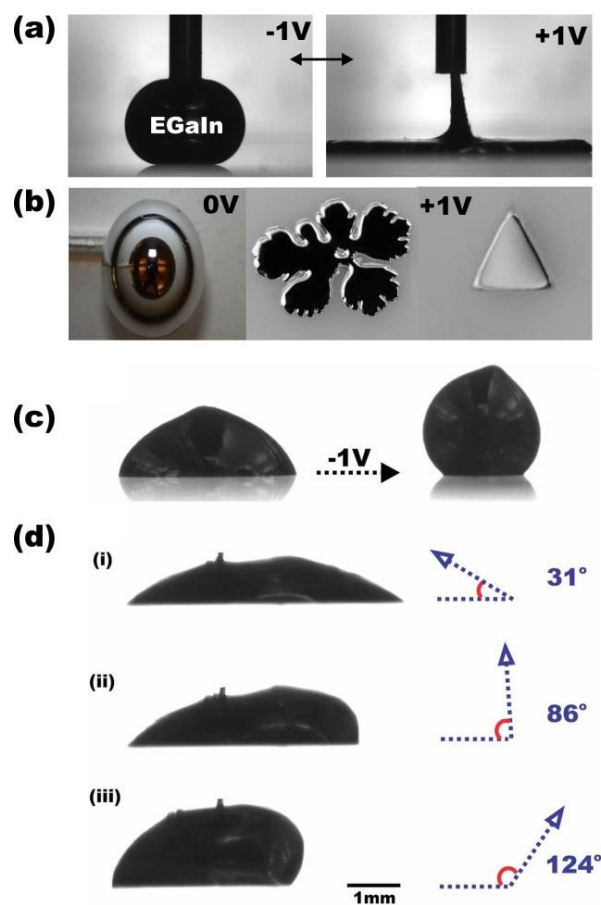


Figure 6: Giant and switchable surface activity of liquid metals using oxide as surfactant in an electrochemical environment. (a-b) A pendant or sessile drop of liquid metal, submerged into electrolyte, dramatically spreads into many different patterns (i.e., pancake, fractal or triangle). The oxide acts as a surfactant that lowers the surface tension of the metal and allows it to spread without bound. (c) Changing the polarity of the applied bias removes the oxide via electrochemical reduction. Removal of the oxide induces capillary action. (d) Removal of the oxide locally allows a drop to asymmetrically de-wet from the substrate. All of the images have been adapted from reference ⁹⁵.

Electrochemical studies can elucidate the kinetics of surface oxidation/reduction^{96–101}. Passive oxide films^{102–107} (i.e., those that do not grow thicker with time) on metals, such as the one formed on gallium, are very common and widely studied for aluminum^{106,108–114}, titanium^{115–118}, and steel^{119,120} (often called valve metals). These films are also important for corrosion protection^{106,121}. These passive films can be removed by scrapping, cutting, yielding, rupturing, scratching and shearing^{115,116,118,122–128} to facilitate the study of oxidation. The electrochemical behavior of gallium has been studied in aqueous, acidic and alkaline environments^{129–137}. Electrochemistry of indium has been carried out in chloride, alkaline, acidic and in aqueous environments^{138–146} as well. The Pourbaix¹⁴⁷ diagram predicts the behavior of the oxide versus electric potential and the pH of the aqueous environment.

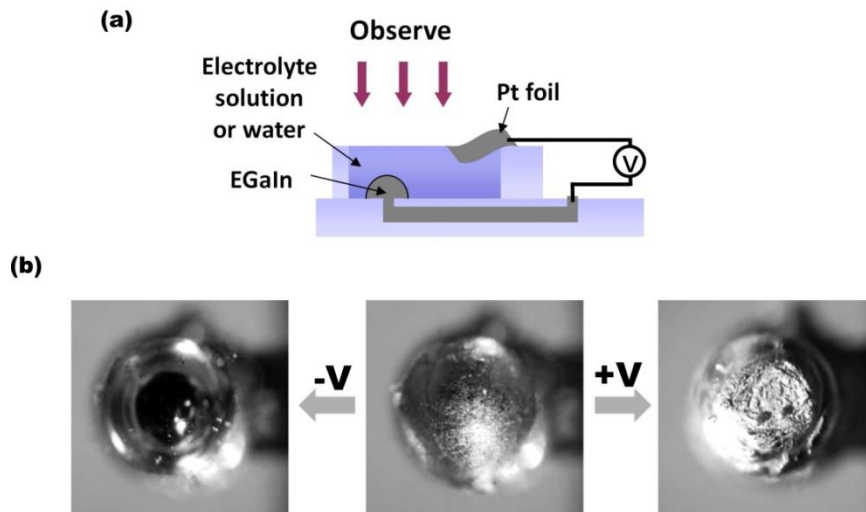


Figure 7: In an (a) electrochemical environment the oxide skin can be (b) removed or grown depending upon the direction of bias¹⁴⁸.

The thickness of the oxide skin on liquid metal can be tuned electrochemically^{148,149}. This property has been harnessed to form memory resistive devices¹⁴⁹ and diodes¹⁴⁸ where the resistance to current increases as the oxide thickness increases. Figure 7 summarizes this result.

1.4 APPLICATIONS OF LIQUID METALS

Flexible devices consisting of thin foils of rigid materials typically cannot be stretched significantly because the materials that comprise them are not inherently stretchable. Soft, deformable, and stretchable electronics can be integrated into bandages, textiles, artificial muscles and soft robots.

The remarkable properties of gallium alloys have recently been utilized for the formation of soft and deformable electronic devices that can change their shape in response to external stimuli (i.e., pressure). A number of new applications based on patterning and shape reconfiguring on demand are briefly summarized in these two sections.

1.4.1 PATTERNING LIQUID METAL

Soft and stretchable electronics devices that contain liquid metal rely on the ability to pattern liquid metal alloys on different substrates rapidly and reliably. A majority of the patterning techniques to date utilize the wetting properties of the oxide and the viscoelastic nature of the

oxide-coated metal. Table 1 lists some of the key processes to pattern liquid metal on different substrates along with the minimum size reported to date. These fabrication methods are still at the exploratory stage and yet to be characterized for larger scale of production.

Table I: List of technologies to date for patterning liquid metal

Name	Year
1. Injection into Microchannels	2008
2. Inkjet Printing or Direct Writing	2013
3. Microcontact Printing	2013
4. Stencil lithography	2013
5. Masked Deposition	2013
6. Freeze Casting	2013
7. Imprinting	2014
8. Tape transfer	2014
9. Laser Ablation	2014

Soft lithography and replica molding techniques are widely used and the devices are highly reproducible. Replica molding is a widely used casting process to inversely replicate a topographical master for making microfluidic channels. The resulting inverse replica of the master constitutes the channel through which liquids may be injected.

Highly flexible, stretchable and reversibly deformable devices have been fabricated by injecting liquid metal into elastomeric microfluidic channels using this method as shown in **Figure 8**. Although this method is very effective for producing devices with the smallest dimensions >10 microns, it is a time consuming batch process. Starting from designing a

photo mask, this method requires several hours to fabricate and characterize a single device depending upon the nature of the experiment.

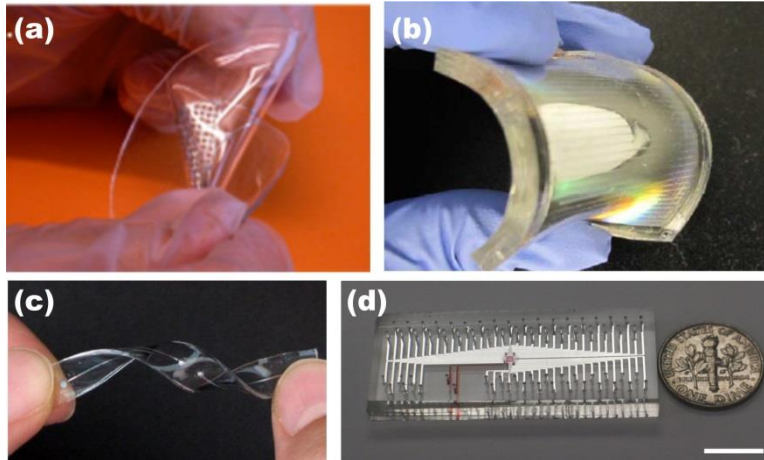


Figure 8: Soft lithographic approach to make microfluidic channels filled with liquid metals. (a) A stretchable un-balanced loop antenna, (b) A flexible patch antenna, (c) A deformable dipole antenna, (d) A soft interconnect for CMOS chip. (a) is adapted from ¹⁰, (b) is from ¹⁵⁰, (c) is adapted from ⁴⁶ and (d) is from ¹⁵¹.

This method requires operator skills for successful replication of each master, fabrication of the elastomeric device and lastly, injection of liquid metal into micro channels. The yield stress properties of the liquid metal limit the minimum channel size into which the metal may be injected. As the channel dimension decreases, applied pressure to force liquid metal into microchannel increases.

Micro-contact printing¹⁵² deposits discrete drops, lines and arrays of patterns. Here, the printer works like a pixel printer and the printer head is controlled by a motorized XYZ stage. The tip of the printer, dips into the liquid metal pool, is wetted by the oxide skin, and then the wet tip moves away from the pool and touches the substrate to deposit a discrete dot of liquid metal or draw lines. Spatial positions of the drops or arrays are controlled by a computer program. Using this method ~ 350 micron droplet can be deposited whereas two lines can be deposited with ~ 200 micron separation distance.

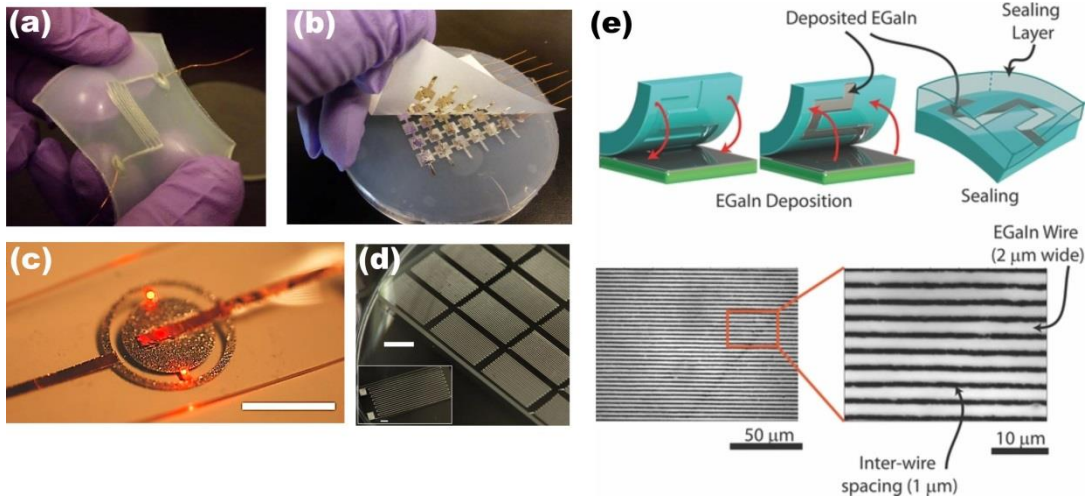


Figure 9: Different ways of producing shapes and patterns. (a) A comb capacitor by using microcontact printing method. (b) An array of liquid metal by using a stencil mask. (c) Demonstration of a liquid metal circuit using tape transfer method, (d) Directly written liquid metal lines, and (e) Liquid metal lines by imprinting method. Photographs for this figure are adapted from (a) ¹⁵², (b) ¹⁵³, (c) ¹⁵⁴ (d) ⁷⁵ and (e) ¹⁵⁵.

Microcontact printing avoids the use of lithographic steps but the minimum features are one order of magnitude higher than those formed by soft lithography. This deposition of droplets is serial and requires the use of precise hardware control. It also works only on substrates to which the oxide-coated metal adheres.

Liquid metal has been patterned using **stencil lithography**¹⁵³ or **tape transfer**¹⁵⁴ methods. Using a stencil mask on top of a substrate, a puddle of liquid metal can be rolled and later the stencil along with excess metal is removed to form patterns and shapes. Patterns are defined by the openings in the stencil. Tape transfer is another method that utilizes similar working principle as stencil lithography. These techniques are capable of forming ~ 100 micron scale width lines. **Imprinting**¹⁵⁵ utilizes compressive force to push metal into micron scale grooves. Examples of devices based on these fabrication techniques are mentioned in **Figure 9**.

The ability to shape liquids into free standing, stable 3D micro structures is extremely difficult and nearly impossible due to the dominance of interfacial tension over gravity. At the sub-mm scale liquid jet breaks up into tiny droplets or droplets of liquid coalesce into large bead. In contrast, liquid metal pendant drops can be stacked on top of each other and form out of plane 3D structures. Utilizing the viscoelastic nature of the oxidized metal droplets, a number of different 3D microstructures have been demonstrated. 3D printing⁷⁴ of liquid metals, as shown in **Figure 10**, is obtained by, a) applying sudden burst pressure that forces metal drop out of the syringe needle, b) stacking pendant drops on top of each other, c)

extruding wires, and d) injecting metals into elastomeric channel which is followed by dissolving the channel.

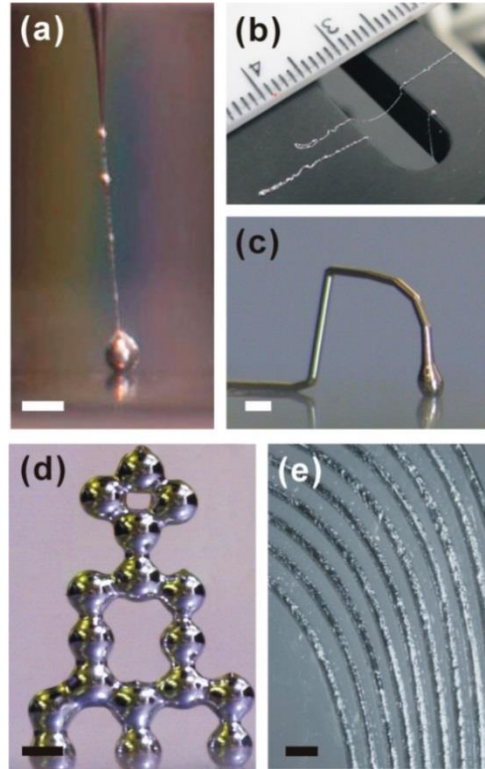


Figure 10: 3D printing of free-standing liquid metal structures. (a) Sudden burst pressure forces liquid metal out of the syringe tip, which extends as a fiber to the substrate. The fiber is stabilized by the oxide layer. (b) Resulting fibers are strong enough to span a gap. (c) Extruded wire that is bent into the shape of an arch. (d) Stacks of liquid metal droplets. (e) Liquid metal injected into microchannels remains mechanically stable after dissolving all of the channel walls except the substrate. Scale bars are all 500 μm .” The caption and this image has been adapted directly from reference ⁴⁶.

All of these structures are stabilized by utilizing the oxide skin that forms rapidly in air. 3D printing of room temperature alloys could play a major role of producing electronics on demand without the need of other complicated fabrication processes.

Direct writing⁷⁵ is another common approach of depositing temperature sensitive materials, especially polymers, layer by layers on a substrate and build different but industrially important objects. It is possible to print conductive inks on elastomer surface¹⁵⁶. However, these inks are not suitable for applications where higher conductivity or improved mechanical properties are needed. Moreover, out of plane structures, like 3D printing of liquid metal droplets, are not possible from direct writing of these conductive inks.

Direct writing addresses the challenge associated with speed of deposition in microcontact printing process. These processes also do not require any steps involved in lithography and it exploits the wetting properties of the oxide and the flow properties of the liquid metal. In direct writing process, metal is continuously forced by a syringe pump out of a nozzle that defines the size of the resolved features, and the motion of the nozzle creates the traces. The mechanical property of the oxide skin is also important to stabilize the written traces on glass or elastomer surface. Strong wetting behavior of the oxide pins the traces to the substrate and they do not damage during encapsulation by elastomer coating. Approximately ~80 micron traces were deposited by this technique.

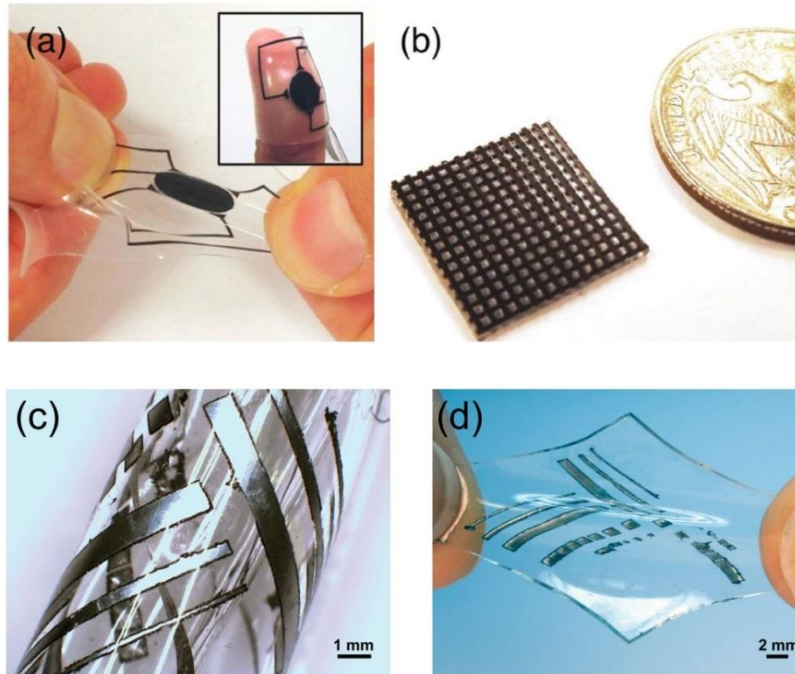


Figure 11: Soft and stretchable liquid metal embedded polymers. (a) Patterns are created by using laser ablation technique. (b) Masked deposition technique to make patterns that avoids the use of lithography or contact printing. Images are adapted from (a) ¹⁵⁷, and (b) ¹⁵⁸.

Laser ablation¹⁵⁷ and **masked deposition**¹⁵⁸ techniques can also create metallic patterns on elastomeric substrates (cf. Figure 11). Laser ablation method utilizes CO₂ lasers to ablate materials and create patterns on a composite layer which is composed of PDMS-metal-PDMS. Later, additional PDMS seals this patterned layer to make soft, stretchable and function sensors. Laser ablation assisted patterning is a direct and fast method of producing shapes that eliminates the need of soft lithography, customized or automated printing, and

mask for stencil lithography. Masked deposition is another recent approach that does not require any steps involved in soft lithography.

1.4.2 RECONFIGURABLE DEVICES

The ability to reconfigure the shape and therefore, the function of electronic devices offers the opportunity to create more dynamic devices. Most electronic devices (e.g., antennas and circuit boards) have a singular, static shape that defines their performance. Conventional shape reconfigurable devices, in contrast, can alter their functional behavior by changing the electrical paths, which typically involves mechanical or electrical switches (e.g., micro-electro mechanical systems, diodes, RF MEMS capacitors)⁸ that selectively connect and disconnect active segments. Efficient integration of these switches at different arrangements and layouts, therefore, require strategic design and complex fabrication steps¹⁵⁹.

Shape reconfigurable devices composed of liquid metal encased in elastomer have been demonstrated⁶. These devices can change their physical shape without the need of external switches, and therefore, function in response to external stimuli. The conductive element – room temperature liquid metal – in these devices flows in response to applied stress, and therefore, reversibility can be attained without the loss of electrical continuity. Present antenna architectures from liquid metal alloys are mechanically stretchable, flexible and offer numerous possibilities where a liquid conductor is needed. One form of a RF antenna – a dipole antenna - is shown in **Figure 12**. Elongating a dipole antenna, for example, lowers the

resonant frequency once stretched in a predictable manner and then the antenna becomes a strain sensor.

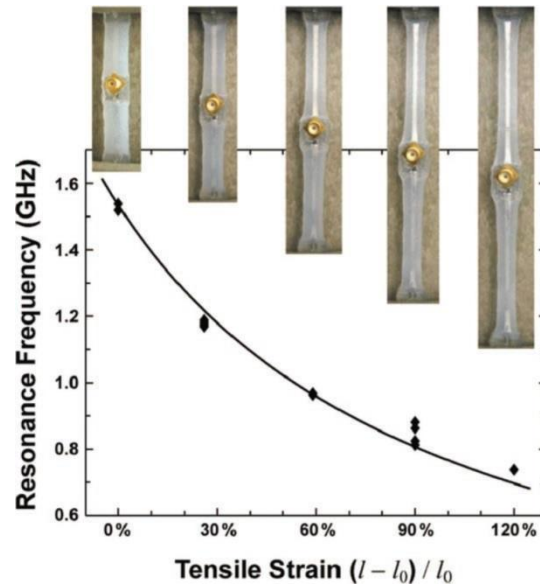


Figure 12: Stretchable radio frequency liquid metal antennas from polymers other than PDMS. The antenna resonates at different frequencies as the length changes upon strain. This image has been adapted from reference ⁷.

Mechanically stretchable antennas also find application as strain sensors¹⁶⁰. Soft sensors utilize the principle of mechanically stretchable antennas to sense and detect deformation of soft structures and translate this deformation in terms of some measurable quantities so that real time monitoring can be achieved^{23,161}.

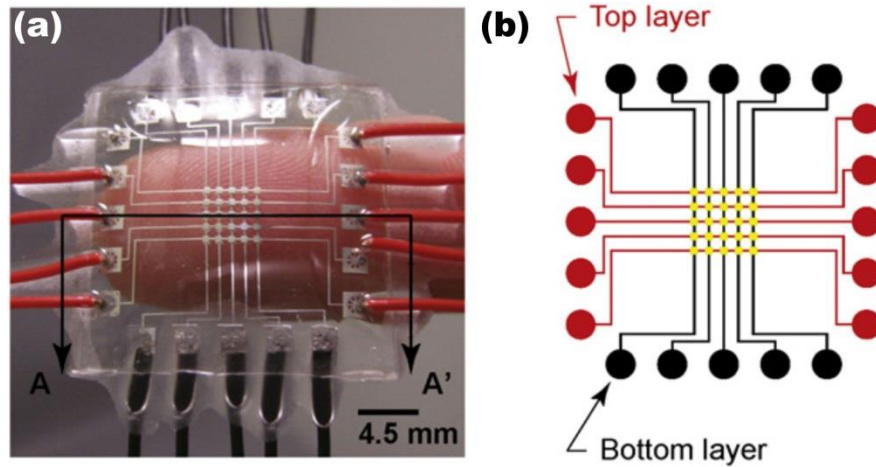


Figure 13: Liquid metal filled capacitive sensors for normal force detection and measurement. (a) Photograph of the prototype device. No solid electronic parts are used in the device. (b) Images of the sensor array. This figure has been directly adapted from reference ¹⁶².

One such example has recently mimicked the performance of human fingers by utilizing liquid metal that detects the external pressure, applied strain, and temperature. For the demonstration of normal force sensor, two layers of liquid metal filled PDMS are stacked against a layer of air filled chamber. The metal filled PDMS layer had some individual tactile elements capable of sensing loads ranging from 0-2.5N. One such example is shown in **Figure 13**.

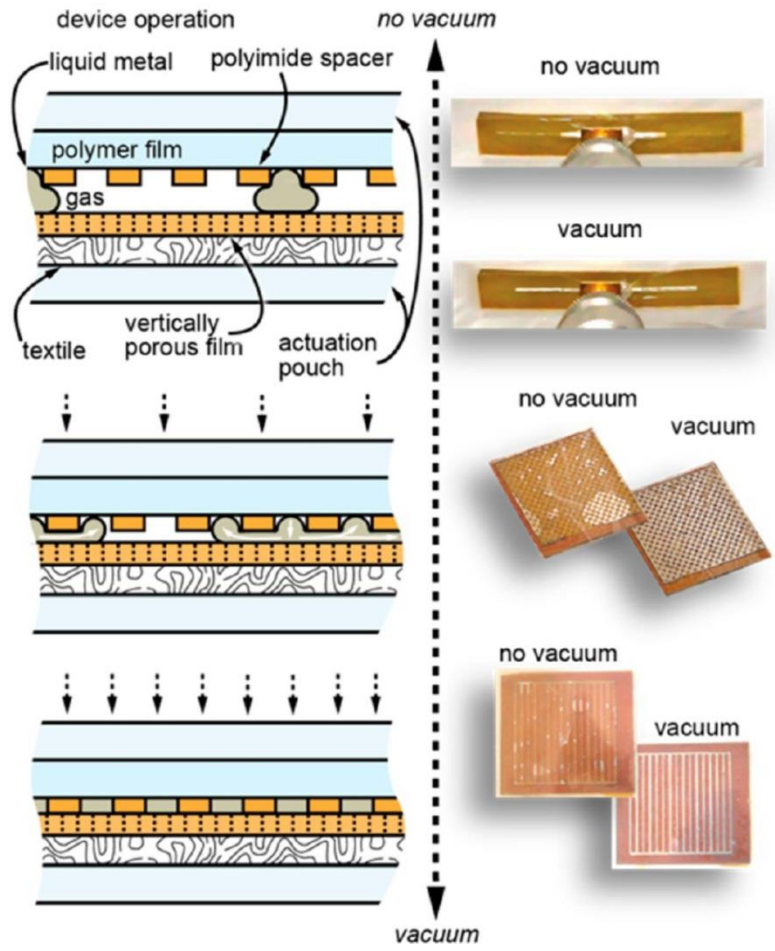


Figure 14: Schematic depiction of a reversible vacuum pressure actuated liquid metal device in the presence of acid vapor to remove the oxide. Examples at the right include antennas, shields and polarizers from top to bottom. This image has been taken from ref⁴⁶

In this example, physical deformation changes the dimension of the elastomeric channel that in turn changes the electrical resistance. This concept of sensing and detecting applied pressure has been utilized for electronic skin and soft robotics as well. Radio frequency

radiation sensors and large area wireless strain sensors have recently utilized rigid components along with microfluidic passive components for high level of performance as well^{23,161}.

Liquid metal filled microchannels also form useful soft electrodes^{13-15,86,163,164}. These electrodes are easy to fabricate and align along the length of the fluid flow and therefore, can be exploited to use as coulter counter or create chaotic advection for enhanced fluid mixing. It is also possible to make soft interconnects from liquid metal which can smartly be integrated into CMOS circuits¹⁵¹. Liquid metal filled wires on self-healing polymers have also been severed mechanically and electrically to form reconfigurable circuits and 3D elements¹⁶⁵. When the structures are cut with a razor, liquid metal remain flush with the channel, and when the structures are pressed together, the polymer selfheal via hydrogen bonding and the metal remains conductive.

Majority of the shape reconfiguration of the aforementioned devices relies on mechanical stretching of the elastomer which in turn elongates the conductive liquid metal. The oxide of liquid metal has a tendency to adhere to the walls of microchannels, impedes flow the liquid metal and thus the use of gallium alloys in applications requiring the reversible control of micro-scale switches, pumps, optics, or shape reconfigurable electronics¹⁶⁶ utilize mercury. Vapor or liquid of a strong acid or base (e.g., HCl or NaOH) can address this issue by removing the oxide^{5,167,168}. One recent example, as shown in Figure 14, utilizes this concept to form reconfigurable circuits. Rather than utilizing pneumatic pressure, in presence of acid,

the metal is actually pulled into the relief structures by vacuum to form reconfigurable antennas. Apart from using acid/base, non-stick surfaces have also been utilized to minimize improve non wetting behavior of the liquid metal alloys¹⁶⁷.

1.5 THESIS OUTLINE

A majority of the applications based on liquid metals are static. This dissertation combines fundamental research – intended to provide better understanding of the metal/oxide interface – with applied research focused on shape reconfigurable components composed of liquid metal. Overall, this dissertation aims to contribute to the development of a new paradigm of microelectronic devices that can be controlled and manipulated on demand in a manner that is completely reversible. The next few sections briefly outline the approach of this dissertation.

Chapter 2 and **Chapter 3** discuss a shape shifting antenna and microstrip fluidic filter . The goal of this work is to control the way in which metal changes shape, and therefore function, in microchannels by using pressure to force the metal further into engineered channels.

The mechanical properties of EGaIn as a composite can be tuned by modifying the skin, which would also likely modify the chemical and electrical properties of the interface. Fundamental studies of the interfacial properties of EGaIn will be carried out by surface measurements. Chapter 4 describes this work.

Due to the presence of the oxide skin, it is not straightforward to get the metal to withdraw from microchannels without leaving metal residue on the walls of the channel. The ability to withdraw liquid metal from micro channel is critical for truly reconfigurable systems (i.e., wires, interconnects, antennas, filters, valves, mixers) that change their function by changing the shape of the metal on demand. The use of pneumatic pressure to remove the metal seems like an obvious approach for pushing or pulling the metal out of the channels but it leaves significant metal residue inside the channels. A mild to moderately concentrated acid solution can remove the oxide from the surface of EGaIn and induce capillary withdraw in an uncontrollable fashion, which is undesirable. **Chapter 5** describes a simple approach to withdraw a fluidic metal wire from microfluidic channels in response to an applied electric potential in the presence of an electrolyte. This electrochemical approach reduces the passivating oxide skin and induces capillary motion of the metal from the microfluidic channels. Since these processes are driven by an external voltage in presence of an electrolyte, we define recapillarity (reduction capillarity) as the process of reducing the oxide skin on the metal to induce capillary action.

Chapter 6 utilizes the principles of recapillarity to induce localized instabilities in a liquid metal alloy (eutectic gallium indium, EGaIn) using low voltages. These instabilities can be turned on or off to pattern 2D films of the metal. The patterning process begins by spreading a film of the metal on a substrate. A thin oxide layer that forms spontaneously on the surface of the metal stabilizes the film despite the large surface tension and low viscosity of the metal. In the absence of the oxide, the metal film beads up to minimize interfacial energy.

The use of localized electrochemical reduction of the oxide in the presence of electrolyte induces capillary withdrawal of the metal (so-called ‘recapillarity’). The resulting patterns and shapes of the liquid metal can be controlled by the placement of the counter electrode with respect to the metal, as well as the duration of the applied current. This patterning method is similar in spirit to the Etch-a-Sketch™ toy, but is distinguished by the use of capillary withdrawal rather than physical scribing.

The presence of the oxide skin on the surface of the liquid metal causes it to stick to most of the surfaces, which limits the ability to easily reconfigure its shape on demand. **Chapter 7** shows that, water can provide an interfacial slip layer between EGaIn and other surfaces, which allows the metal to flow smoothly through capillaries and across surfaces without sticking. The slip layer provides new opportunities to control and actuate liquid metal plugs in microchannels – including the use of continuous electrowetting—enabling new possibilities for shape reconfigurable electronics, sensors, actuators and antennas.

1.6 REFERENCES

- (1) Regan, M. J.; Tostmann, H.; Pershan, P. S.; Magnussen, O. M.; DiMasi, E.; Ocko, B. M.; Deutsch, M. X-Ray Study of the Oxidation of Liquid-Gallium Surfaces. *Phys. Rev. B Condens. Matter* **1997**, *55*, 10786–10790.
- (2) FRENCH, S. J.; SAUNDERS, D. J.; INGLE, G. W. THE SYSTEM GALLIUM-INDIUM. *J. Phys. Chem.* **1937**, *42*, 265–274.
- (3) Zrnic, D.; Swatik, D. S. On the Resistivity and Surface Tension of the Eutectic Alloy of Gallium and Indium. *J. Common Met.* **1969**, *18*, 67–68.
- (4) König, U.; Keck, W. Measurement of the Surface Tension of Gallium and Indium in a Hydrogen Atmosphere by the Sessile Drop Method. *J. Common Met.* **1983**, *90*, 299–303.
- (5) Dickey, M. D.; Chiechi, R. C.; Larsen, R. J.; Weiss, E. A.; Weitz, D. A.; Whitesides, G. M. Eutectic Gallium-Indium (EGaIn): A Liquid Metal Alloy for the Formation of Stable Structures in Microchannels at Room Temperature. *Adv. Funct. Mater.* **2008**, *18*, 1097–1104.
- (6) So, J. H.; Thelen, J.; Qusba, A.; Hayes, G. J.; Lazzi, G.; Dickey, M. D. Reversibly Deformable and Mechanically Tunable Fluidic Antennas. *Adv. Funct. Mater.* **2009**, *19*, 3632–3637.
- (7) Kubo, M.; Li, X.; Kim, C.; Hashimoto, M.; Wiley, B. J.; Ham, D.; Whitesides, G. M. Stretchable Microfluidic Radiofrequency Antennas. *Adv. Mater.* **2010**, *22*, 2749–2752.

- (8) Khan, M. R.; Hayes, G. J.; So, J.-H.; Lazzi, G.; Dickey, M. D. A Frequency Shifting Liquid Metal Antenna with Pressure Responsiveness. *Appl. Phys. Lett.* **2011**, *99*, 013501–013503.
- (9) Cheng, S.; Wu, Z.; Hallbjorner, P.; Hjort, K.; Rydberg, A. Foldable and Stretchable Liquid Metal Planar Inverted Cone Antenna. *IEEE Trans. Antennas Propag.* **2009**, *57*, 3765–3771.
- (10) Cheng, S.; Rydberg, A.; Hjort, K.; Wu, Z. Liquid Metal Stretchable Unbalanced Loop Antenna. *Appl. Phys. Lett.* **2009**, *94*, 144103–144103–3.
- (11) Kim, H.-J.; Son, C.; Ziaie, B. A Multiaxial Stretchable Interconnect Using Liquid-Alloy-Filled Elastomeric Microchannels. *Appl. Phys. Lett.* **2008**, *92*, 011904–011904–3.
- (12) Kim, H.-J.; Maleki, T.; Wei, P.; Ziaie, B. A Biaxial Stretchable Interconnect With Liquid-Alloy-Covered Joints on Elastomeric Substrate. *J. Microelectromechanical Syst.* **2009**, *18*, 138–146.
- (13) Chiechi, R. C.; Weiss, E. A.; Dickey, M. D.; Whitesides, G. M. Eutectic Gallium–Indium (EGaIn): A Moldable Liquid Metal for Electrical Characterization of Self-Assembled Monolayers. *Angew. Chem. Int. Ed.* **2008**, *47*, 142–144.
- (14) Thuo, M. M.; Reus, W. F.; Nijhuis, C. A.; Barber, J. R.; Kim, C.; Schulz, M. D.; Whitesides, G. M. Odd–Even Effects in Charge Transport across Self-Assembled Monolayers. *J. Am. Chem. Soc.* **2011**, *133*, 2962–2975.
- (15) So, J.-H.; Dickey, M. D. Inherently Aligned Microfluidic Electrodes Composed of Liquid Metal. *Lab Chip* **2011**, *11*, 905–911.

- (16) Forrest, S. R. The Path to Ubiquitous and Low-Cost Organic Electronic Appliances on Plastic. *Nature* **2004**, *428*, 911–918.
- (17) Post, E. R.; Orth, M.; Russo, P. R.; Gershenfeld, N. E-Broidery: Design and Fabrication of Textile-Based Computing. *IBM Syst. J.* **2000**, *39*, 840–860.
- (18) Gregory, R. V.; Kimbrell, W. C.; Kuhn, H. H. Conductive Textiles. *Synth. Met.* **1989**, *28*, 823–835.
- (19) Rogers, J. A.; Bao, Z.; Baldwin, K.; Dodabalapur, A.; Crone, B.; Raju, V. R.; Kuck, V.; Katz, H.; Amundson, K.; Ewing, J.; et al. Paper-like Electronic Displays: Large-Area Rubber-Stamped Plastic Sheets of Electronics and Microencapsulated Electrophoretic Inks. *Proc. Natl. Acad. Sci. U. S. A.* **2001**, *98*, 4835–4840.
- (20) Rogers, J. A. Toward Paperlike Displays. *Science* **2001**, *291*, 1502–1503.
- (21) Chen, Y.; Au, J.; Kazlas, P.; Ritenour, A.; Gates, H.; McCreary, M. Electronic Paper: Flexible Active-Matrix Electronic Ink Display. *Nature* **2003**, *423*, 136–136.
- (22) Gelinck, G. H.; Huitema, H. E. A.; van Veenendaal, E.; Cantatore, E.; Schrijnemakers, L.; van der Putten, J. B. P. H.; Geuns, T. C. T.; Beenhakkers, M.; Giesbers, J. B.; Huisman, B.-H.; et al. Flexible Active-Matrix Displays and Shift Registers Based on Solution-Processed Organic Transistors. *Nat. Mater.* **2004**, *3*, 106–110.
- (23) Someya, T.; Kato, Y.; Sekitani, T.; Iba, S.; Noguchi, Y.; Murase, Y.; Kawaguchi, H.; Sakurai, T. Conformable, Flexible, Large-Area Networks of Pressure and Thermal Sensors with Organic Transistor Active Matrixes. *Proc. Natl. Acad. Sci. U. S. A.* **2005**, *102*, 12321–12325.

- (24) Baude, P. F.; Ender, D. A.; Haase, M. A.; Kelley, T. W.; Muyres, D. V.; Theiss, S. D. Pentacene-Based Radio-Frequency Identification Circuitry. *Appl. Phys. Lett.* **2003**, *82*, 3964–3966.
- (25) Cantatore, E.; Geuns, T. C. T.; Gelinck, G. H.; van Veenendaal, E.; Gruijthuijsen, A. F. A.; Schrijnemakers, L.; Drews, S.; de Leeuw, D. M. A 13.56-MHz RFID System Based on Organic Transponders. *IEEE J. Solid-State Circuits* **2007**, *42*, 84–92.
- (26) Mayer, A.; Scully, S.; Hardin, B.; Rowell, M.; Mcgehee, M. Polymer-Based Solar Cells. *Mater. Today* **2007**, *10*, 28–33.
- (27) Ouyang, J.; Chu, C.-W.; Szmanda, C. R.; Ma, L.; Yang, Y. Programmable Polymer Thin Film and Non-Volatile Memory Device. *Nat. Mater.* **2004**, *3*, 918–922.
- (28) Scott, J. C.; Bozano, L. D. Nonvolatile Memory Elements Based on Organic Materials. *Adv. Mater.* **2007**, *19*, 1452–1463.
- (29) Yu, G.; Gao, J.; Hummelen, J. C.; Wudl, F.; Heeger, A. J. Polymer Photovoltaic Cells: Enhanced Efficiencies via a Network of Internal Donor-Acceptor Heterojunctions. *Science* **1995**, *270*, 1789–1791.
- (30) Saito, T.; Furuta, T.; Hwang, J.-H.; Kuramoto, S.; Nishino, K.; Suzuki, N.; Chen, R.; Yamada, A.; Ito, K.; Seno, Y.; et al. Multifunctional Alloys Obtained via a Dislocation-Free Plastic Deformation Mechanism. *Science* **2003**, *300*, 464–467.
- (31) Lacour, S. P.; Jones, J.; Wagner, S.; Li, T.; Suo, Z. Stretchable Interconnects for Elastic Electronic Surfaces. *Proc. IEEE* **2005**, *93*, 1459–1467.
- (32) Kim, D.-H.; Ghaffari, R.; Lu, N.; Rogers, J. A. Flexible and Stretchable Electronics for Biointegrated Devices. *Annu. Rev. Biomed. Eng.* **2012**, *14*, 113–128.

- (33) Lacour, S. P.; Chan, D.; Wagner, S.; Li, T.; Suo, Z. Mechanisms of Reversible Stretchability of Thin Metal Films on Elastomeric Substrates. *Appl. Phys. Lett.* **2006**, *88*, 204103–204103–3.
- (34) Li, T.; Huang, Z.; Suo, Z.; Lacour, S. P.; Wagner, S. Stretchability of Thin Metal Films on Elastomer Substrates. *Appl. Phys. Lett.* **2004**, *85*, 3435–3437.
- (35) Chandler, J. E.; Messer, H. H.; Ellender, G. Cytotoxicity of Gallium and Indium Ions Compared with Mercuric Ion. *J. Dent. Res.* **1994**, *73*, 1554–1559.
- (36) Sheka, I. A.; Chaus, I. S.; Mitiureva, T. T. *The Chemistry of Gallium*; Elsevier: New York, 1966.
- (37) Anderson, T. J.; Ansara, I. The Ga-In (Gallium-Indium) System. *J. Phase Equilibria* **1991**, *12*, 67–72.
- (38) Briggs, L. J. Gallium: Thermal Conductivity; Supercooling; Negative Pressure. *J. Chem. Phys.* **1957**, *26*, 784–786.
- (39) Popova, T. I.; Bagotskaya, I. A.; Moorhead, E. D. *Encyclopedia of Electrochemistry of the Elements*; Marcel Dekker Inc.: New York,, 1978.
- (40) Sheka, I. A.; Chaus, I. S.; Mitiureva, T. T. *The Chemistry of Gallium*; Elsevier: New York, 1966.
- (41) Narh, K. A.; Dwivedi, V. P.; Grow, J. M.; Stana, A.; Shih, W.-Y. The Effect of Liquid Gallium on the Strengths of Stainless Steel and Thermoplastics. *J. Mater. Sci.* **1998**, *33*, 329–337.

- (42) Prokhorenko, V. Y.; Roshchupkin, V. V.; Pokrasin, M. A.; Prokhorenko, S. V.; Kotov, V. V. Liquid Gallium: Potential Uses as a Heat-Transfer Agent. *High Temp.* **2000**, *38*, 954–968.
- (43) Jach, J.; Sebba, F. The Melting of Gallium. *Trans. Faraday Soc.* **1954**, *50*, 226–231.
- (44) Maiboroda, V. P. Investigation of Gallium and Indium during Melting. *Thin Solid Films* **1991**, *195*, 357–366.
- (45) Lyapin, A. G.; Gromnitskaya, E. L.; Yagafarov, O. F.; Stal'gorova, O. V.; Brazhkin, V. V. Elastic Properties of Crystalline and Liquid Gallium at High Pressures. *J. Exp. Theor. Phys.* **2008**, *107*, 818–827.
- (46) Dickey, M. D. Emerging Applications of Liquid Metals Featuring Surface Oxides. *ACS Appl. Mater. Interfaces* **2014**, *6*, 18369–18379.
- (47) Cademartiri, L.; Thuo, M. M.; Nijhuis, C. A.; Reus, W. F.; Tricard, S.; Barber, J. R.; Sodhi, R. N. S.; Brodersen, P.; Kim, C.; Chiechi, R. C.; et al. Electrical Resistance of Ag-TS-S(CH₂)_(n-1)CH₃//Ga₂O₃/EGaIn Tunneling Junctions. *J. Phys. Chem. C* **2012**, *116*, 10848–10860.
- (48) Zinkevich, M.; Aldinger, F. Thermodynamic Assessment of the Gallium-Oxygen System. *J. Am. Ceram. Soc.* **2004**, *87*, 683–691.
- (49) Roy, R.; Hill, V. G.; Osborn, E. F. Polymorphism of Ga₂O₃ and the System Ga₂O₃—H₂O. *J. Am. Chem. Soc.* **1952**, *74*, 719–722.
- (50) Lorenz, M. R.; Woods, J. F.; Gambino, R. J. Some Electrical Properties of the Semiconductor B-Ga₂O₃. *J. Phys. Chem. Solids* **1967**, *28*, 403–404.

- (51) Ueda, N.; Hosono, H.; Waseda, R.; Kawazoe, H. Anisotropy of Electrical and Optical Properties in B-Ga₂O₃ Single Crystals. *Appl. Phys. Lett.* **1997**, *71*, 933–935.
- (52) Harwig, T.; Schoonman, J. Electrical Properties of B-Ga₂O₃ Single Crystals. II. *J. Solid State Chem.* **1978**, *23*, 205–211.
- (53) Harwig, T.; Wubs, G. J.; Dirksen, G. J. Electrical Properties of B-Ga₂O₃ Single Crystals. *Solid State Commun.* **1976**, *18*, 1223–1225.
- (54) Fleischer, M.; Meixner, H. Electron Mobility in Single- and Polycrystalline Ga₂O₃. *J. Appl. Phys.* **1993**, *74*, 300–305.
- (55) Shan, F. K.; Liu, G. X.; Lee, W. J.; Lee, G. H.; Kim, I. S.; Shin, B. C. Structural, Electrical, and Optical Properties of Transparent Gallium Oxide Thin Films Grown by Plasma-Enhanced Atomic Layer Deposition. *J. Appl. Phys.* **2005**, *98*, 023504.
- (56) Tippins, H. Optical Absorption and Photoconductivity in the Band Edge of B-Ga₂O₃. *Phys. Rev.* **1965**, *140*, A316–A319.
- (57) Hajnal, Z.; Miró, J.; Kiss, G.; Réti, F.; Deák, P.; Herndon, R. C.; Kuperberg, J. M. Role of Oxygen Vacancy Defect States in the N-Type Conduction of B-Ga₂O₃. *J. Appl. Phys.* **1999**, *86*, 3792–3796.
- (58) Ogita, M.; Higo, K.; Nakanishi, Y.; Hatanaka, Y. Ga₂O₃ Thin Film for Oxygen Sensor at High Temperature. In; Elsevier Science, 2001; pp. 721–725.
- (59) Kohl, D.; Ochs, T.; Geyer, W.; Fleischer, M.; Meixner, H. Adsorption and Decomposition of Methane on Gallium Oxide Films. *Sens. Actuators B Chem.* **1999**, *59*, 140–145.

- (60) Fleischer, M.; Kornely, S.; Weh, T.; Frank, J.; Meixner, H. Selective Gas Detection with High-Temperature Operated Metal Oxides Using Catalytic Filters. *Sens. Actuators B Chem.* **2000**, *69*, 205–210.
- (61) Orita, M.; Ohta, H.; Hirano, M.; Hosono, H. Deep-Ultraviolet Transparent Conductive B-Ga₂O₃ Thin Films. *Appl. Phys. Lett.* **2000**, *77*, 4166–4168.
- (62) Petre, A. L.; Auroux, A.; Gélín, P.; Caldararu, M.; Ionescu, N. I. Acid–base Properties of Supported Gallium Oxide Catalysts. *Thermochim. Acta* **2001**, *379*, 177–185.
- (63) Shimizu, K.; Satsuma, A.; Hattori, T. Selective Catalytic Reduction of NO by Hydrocarbons on Ga₂O₃/Al₂O₃ Catalysts. *Appl. Catal. B Environ.* **1998**, *16*, 319–326.
- (64) Nagarajan, L.; De Souza, R. A.; Samuelis, D.; Valov, I.; Borger, A.; Janek, J.; Becker, K.-D.; Schmidt, P. C.; Martin, M. A Chemically Driven Insulator-Metal Transition in Non-Stoichiometric and Amorphous Gallium Oxide. *Nat. Mater.* **2008**, *7*, 391–398.
- (65) Rebien, M.; Henrion, W.; Hong, M.; Mannaerts, J. P.; Fleischer, M. Optical Properties of Gallium Oxide Thin Films. *Appl. Phys. Lett.* **2002**, *81*, 250–252.
- (66) Sharma, S.; Sunkara, M. K. Direct Synthesis of Gallium Oxide Tubes, Nanowires, and Nanopaintbrushes. *J Am Chem Soc* **2002**, *124*, 12288–12293.
- (67) Chopra, K. L.; Major, S.; Pandya, D. K. Transparent conductors—A Status Review. *Thin Solid Films* **1983**, *102*, 1–46.

- (68) Shi, W. S.; Zheng, Y. F.; Wang, N.; Lee, C.-S.; Lee, S.-T. A General Synthetic Route to III–V Compound Semiconductor Nanowires. *Adv. Mater.* **2001**, *13*, 591–594.
- (69) Dai, Z. R.; Pan, Z. W.; Wang, Z. L. Gallium Oxide Nanoribbons and Nanosheets. *J. Phys. Chem. B* **2002**, *106*, 902–904.
- (70) Zhang, H. Z.; Kong, Y. C.; Wang, Y. Z.; Du, X.; Bai, Z. G.; Wang, J. J.; Yu, D. P.; Ding, Y.; Hang, Q. L.; Feng, S. Q. Ga₂O₃ Nanowires Prepared by Physical Evaporation. *Solid State Commun.* **1999**, *109*, 677–682.
- (71) Regan, M. J.; Pershan, P. S.; Magnussen, O. M.; Ocko, B. M.; Deutsch, M.; Berman, L. E. X-Ray Reflectivity Studies of Liquid Metal and Alloy Surfaces. *Phys. Rev. B* **1997**, *55*, 15874–15884.
- (72) Khan, M. R.; Hayes, G. J.; Zhang, S.; Dickey, M. D.; Lazzi, G. A Pressure Responsive Fluidic Microstrip Open Stub Resonator Using a Liquid Metal Alloy. *IEEE Microw. Wirel. Compon. Lett.* **2012**, *22*, 577–579.
- (73) Larsen, R. J.; Dickey, M. D.; Whitesides, G. M.; Weitz, D. A. Viscoelastic Properties of Oxide-Coated Liquid Metals. *J. Rheol.* **2009**, *53*, 1305–1326.
- (74) Ladd, C.; So, J.-H.; Muth, J.; Dickey, M. D. 3D Printing of Free Standing Liquid Metal Microstructures. *Adv. Mater.* **2013**, *25*, 5081–5085.
- (75) Boley, J. W.; White, E. L.; Chiu, G. T.-C.; Kramer, R. K. Direct Writing of Gallium-Indium Alloy for Stretchable Electronics. *Adv. Funct. Mater.* **2014**, *24*, 3501–3507.
- (76) Zhu, S.; So, J.-H.; Mays, R.; Desai, S.; Barnes, W. R.; Pourdeyhimi, B.; Dickey, M. D. Ultrastretchable Fibers with Metallic Conductivity Using a Liquid Metal Alloy Core. *Adv. Funct. Mater.* **2012**, n/a–n/a.

- (77) Cheng, S.; Wu, Z. Microfluidic Stretchable RF Electronics. *Lab. Chip* **2010**, *10*, 3227–3234.
- (78) Majidi, C.; Kramer, R.; Wood, R. J. A Non-Differential Elastomer Curvature Sensor for Softer-than-Skin Electronics. *Smart Mater. Struct.* **2011**, *20*, 105017.
- (79) Majidi, C.; Wood, R. J. Tunable Elastic Stiffness with Microconfined Magnetorheological Domains at Low Magnetic Field. *Appl. Phys. Lett.* **2010**, *97*, 164104–164104–3.
- (80) Wang, J.; Liu, S.; Vardeny, Z. V.; Nahata, A. Liquid Metal-Based Plasmonics. *Opt. Express* **2012**, *20*, 2346–2353.
- (81) Doudrick, K.; Liu, S.; Mutunga, E. M.; Klein, K. L.; Damle, V.; Varanasi, K. K.; Rykaczewski, K. Different Shades of Oxide: From Nanoscale Wetting Mechanisms to Contact Printing of Gallium-Based Liquid Metals. *Langmuir* **2014**, *30*, 6867–6877.
- (82) Li, G.; Parmar, M.; Kim, D.; Lee, J.-B. (JB); Lee, D.-W. PDMS Based Coplanar Microfluidic Channels for the Surface Reduction of Oxidized Galinstan. *Lab. Chip* **2013**, *14*, 200–209.
- (83) Khan, M.; Trlica, C.; Dickey, M. Recapillarity: Electrochemically Controlled Capillary Withdrawal of a Liquid Metal Alloy From Microchannels. *Adv. Funct. Mater.* *In press*.
- (84) Kim, D.; Lee, D.-W.; Choi, W.; Lee, J.-B. A Super-Lyophobic PDMS Micro-Tunnel as a Novel Microfluidic Platform for Oxidized Galinstan. In *2012 IEEE 25th International Conference on Micro Electro Mechanical Systems (MEMS)*; 2012; pp. 1005–1008.

- (85) Kramer, R. K.; Boley, J. W.; Stone, H. A.; Weaver, J. C.; Wood, R. J. Effect of Microtextured Surface Topography on the Wetting Behavior of Eutectic Gallium-Indium Alloys. *Langmuir* **2013**.
- (86) Zhang, Y.; Zhao, Z.; Fracasso, D.; Chiechi, R. C. Bottom-Up Molecular Tunneling Junctions Formed by Self-Assembly. *Isr. J. Chem.* **2014**, *54*, 513–533.
- (87) Kim, D.; Thissen, P.; Viner, G.; Lee, D.-W.; Choi, W.; Chabal, Y. J.; Lee, J.-B. (J. B. . Recovery of Nonwetting Characteristics by Surface Modification of Gallium-Based Liquid Metal Droplets Using Hydrochloric Acid Vapor. *ACS Appl. Mater. Interfaces* **2013**, *5*, 179–185.
- (88) Dickey, M. D.; Chiechi, R. C.; Larsen, R. J.; Weiss, E. A.; Weitz, D. A.; Whitesides, G. M. Eutectic Gallium-Indium (EGaIn): A Liquid Metal Alloy for the Formation of Stable Structures in Microchannels at Room Temperature. *Adv. Funct. Mater.* **2008**, *18*, 1097–1104.
- (89) Li, G.; Parmar, M.; Kim, D.; Lee, J.-B. (JB); Lee, D.-W. PDMS Based Coplanar Microfluidic Channels for the Surface Reduction of Oxidized Galinstan. *Lab. Chip* **2013**, *14*, 200–209.
- (90) Kim, D.; Lee, D.-W.; Choi, W.; Lee, J.-B. A Super-Lyophobic PDMS Micro-Tunnel as a Novel Microfluidic Platform for Oxidized Galinstan. In *2012 IEEE 25th International Conference on Micro Electro Mechanical Systems (MEMS)*; 2012; pp. 1005–1008.

- (91) Kim, D.; Jung, D.; Yoo, J. H.; Lee, Y.; Choi, W.; Lee, G. S.; Yoo, K.; Lee, J.-B. Stretchable and Bendable Carbon Nanotube on PDMS Super-Lyophobic Sheet for Liquid Metal Manipulation. *J. Micromechanics Microengineering* **2014**, *24*, 055018.
- (92) Jackel, J. L.; Hackwood, S.; Beni, G. Electrowetting Optical Switch. *Appl. Phys. Lett.* **1982**, *40*, 4–5.
- (93) Maltezos, G.; Nortrup, R.; Jeon, S.; Zaumseil, J.; Rogers, J. A. Tunable Organic Transistors That Use Microfluidic Source and Drain Electrodes. *Appl. Phys. Lett.* **2003**, *83*, 2067–2069.
- (94) Rodrigo, D.; Jofre, L.; Cetiner, B. A. Circular Beam-Steering Reconfigurable Antenna With Liquid Metal Parasitics. *IEEE Trans. Antennas Propag.* **2012**, *60*, 1796–1802.
- (95) Khan, M. R.; Eaker, C. B.; Bowden, E. F.; Dickey, M. D. Giant and Switchable Surface Activity of Liquid Metal via Surface Oxidation. *Proc. Natl. Acad. Sci.* **2014**, *111*, 14047–14051.
- (96) Pajkossy, T. Electrochemistry at Fractal Surfaces. *J. Electroanal. Chem. Interfacial Electrochem.* **1991**, *300*, 1–11.
- (97) Pajkossy, T.; Nyikos, L. Diffusion to Fractal surfaces—II. Verification of Theory. *Electrochimica Acta* **1989**, *34*, 171–179.
- (98) Pajkossy, T.; Nyikos, L. Diffusion to Fractal surfaces—III. Linear Sweep and Cyclic Voltammograms. *Electrochimica Acta* **1989**, *34*, 181–186.
- (99) Nyikos, L.; Pajkossy, T. Diffusion to Fractal Surfaces. *Electrochimica Acta* **1986**, *31*, 1347–1350.

- (100) Nyikos, L.; Pajkossy, T.; Borosy, A. P.; Martemyanov, S. A. Diffusion to Fractal surfaces—IV. The Case of the Rotating Disc Electrode of Fractal Surface. *Electrochimica Acta* **1990**, *35*, 1423–1424.
- (101) Imre, A.; Pajkossy, T.; Nyikos, L. Electrochemical Determination of the Fractal Dimension of Fractured Surfaces. *Acta Metall. Mater.* **1992**, *40*, 1819–1826.
- (102) Young, L. *Anodic Oxide Films.*; Academic Press, 1961.
- (103) Ikonopisov, S. Theory of Electrical Breakdown during Formation of Barrier Anodic Films. *Electrochimica Acta* **1977**, *22*, 1077–1082.
- (104) Kiss, L. Modeling the Environment Influence on the Anodic Metal Dissolution. *Russ. J. Electrochem.* **2000**, *36*, 1051–1056.
- (105) Hurlen, T.; Simon, C.; Wilhelmssen, W.; Hornkjøl, S.; Gulbrandsen, E. Model Studies on Passive Metal Electrodes. *Electrochimica Acta* **1989**, *34*, 519–524.
- (106) Hans-Henning Strehblow; Vincent Maurice. Passivity of Metals. In *Corrosion Mechanisms in Theory and Practice, Third Edition*; Corrosion Technology; CRC Press, 2011; pp. 235–326.
- (107) Macdonald, D. D. Passivity—the Key to Our Metals-Based Civilization. *Pure Appl. Chem.* **1999**, *71*.
- (108) Lohrengel, M. M. Thin Anodic Oxide Layers on Aluminium and Other Valve Metals: High Field Regime. *Mater. Sci. Eng. R Rep.* **1993**, *11*, 243–294.
- (109) Alwitt, R. S. The Anodic Oxidation of Aluminum in the Presence of a Hydrated Oxide. *J. Electrochem. Soc.* **1967**, *114*, 843–848.

- (110) Diggle, J. W.; Downie, T. C.; Goulding, C. W. Anodic Oxide Films on Aluminum. *Chem. Rev.* **1969**, *69*, 365–405.
- (111) Lenderink, H. J. W.; Linden, M. V. D.; De Wit, J. H. W. Corrosion of Aluminium in Acidic and Neutral Solutions. *Electrochimica Acta* **1993**, *38*, 1989–1992.
- (112) Kim, J.; Pyun, S. Effects of Electrolyte Composition and Applied Potential on the Repassivation Kinetics of Pure Aluminium. *Electrochimica Acta* **1995**, *40*, 1863–1869.
- (113) Moshier, W. C.; Davis, G. D.; Ahearn, J. S. The Corrosion and Passivity of Aluminum Exposed to Dilute Sodium Sulfate Solutions. *Corros. Sci.* **1987**, *27*, 785–801.
- (114) Hassel, A. W.; Lohrengel, M. M. Initial Stages of Cathodic Breakdown of Thin Anodic Aluminium Oxide Films. *Electrochimica Acta* **1995**, *40*, 433–437.
- (115) Beck, T. R. Electrochemistry of Freshly-Generated Titanium surfaces—I. Scraped-Rotating-Disk Experiments. *Electrochimica Acta* **1973**, *18*, 807–814.
- (116) Beck, T. R. Electrochemistry of Freshly-Generated Titanium surfaces—II. Rapid Fracture Experiments. *Electrochimica Acta* **1973**, *18*, 815–827.
- (117) Gong, D.; Grimes, C. A.; Varghese, O. K.; Hu, W.; Singh, R. S.; Chen, Z.; Dickey, E. C. Titanium Oxide Nanotube Arrays Prepared by Anodic Oxidation. *J. Mater. Res.* **2001**, *16*, 3331–3334.
- (118) Beck, T. R. Stress Corrosion Cracking of Titanium Alloys II . An Electrochemical Mechanism. *J. Electrochem. Soc.* **1968**, *115*, 890–896.

- (119) Hines, J. G. On the Propagation of Stress-Corrosion Cracks in Metals. *Corros. Sci.* **1961**, *1*, 21–48.
- (120) Burstein, G. T.; Marshall, P. I. Growth of Passivating Films on Scratched 304L Stainless Steel in Alkaline Solution. *Corros. Sci.* **1983**, *23*, 125–137.
- (121) Roberge, P. R. *Corrosion Engineering: Principles and Practice*; McGraw-Hill, 2008.
- (122) Hoar, T. P.; Scully, J. C. Mechanochemical Anodic Dissolution of Austenitic Stainless Steel in Hot Chloride Solution at Controlled Electrode Potential. *J. Electrochem. Soc.* **1964**, *111*, 348–352.
- (123) Hagyard, T.; Williams, J. R. Potential of Aluminium in Aqueous Chloride Solutions. Part 1. *Trans. Faraday Soc.* **1961**, *57*, 2288–2294.
- (124) Burstein, G. T.; Newman, R. C. Anodic Behaviour of Scratched Silver Electrodes in Alkaline Solution. *Electrochimica Acta* **1980**, *25*, 1009–1013.
- (125) Podesta, J. J.; Rothwell, G. P.; Hoar, T. P. Yield-Assisted Anodic Dissolution of Brasses in Ammoniacal Solutions. *Corros. Sci.* **1971**, *11*, 241–248.
- (126) Tomashov, N. D.; Verzhinina, L. P. Kinetics of Some Electrode Processes on a Continuously Renewed Surface of Solid Metal. *Electrochimica Acta* **1970**, *15*, 501–517.
- (127) Anderson, T. N.; Anderson, J. L.; Eyring, H. Nature of Fresh Metal Surfaces in Aqueous Solutions. *J. Phys. Chem.* **1969**, *73*, 3562–3570.
- (128) Hagyard, T.; Earl, W. B. Potential of Aluminum in Aqueous Chloride Solutions. *J. Electrochem. Soc.* **1967**, *114*, 694–698.

- (129) Hurlen, T. Anodic Dissolution of Liquid Gallium in Alkaline Solutions. *Electrochimica Acta* **1964**, *9*, 1449–1452.
- (130) Armstrong, R. D.; Race, W. P.; Thirsk, H. R. The Anodic Behaviour of Gallium in Alkaline Solution. *J. Electroanal. Chem.* **1971**, *31*, 405–411.
- (131) Horasawa, N.; Takahashi, S.; Marek, M. Electrochemical Behavior of Amalgams and a Gallium Alloy in Two Electrolytes. *J Dent Res* **1997**, *76*, 1481–1481.
- (132) Bagotska, I.; Morozov, A. M.; Grigoryev, N. On Zero-Charge Potential of Gallium in Aqueous Solutions and Origin of High Capacitance at Gallium/solution Interface. *Electrochim Acta* **1968**, *13*, 873–876.
- (133) Frumkin, A.; Polianovskaya, N.; Grigoryev, N.; Bagotskaya, I. Electrocapillary Phenomena on Gallium. *Electrochimica Acta* **1965**, *10*, 793–802.
- (134) Perkins, R. S. Gallium Oxidation in Alkaline Solution. *J. Electrochem. Soc.* **1972**, *119*, 713–715.
- (135) Perkins, R. Anodic-Oxidation of Gallium in Alkaline-Solution. *J. Electroanal. Chem.* **1979**, *101*, 47–57.
- (136) Varadharaj, A.; Rao, G. Cyclic Voltammetric Studies on Gallium Film Electrodes in Alkaline Media. *J. Chem. Sci.* **1990**, *102*, 177–187.
- (137) Hurlen, T. Anodic Dissolution of Liquid Gallium in Alkaline Solutions. *Electrochimica Acta* **1964**, *9*, 1449–1452.
- (138) Duncan, S. J.; Burstein, G. T. Kinetics of Anodic Oxide Film Growth on Indium in Alkaline Solution. *J. Appl. Electrochem.* **1987**, *17*, 196–204.

- (139) Saidman, S. B.; Bessone, J. B. Anodic Behaviour of Indium in Sodium Chloride Solutions. *Electrochimica Acta* **1991**, *36*, 2063–2067.
- (140) Zhou, H.; Xu, M.; Huang, Q.; Cai, Z.; Li, W. Anodic Behavior of Indium in KOH Solution. *J. Appl. Electrochem.* **2009**, *39*, 1739–1744.
- (141) Miller, B.; Visco, R. E. Ring-Disk Amperometry: A Study of Indium Dissolution. *J. Electrochem. Soc.* **1968**, *115*, 251–258.
- (142) Piercy, R.; Hampson, N. A. The Electrochemistry of Indium. *J. Appl. Electrochem.* **1975**, *5*, 1–15.
- (143) Metikoš-Huković, M.; Omanović, S. Thin Indium Oxide Film Formation and Growth: Impedance Spectroscopy and Cyclic Voltammetry Investigations. *J. Electroanal. Chem.* **1998**, *455*, 181–189.
- (144) Omanović, S.; Metikoš-Huković, M. Thin Oxide Films on Indium: Impedance Spectroscopy Investigation of Reductive Decomposition. *Thin Solid Films* **1995**, *266*, 31–37.
- (145) Omanović, S.; Metikoš-Huković, M. The Ionic Conductance of Barrier Anodic Oxide Films on Indium. *Solid State Ion.* **1995**, *78*, 69–78.
- (146) Omanović, S.; Metikoš-Huković, M. Indium as a Cathodic Material: Catalytic Reduction of Formaldehyde. *J. Appl. Electrochem.* **1997**, *27*, 35–41.
- (147) Pourbaix. *Atlas of Electrochemical Equilibria in Aqueous Solutions*; Second English Edition.; Natl Assn of Corrosion, 1974.
- (148) So, J.; Koo, H.; Dickey, M. D.; Velev, O. D. Ionic Current Rectification in Soft-Matter Diodes with Liquid-Metal Electrodes. *Adv. Funct. Mater.* **2012**, *22*, 625–631.

- (149) Koo, H.; So, J.; Dickey, M. D.; Velev, O. D. Towards All-Soft Matter Circuits: Prototypes of Quasi-Liquid Devices with Memristor Characteristics. *Adv. Mater.* **2011**, *23*, 3559–3564.
- (150) Hayes, G. J.; So, J.-H.; Qusba, A.; Dickey, M. D.; Lazzi, G. Flexible Liquid Metal Alloy (EGaIn) Microstrip Patch Antenna. *IEEE Trans. Antennas Propag.* **2012**, *60*, 2151–2156.
- (151) Zhang, B.; Dong, Q.; Korman, C. E.; Li, Z.; Zaghoul, M. E. Flexible Packaging of Solid-State Integrated Circuit Chips with Elastomeric Microfluidics. *Sci. Rep.* **2013**, *3*.
- (152) Tabatabai, A.; Fassler, A.; Usiak, C.; Majidi, C. Liquid-Phase Gallium–Indium Alloy Electronics with Microcontact Printing. *Langmuir* **2013**, *29*, 6194–6200.
- (153) Wissman, J.; Lu, T.; Majidi, C. Soft-Matter Electronics with Stencil Lithography. In *2013 IEEE Sensors*; 2013; pp. 1–4.
- (154) Jeong, S. H.; Hjort, K.; Wu, Z. Tape Transfer Printing of a Liquid Metal Alloy for Stretchable RF Electronics. *Sensors* **2014**, *14*, 16311–16321.
- (155) Gozen, B. A.; Tabatabai, A.; Ozdoganlar, O. B.; Majidi, C. High-Density Soft-Matter Electronics with Micron-Scale Line Width. *Adv. Mater.* **2014**, *26*, 5211–5216.
- (156) Hon, K. K. B.; Li, L.; Hutchings, I. M. Direct Writing technology—Advances and Developments. *CIRP Ann. - Manuf. Technol.* **2008**, *57*, 601–620.
- (157) Lu, T.; Finkenauer, L.; Wissman, J.; Majidi, C. Rapid Prototyping for Soft-Matter Electronics. *Adv. Funct. Mater.* **2014**, n/a–n/a.

- (158) Kramer, R. K.; Majidi, C.; Wood, R. J. Masked Deposition of Gallium-Indium Alloys for Liquid-Embedded Elastomer Conductors. *Adv. Funct. Mater.* **2013**, n/a–n/a.
- (159) Chang, K. *Encyclopedia of RF and Microwave Engineering*; John Wiley,: Hoboken, N.J., 2005.
- (160) Lipomi, D. J.; Vosgueritchian, M.; Tee, B. C.-K.; Hellstrom, S. L.; Lee, J. A.; Fox, C. H.; Bao, Z. Skin-like Pressure and Strain Sensors Based on Transparent Elastic Films of Carbon Nanotubes. *Nat. Nanotechnol.* **2011**, *6*, 788–792.
- (161) Cheng, S.; Wu, Z. A Microfluidic, Reversibly Stretchable, Large-Area Wireless Strain Sensor. *Adv. Funct. Mater.* **2011**, *21*, 2282–2290.
- (162) Nawaz, A. A.; Mao, X.; Stratton, Z. S.; Huang, T. J. Unconventional Microfluidics: Expanding the Discipline. *Lab. Chip* **2013**, *13*, 1457–1463.
- (163) Cheng, S.; Wu, Z. Microfluidic Electronics. *Lab. Chip* **2012**, *12*, 2782.
- (164) Nijhuis, C. A.; Reus, W. F.; Whitesides, G. M. Molecular Rectification in Metal–SAM–Metal Oxide–Metal Junctions. *J. Am. Chem. Soc.* **2009**, *131*, 17814–17827.
- (165) Palleau, E.; Reece, S.; Desai, S. C.; Smith, M. E.; Dickey, M. D. Self-Healing Stretchable Wires for Reconfigurable Circuit Wiring and 3D Microfluidics. *Adv. Mater.* **2013**, *25*, 1589–1592.
- (166) Giguere, P. A.; Lamontagne, D. Polarography with a Dropping Gallium Electrode. *Science* **1954**, *120*, 390–391.
- (167) Kim, D.; Thissen, P.; Viner, G.; Lee, D.-W.; Choi, W.; Chabal, Y. J.; Lee, J.-B. (J. B. . Recovery of Nonwetting Characteristics by Surface Modification of Gallium-

Based Liquid Metal Droplets Using Hydrochloric Acid Vapor. *ACS Appl. Mater. Interfaces* **2013**, *5*, 179–185.

- (168) Kim, D.; Lee, Y.; Lee, D.; Choi, W.; Lee, J.-B. J. B. Hydrochloric Acid-Impregnated Paper for Liquid Metal Microfluidics. In *2013 Transducers Eurosensors XXVII: The 17th International Conference on Solid-State Sensors, Actuators and Microsystems (TRANSDUCERS EUROSENSORS XXVII)*; 2013; pp. 2620–2623.

CHAPTER 2

A FREQUENCY SHIFTING LIQUID METAL

ANTENNA WITH PRESSURE RESPONSIVENESS*

**This work has been published in Applied Physics Letters. Contributors to this work: G. Hayes, Ju-Hee So, G. Lazzi.*

2.1 INTRODUCTION

This chapter describes antennas fabricated from a liquid metal alloy that can change their electrical length and thus, frequency in response to pressure. Most antennas have a singular, static shape that defines their performance. Reconfigurable antennas, in contrast, can alter their functional behavior (e.g., frequency, bandwidth, or polarization)^{1,2} by changing the shape of conductive elements of the antenna³. This approach typically involves mechanical or electrical switches (e.g., MEMS, diodes, RF MEMS capacitors)³⁻¹⁴ that selectively connect and disconnect conductive segments to the antenna. Stretchable antennas composed of liquid metal encased in elastomer can change their physical shape, and therefore resonant frequency, in response to strain¹⁵⁻¹⁷. Here, we present an antenna architecture that can change its shape in a simple manner by inducing the conductive antenna elements to flow (and merge) in response to external stimuli without using any external switches. The challenge with this approach is to control the way the liquid metal changes its shape so that the response is predictable and rapid. We address this challenge by harnessing the rheological properties of a low viscosity¹⁸, conductive¹⁹ liquid metal alloy (eutectic gallium indium²⁰, EGaIn, 75% gallium and 25% indium) that is stabilized mechanically within microchannels despite its large surface tension due to the presence of a solid oxide skin¹⁸ that forms spontaneously on its surface and does not grow thicker with time (i.e., it is passivating²¹). Previous rheological measurements confirm the elastic nature of the skin and establish that it yields beyond a critical stress²². We designed a microfluidic channel in such a way that an initially short dipole antenna (~25 mm long) would merge with adjacent segments of metal to create an elongated dipole (~51 mm long) when exposed to a pressure above the critical

value required to yield the skin. The merging process changes the shape, and therefore resonant frequency (in three distinct states), in a predictable manner. Because the process of merging is irreversible in its current form, the resonant frequency of the antenna represents a spectral memory state that records the pressure to which it is exposed and offers a simple approach for sensing and recording stimuli (e.g., pressure) wirelessly. This chapter demonstrates and models this frequency-shifting fluidic antenna and elucidates the mechanism by which it changes its shape.

2.2 RESULTS

Figure 1 describes the concept of frequency shifting antennas formed by injecting liquid metal into microfluidic channels composed of polydimethylsiloxane (PDMS)^{23–25}. The antenna geometry consists of a single row of four collinear segments (each 1 mm wide, 12.6 mm long, 50 μm thick) placed end-to-end. Initially, the two innermost segments comprise the dipole. Two rows of posts (each row consists of 50 μm diameter posts with a 100 μm center-to-center spacing) separate the two innermost segments from the two outermost segments [Figure 1(b)]. During the fabrication process²⁶, the metal is injected by hand through the inlet holes (an outlet vent allows air to escape the channel during filling), fills the channels readily, and is stabilized mechanically at the posts by a thin oxide skin [Figure 1(c)]. It does not flow between the posts (the posts acts as Laplace barriers²⁷) as long as the critical pressure is not exceeded (the critical pressure depends on the geometry of the posts and is approximately 7 psi for the present geometry)¹⁸.

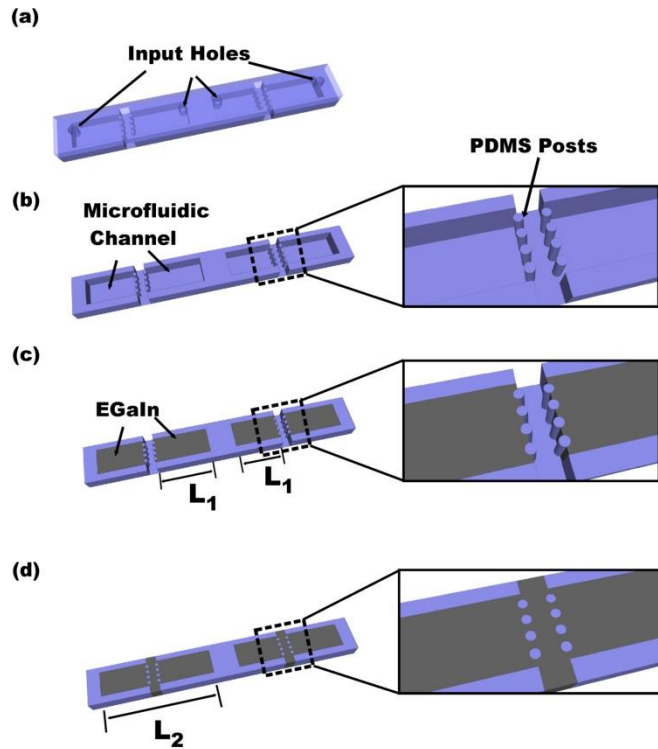


Figure 1. A depiction of an antenna that reconfigures its shape in response to pressure (not to scale). a) Empty microchannels with inlet holes (not shown in remaining depictions) b) Rows of posts separate the two outermost segments of the antenna from the two innermost segments. c) Injecting liquid metal into the microfluidic channels produces four antenna segments. Initially, the two innermost liquid segments of length L_1 define the dipole antenna. The metal will not flow through the posts until the applied pressure exceeds the critical pressure required to yield the skin that mechanically stabilizes the liquid. d) The four sections of metal merge into two longer sections (each of length, L_2), which lowers the resonant frequency.

Pressures that exceed the critical pressure force the metal to flow between the posts and thereby merge the outermost segments with the inner segments [Figure 1(d)] to increase the physical and electrical length of the dipole.

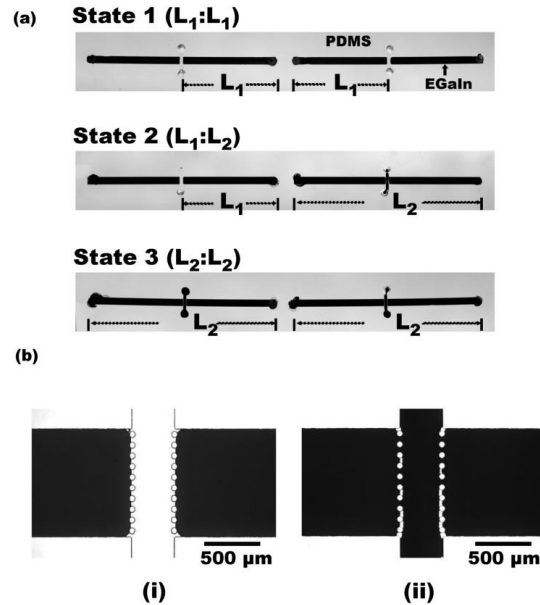


Figure 2: Photographs of a shape reconfigurable antenna in three different states. Length L_1 is 12.6 mm. a) State 1 consists of four isolated segments of liquid metal embedded in elastomer. The two innermost segments, $L_1:L_1$, define the antenna. Applying pressure to the right side of the antenna causes two of the sections to merge such that the dipole assumes a different geometry, State 2 ($L_1:L_2$). Merging both outermost segments with the innermost segments forms State 3 ($L_2:L_2$). b) Micrographs of the region between the segments of metal. i) A narrow gap defined by two rows of posts initially separates the segments. ii) By applying sufficient pressure at the inlet, the metal flows through the posts and merges into an electrically continuous segment.

Figure 2 shows photographs of the antennas in three different states. The two innermost segments comprise the initial dipole antenna with lengths L_1 (“state 1”). Pressure applied to one input hole ruptures the oxide skin to produce “state 2” by increasing the length of one arm of the dipole ($L_2 > L_1$). Pressure applied to the other input hole produces “state 3” in which the dipole consists of two arms, each of length L_2 . Figure 2(b) shows micrographs of the gap between the PDMS posts before and after merging the metal.

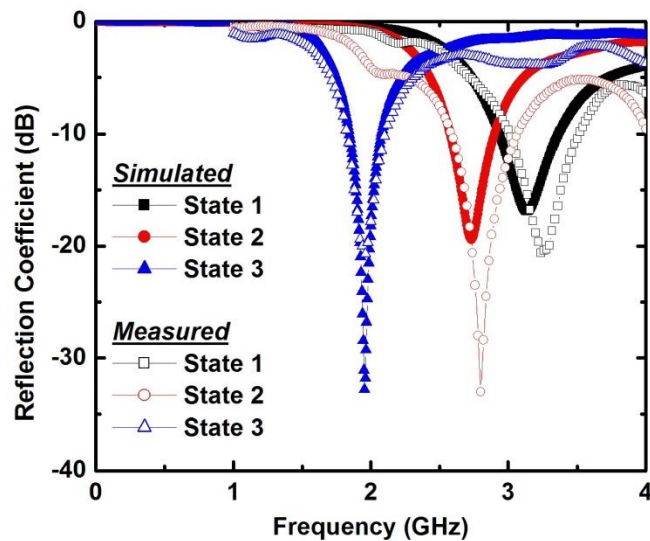


Figure 3. Three distinct frequency responses illustrating the frequency shifting nature of the antenna. Measured spectra (open symbols) match well with the simulated spectra (filled symbols). As the arms of the antenna get longer (going from State 1 to 2 to 3), the spectral response of the antenna shifts to a lower resonant frequency.

A coaxial balun featuring two electrical leads connected to the two central arms of the dipole excited the antennas¹⁵. A network analyzer measured the spectral responses (reflection

coefficients) of the antennas and CST-MWS²⁸ software simulated the spectral response of the antennas. The simulated models of the different lengths of dipoles included the physical and electrical properties of the PDMS substrate ($\epsilon_r=2.7$ and $\tan\delta = 0.04$) and the liquid metal components¹⁸ ($\sigma = 3.4\times 10^4 \text{ Scm}^{-1}$); Figure 3 shows that the simulation results and measurements are in good agreement. As the length of the dipole increases via merging of the segments (from states 1 to 2 to 3), the resonant frequency shifts to a lower value (from 3.6 to 2.6 to 1.9 GHz, respectively, based on the best impedance match), which is consistent with the simulated spectra. The electrically isolated outermost segments in state 1 exhibited minimum electrical coupling to the innermost segments as confirmed by simulation. During the merging process, the metal would often leave small air gaps between some of the posts [e.g., Figure 2(b)]. Based on the model, the trapped air has a negligible effect on the antenna response due to the sufficient electrical connection of the metal between the other posts.

The merging process occurs extremely fast (within a few milliseconds) due to the low viscosity of the liquid metal and the short distance it has to travel. To elucidate the merging process, a video camera with a fast capture rate (5,000 fps) recorded the liquid metal as it ruptures between the posts due to applied pressure. Figure 4 shows 12 chronological frames that capture the merging process over a window of time spanning 3.6 ms. Rupturing occurred at ~8 psi of applied pressure, which is in sufficient agreement with the predicted yield stress (~7 psi) behavior of the skin of the metal for the given geometry¹⁸.

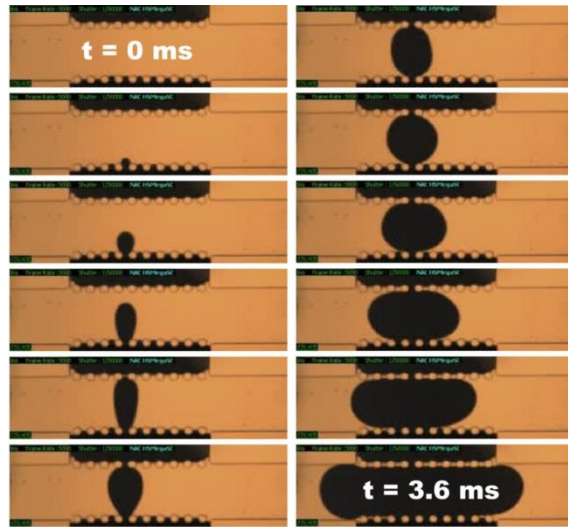


Figure 4. Sequential micrographs of the process of merging liquid metal segments. Images are taken from a high speed video camera and each frame represents about 0.3 milliseconds. Pressure applied to the lower segment causes the liquid metal to rupture through two posts and merge with the adjacent metal to form an electrically continuous wire segment and thereby elongate the antenna.

Typically, the liquid metal only ruptures between one set of posts (c.f., Figure 4). This result is consistent with the critical yield stress property of the metal; once the metal ruptures between two posts, the pressure drop at the other metal / air interfaces is no longer sufficient to rupture the skin. The liquid metal merges with the adjacent segment of metal to form an electrically continuous wire before flowing toward the vent holes. Without optimization (and using only our hands to control the pressure applied to the syringe during the initial filling), the segments merged ~75% of the time. In the failures, the wires did not merge due to small air gaps between the two metal interfaces spanning neighboring posts. The yield increased to

100% by either (1) pushing the metal as far as possible through both rows of posts prior to rupturing to increase the chances of merging, or (2) applying pressure to the inlets of both adjacent segments of the metal and thereby forcing the metal to merge.

2.3 CONCLUSION

This chapter demonstrates antennas that change their shape, and therefore frequency, in response to external stimuli (pressure) without utilizing any external switches or electrical connections by inducing a liquid metal to flow and merge into elongated geometries in a predictable manner. This simple approach controls the shape of the active elements of the antenna by exploiting the rheological behavior of the liquid metal that originates from its oxide skin. Modeling of the different states agreed with the experimental results that show shifts of the reflection coefficient response to lower frequencies as the antenna is elongated. Images from a high speed video helped elucidate the mechanism of merging in which metal ruptures between posts when the applied pressure exceeds a critical value.

The ability of the antenna to change its shape, and therefore function, in response to external stimuli is useful for wireless sensing in which the antenna itself is a sensor. In its current form, the merging process is irreversible and therefore serves as a passive memory element in which hysteretic information is stored in the spectral signature of the antenna. This chapter demonstrates the ability to merge four sections of wires to create three distinct antenna states, but in principle, many different states and geometries are possible. The pressure required to merge the segments could also be tuned by changing the geometry of the

posts. In addition to changing the operational frequency (reflection coefficient), the approach could also be used to tune other antenna parameters, such as radiation pattern and polarization. These antennas could be used in wireless sensing or monitoring radio systems, switches, RFID tags, conformal circuits for health monitoring, or in military applications. An additional advantage of liquid metal antennas is that they adopt the mechanical properties of the encasing material. Antennas encased by elastomer can therefore be bent, twisted and stretched. Here, external pressure altered the shape of the antenna, but it may be possible to use other stimuli (e.g., flexing the antenna) to induce segments of the antenna to merge.

2.4 REFERENCES

- (1) Balanis, C. A. *Modern Antenna Handbook*; Wiley,; Hoboken, NJ, c2008.
- (2) Chang, K. *Encyclopedia of RF and Microwave Engineering*; John Wiley,; Hoboken, N.J., 2005.
- (3) Cetiner, B. A.; Biyikli, N.; Yildirim, B. S.; Damgaci, Y. Nanoelectromechanical Switches for Reconfigurable Antennas. *Microw. Opt. Technol. Lett.* **2010**, *52*, 64–69.
- (4) Ali, M.; Sayem, A. T. M.; Kunda, V. K. A Reconfigurable Stacked Microstrip Patch Antenna for Satellite and Terrestrial Links. *IEEE Trans. Veh. Technol.* **2007**, *56*, 426–435.
- (5) Mirkamali, A.; Hall, P. S. Wideband Frequency Reconfiguration of a Printed Log Periodic Dipole Array. *Microw. Opt. Technol. Lett.* **2010**, *52*, 861–864.
- (6) Huff, G. H.; Bernhard, J. T. Integration of Packaged RF MEMS Switches with Radiation Pattern Reconfigurable Square Spiral Microstrip Antennas. *IEEE Trans. Antennas Propag.* **2006**, *54*, 464–469.
- (7) Cetiner, B. A.; Jafarkhani, H.; Qian, J.-Y.; Yoo, H. J.; Grau, A.; De Flaviis, F. Multifunctional Reconfigurable MEMS Integrated Antennas for Adaptive MIMO Systems. *IEEE Commun. Mag.* **2004**, *42*, 62–70.
- (8) Brown, E. R. On the Gain of a Reconfigurable-Aperture Antenna. *IEEE Trans. Antennas Propag.* **2001**, *49*, 1357–1362.
- (9) Freeman, J. L.; Lamberty, B. J.; Andrews, G. S. Optoelectronically Reconfigurable Monopole Antenna. *Electron. Lett.* **1992**, *28*, 1502.

- (10) Panagamuwa, C. J.; Chauraya, A.; Vardaxoglou, J. C. Frequency and Beam Reconfigurable Antenna Using Photoconducting Switches. *IEEE Trans. Antennas Propag.* **2006**, *54*, 449–454.
- (11) Peroulis, D.; Sarabandi, K.; Katehi, L. P. B. Design of Reconfigurable Slot Antennas. *IEEE Trans. Antennas Propag.* **2005**, *53*, 645–654.
- (12) Piazza, D.; Dandekar, K. R. Reconfigurable Antenna Solution for MIMO-OFDM Systems. *Electron. Lett.* **2006**, *42*, 446.
- (13) Sung, Y. J.; Jang, T. U.; Kim, Y.-S. A Reconfigurable Microstrip Antenna for Switchable Polarization. *IEEE Microw. Wirel. Compon. Lett.* **2004**, *14*, 534–536.
- (14) Kingsley, N.; Anagnostou, D. E.; Tentzeris, M.; Papapolymerou, J. RF MEMS Sequentially Reconfigurable Sierpinski Antenna on a Flexible Organic Substrate With Novel DC-Biasing Technique. *J. Microelectromechanical Syst.* **2007**, *16*, 1185–1192.
- (15) So, J. H.; Thelen, J.; Qusba, A.; Hayes, G. J.; Lazzi, G.; Dickey, M. D. Reversibly Deformable and Mechanically Tunable Fluidic Antennas. *Adv. Funct. Mater.* **2009**, *19*, 3632–3637.
- (16) Cheng, S.; Rydberg, A.; Hjort, K.; Wu, Z. Liquid Metal Stretchable Unbalanced Loop Antenna. *Appl. Phys. Lett.* **2009**, *94*, 144103.
- (17) Kubo, M.; Li, X.; Kim, C.; Hashimoto, M.; Wiley, B. J.; Ham, D.; Whitesides, G. M. Stretchable Microfluidic Radiofrequency Antennas. *Adv. Mater.* **2010**, *22*, 2749–2752.
- (18) Dickey, M. D.; Chiechi, R. C.; Larsen, R. J.; Weiss, E. A.; Weitz, D. A.; Whitesides, G. M. Eutectic Gallium-Indium (EGaIn): A Liquid Metal Alloy for the Formation of Stable Structures in Microchannels at Room Temperature. *Adv. Funct. Mater.* **2008**, *18*, 1097–1104.

- (19) Zrnic, D.; Swatik, D. S. On the Resistivity and Surface Tension of the Eutectic Alloy of Gallium and Indium. *J. Common Met.* **1969**, *18*, 67–68.
- (20) FRENCH, S. J.; SAUNDERS, D. J.; INGLE, G. W. THE SYSTEM GALLIUM-INDIUM. *J. Phys. Chem.* **1937**, *42*, 265–274.
- (21) Regan, M. J.; Tostmann, H.; Pershan, P. S.; Magnussen, O. M.; DiMasi, E.; Ocko, B. M.; Deutsch, M. X-Ray Study of the Oxidation of Liquid-Gallium Surfaces. *Phys. Rev. B Condens. Matter* **1997**, *55*, 10786–10790.
- (22) Larsen, R. J.; Dickey, M. D.; Whitesides, G. M.; Weitz, D. A. Viscoelastic Properties of Oxide-Coated Liquid Metals. *J. Rheol.* **2009**, *53*, 1305–1326.
- (23) McDonald, J. C.; Whitesides, G. M. Poly(dimethylsiloxane) as a Material for Fabricating Microfluidic Devices. *Acc. Chem. Res.* **2002**, *35*, 491–499.
- (24) Jo, B.-H.; Van Lerberghe, L. M.; Motsegood, K. M.; Beebe, D. J. Three-Dimensional Micro-Channel Fabrication in Polydimethylsiloxane (PDMS) Elastomer. *J. Microelectromechanical Syst.* **2000**, *9*, 76–81.
- (25) Duffy, D. C.; McDonald, J. C.; Schueller, O. J. A.; Whitesides, G. M. Rapid Prototyping of Microfluidic Systems in Poly(dimethylsiloxane). *Anal. Chem.* **1998**, *70*, 4974–4984.
- (26) Xia, Y.; Whitesides, G. M. Soft Lithography. *Annu. Rev. Mater. Sci.* **1998**, *28*, 153–184.
- (27) Kreit, E.; Dhindsa, M.; Yang, S.; Hagedon, M.; Zhou, K.; Papautsky, I.; Heikenfeld, J. Laplace Barriers for Electrowetting Thresholding and Virtual Fluid Confinement. *Langmuir* **2010**, *26*, 18550–18556.

(28) CST Computer Simulation Technology Microwave Studio in [Http://www.cst.com](http://www.cst.com).

CHAPTER 3

A PRESSURE RESPONSIVE FLUIDIC MICROSTRIP OPEN STUB RESONATOR USING A LIQUID METAL ALLOY*

**This work has been published in IEEE Microwave component letter. Contributors of this work: Silu Zhang, G. Hayes, G. Lazzi.*

3.1 ABSTRACT

This chapter describes a fluidic microstrip bandstop filter with transmission properties that change in discrete states. The filter consists of a liquid metal alloy - eutectic gallium indium (EGaIn) - as the conductive component in microfluidic channels. The fluidity of EGaIn allows the open stub resonator of the filter to change its length by flowing in response to an applied pressure. A series of posts in the channel defines the length of the stub filled by the metal and dictates the pressure needed for the liquid metal to flow and thereby extend the stub length. The frequency response of the filter changes in response to the changes in the length of the resonator stub. This approach is a simple method for creating tunable filters and impedance matching sections using soft materials that change dimensions in response to pressure.

3.2 INTRODUCTION

This chapter presents a unique fluidic microstrip bandstop filter with a pressure sensitive frequency response. Changing the length of liquid metal in an open stub microfluidic channel alters the frequency response of the filter. Conventional tunable microstrip filters with open stub resonator sections are fabricated from printed circuit board (PCB) technology^{1,2}, using a method of etching patterns on stacked sheets of copper and dielectric. The electrical length of the stub and, therefore, response of the filter may be altered using a number of methods including the incorporation of varactors³, MEMS⁴, or PIN diodes that bridge disconnected segments of the stub⁵ or alter the impedance of the stub. In all of these applications, the

physical geometry remains fixed after assembly. In contrast, our approach allows the stub length to be tuned post-assembly in a simple manner using pressure applied by fingertips. In addition, our approach uses simple and common fabrication techniques (soft lithography), which is useful for rapid prototyping. Also, the soft materials that comprise the filter may be useful for conformal or flexible electronics. By incorporating the liquid metal to form both the transmission line and the resonating element, this approach expands upon reconfigurable components that use liquid metals to alter the resonant performance of coupled structures such as defected ground structures⁶, frequency-selective surfaces⁷, and antennas⁸⁻¹⁰.

Figure 1 and 2 illustrates the geometry of the microstrip filter. Liquid metal - eutectic gallium indium, EGaln (75% Ga and 25% In) - forms the conductive 50 Ω transmission line in a polydimethylsiloxane (PDMS) substrate. The liquid flows into the open stub in response to external pressure and the length of the stub changes in a predictable manner due to several rows of posts that define discrete stub lengths. This approach takes advantage of the fact that EGaln only flows when the applied pressure exceeds a critical value¹¹.

3.3 DESIGN

We designed microchannels with three discrete stub states that correspond to three discrete pressures. Figure 3 illustrates the geometries of each state. Injecting the liquid metal through inlet hole (Port 1) into the transmission line by a syringe forms the initial, transmission line (State 1) of the prototype. The oxide skin on the metal stabilizes it within the transmission line so that it does not withdraw from the channel. A row of posts prevents the metal from

entering the open stub (Figure 4a). These rows of posts act as Laplace barriers¹². A Laplace barrier is a geometric constriction through which a fluid cannot pass unless a critical pressure is exceeded (this pressure depends inversely on the size of the constriction).

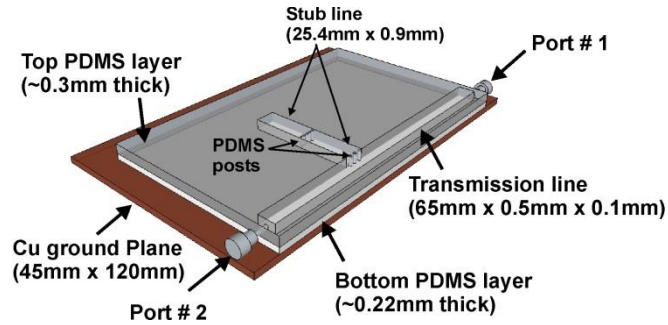


Figure 1. Geometry of bandstop filter with a 50Ω microstrip transmission line from Port 1 to Port 2 and open stub section.

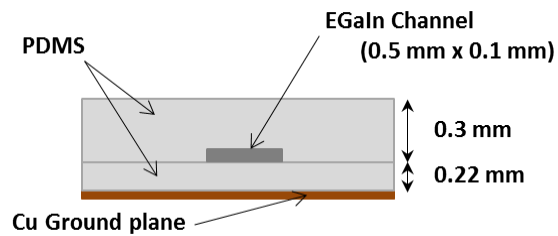


Figure 2. Cross section of a 50Ω microstrip transmission line.

Applying a higher pressure at the inlet (8 psi) achieves State 2. The higher pressure ruptures the oxide skin that spans the first row of posts and induces the liquid metal to flow between the posts up to the second row of posts (i.e., half of the stub line). Since the second row of posts are spaced closer together than the first row of posts, the liquid metal ceases to flow (Figure 4b). Increasing the pressure further (15 psi) causes the metal to flow through the second set of posts and fill the stub completely with liquid metal (Figure 4c) to produce State 3 of the filter. In general, larger applied pressures correspond to longer stub lengths and the transition between states is on the order of milliseconds.

3.4. MEASUREMENT AND SIMULATION

We measured the frequency response of the system in all three states using a network analyzer and simulated the spectral response of the filter using CST Microwave Studio. The simulated models of the different states of the filter include the physical and electrical properties of the PDMS substrate ($\epsilon_r = 2.68$, $\tan\delta = 0.04$) and the EGaIn conductors ($\sigma = 3.4 \times 10^4 \text{ Scm}^{-1}$). The measured reflection coefficient responses (Figure 5) are below -10 dB up to 4.5 GHz in the State 1 with a higher reflection at the various band stop regions corresponding to State 2 and State 3.

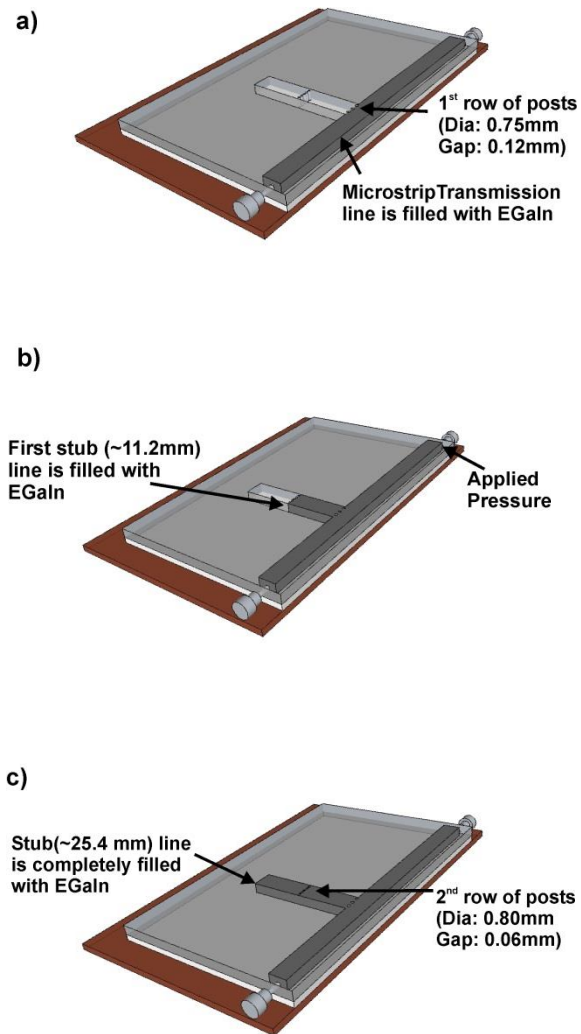


Figure 3. Geometry of bandstop filter: (a) State 1, (b) State 2, and (c) State 3.

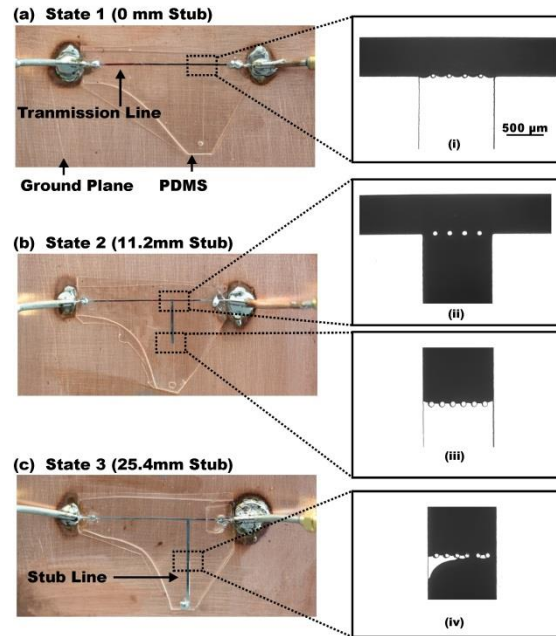


Figure. 4. Photographs (left) and micrographs (right) of the microstrip filter in three different states: (a) State 1 consists of a 50Ω transmission line filled with EGaIn and an empty stub line, (b) State 2 with a partially filled open stub, and (c) State 3 with a fully filled open stub.

Figure 6 indicates that the simulations and measurements have the same resonant frequency. In State 1 the filter behaves like a 50Ω transmission line with low transmission loss (below 1.5 dB up to 4.5 GHz). As the length of the stub increases (from State 1 to 2 to 3), the filtered frequency shifts to lower frequencies. Although the measured resonant frequencies agree with the simulation, the simulated values indicate a higher Q factor than the measured results. This difference may be partially attributed to the measured response including losses due to the microstrip-to-coax transitions at both ends of the assembly.

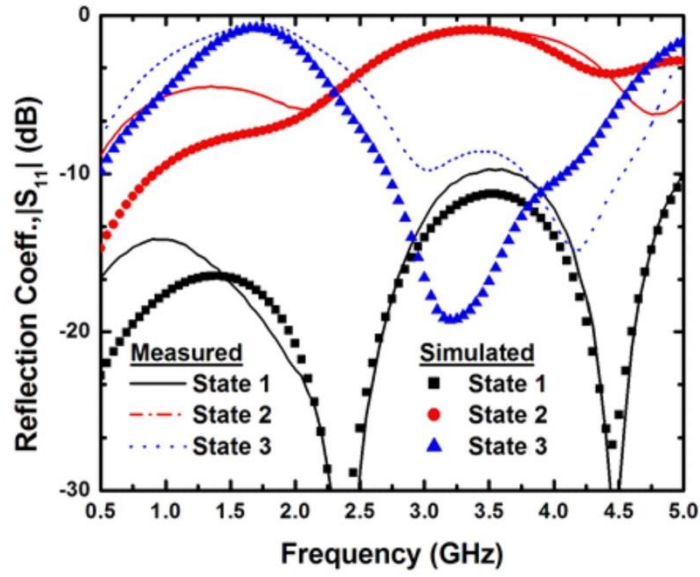


Figure 5. Measured reflection coefficient for each state of the filter.

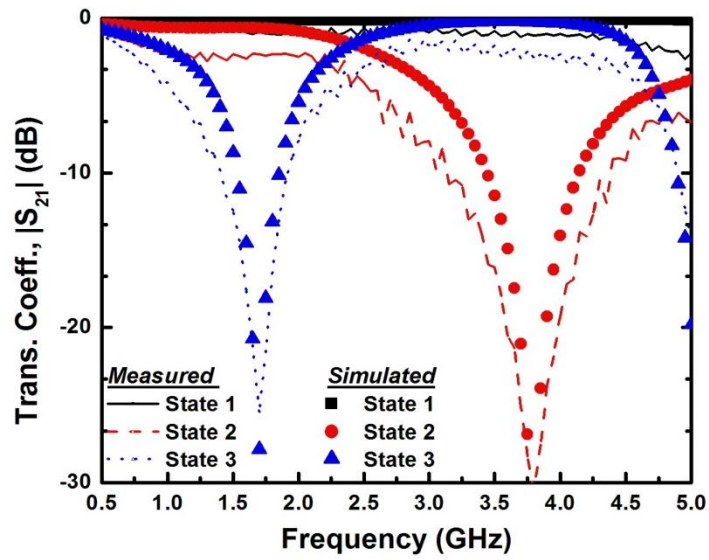


Figure 6. Measured and simulated transmission coefficient response for each state of the microstrip filter.

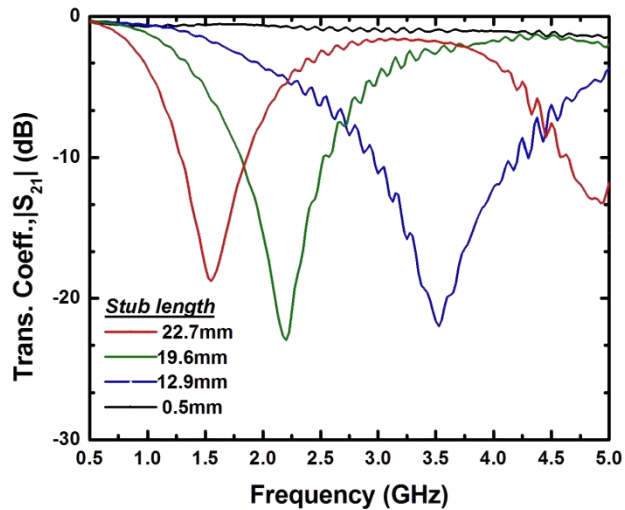


Figure 7. Measured transmission coefficient of a prototype with an open stub shortened from 22.7 mm to 0.5 mm.

Also, the actual losses of the PDMS may be larger than the simulated model and the thickness of the PDMS top layer may be thicker than the model. Regardless, the measurements show that the transmission properties may be switched dramatically using pressures that can be generated by fingertips.

The change in stub length is not inherently reversible due to the stability of the oxide skin. We investigated the reversibility of the bandstop filter response by destabilizing the oxide skin¹³ to reverse an open stub from 22.7 mm down to 0.5 mm. Figure 7 shows the shift in transmission coefficient from 1.5 GHz at 22.7 mm to 0.5 mm with a response similar to a transmission line.

3.5 CONCLUSION

We fabricated and characterized a tunable microstrip bandstop filter incorporating a novel fluidic transmission line and open stub resonator section. The electrical length of the resonator increases in discrete steps with increasing pressure that allows the assembly to transition from transmission line to a tunable bandstop filter. The end user can manually tune the electrical performance of a circuit by applying pressure to achieve a desired physical length of the open stub that remains fixed upon release of the pressure; the device is therefore also a sensor of pressure. This system has the appeal of being built using simple techniques incorporating soft materials, which may be useful for conformal or wearable applications. For simplicity, we use a Cu ground plane, but previous work shows it is possible to form ground planes from liquid metal¹⁴.

3.6 REFERENCES

- (1) Carano, M.; Fjelstad, J. Electronic Materials and Processes Handbook. In *Electronic Materials and Processes Handbook*; McGraw-Hill, 2004; pp. 1–61.
- (2) Lerdwanittip, R.; Namsang, A.; Akkaraekthalin, P. Bandpass Filters Using T-Shape Stepped Impedance Resonators for Wide Harmonics Suppression and Their Application for a Diplexer. *JSTS Journal Semicond. Technol. Sci.* **2011**, *11*, 65–72.
- (3) Taslimi, A.; Mouthaan, K. Wideband Tunable Stubs Using Phase Shifters. In *2010 IEEE International Conference on Wireless Information Technology and Systems (ICWITS)*; 2010; pp. 1–4.
- (4) Takacs, A.; Neculoiu, D.; Vasilache, D.; Muller, A.; Pons, P.; Bary, L.; Calmon, P.; Aubert, H.; Plana, R. Tunable Bandstop and Bandpass MEMS Filters for Millimeter Wave Applications. In *Microwave Conference, 2008. EuMC 2008. 38th European*; 2008; pp. 591–594.
- (5) Kim, C. H.; Chang, K. Ring Resonator Bandpass Filter With Switchable Bandwidth Using Stepped-Impedance Stubs. *IEEE Trans. Microw. Theory Tech.* **2010**, *58*, 3936–3944.
- (6) Guo, S.; Lei, B. J.; Hu, W.; Shiroma, W. A.; Ohta, A. T. A Tunable Low-Pass Filter Using a Liquid-Metal Reconfigurable Periodic Defected Ground Structure. In *Microwave Symposium Digest (MTT), 2012 IEEE MTT-S International*; 2012; pp. 1–3.
- (7) Lei, B. J.; Zamora, A.; Chun, T. F.; Ohta, A. T.; Shiroma, W. A. A Wideband, Pressure-Driven, Liquid-Tunable Frequency Selective Surface. *IEEE Microw. Wirel. Compon. Lett.* **2011**, *21*, 465–467.

- (8) Rashed Khan, M.; Hayes, G. J.; So, J.-H.; Lazzi, G.; Dickey, M. D. A Frequency Shifting Liquid Metal Antenna with Pressure Responsiveness. *Appl. Phys. Lett.* **2011**, *99*, 013501–013501–3.
- (9) Wang, J.; Liu, S.; Nahata, A. Reconfigurable Plasmonic Devices Using Liquid Metals. *Opt. Express* **2012**, *20*, 12119–12126.
- (10) Wang, J.; Liu, S.; Vardeny, Z. V.; Nahata, A. Liquid Metal-Based Plasmonics. *Opt. Express* **2012**, *20*, 2346–2353.
- (11) Dickey, M. D.; Chiechi, R. C.; Larsen, R. J.; Weiss, E. A.; Weitz, D. A.; Whitesides, G. M. Eutectic Gallium-Indium (EGaIn): A Liquid Metal Alloy for the Formation of Stable Structures in Microchannels at Room Temperature. *Adv. Funct. Mater.* **2008**, *18*, 1097–1104.
- (12) Kreit, E.; Dhindsa, M.; Yang, S.; Hagedorn, M.; Zhou, K.; Papautsky, I.; Heikenfeld, J. Laplace Barriers for Electrowetting Thresholding and Virtual Fluid Confinement. *Langmuir* **2010**, *26*, 18550–18556.
- (13) So, J.-H.; Dickey, M. D. Inherently Aligned Microfluidic Electrodes Composed of Liquid Metal. *Lab. Chip* **2011**, *11*, 905–911.
- (14) Hayes, G. J.; So, J.-H.; Qusba, A.; Dickey, M. D.; Lazzi, G. Flexible Liquid Metal Alloy (EGaIn) Microstrip Patch Antenna. *IEEE Trans. Antennas Propag.* **2012**, *60*, 2151–2156.

Chapter 4

**INVESTIGATING THE INTERFACE BETWEEN THE
WALL AND A LIQUID METAL ALLOY IN
MICROCHANNELS***

**Contributors to this work: Ju-Hee So, Etienne Palleau, Kory Gray, John Muth*

4.1 ABSTRACT

Eutectic gallium indium (EGaIn) is a low viscosity liquid at room temperature that can be injected into microchannels to form electrical components including electrodes, antennas, and interconnects. The metal rapidly reacts with oxygen to form a surface oxide. Injecting the metal into air impermeable microchannels offers the potential to form oxide-free metal contacts to surfaces at room temperature. However, energy dispersive X-ray spectroscopy shows that EGaIn also forms a surface oxide at the interface with the walls of air impermeable microchannels. The air permeability and the surface chemistry of the walls also affect the morphology of the interface. The metal forms dimples when injected into air-impermeable glass microchannels but does not in air permeable (PDMS) microchannels. Channels pre-filled with acid form a smooth interface with the metal regardless of the air-permeability of the walls since the acid prevents the oxide from forming. Taken in sum, the results here show that (1) the oxide is present in all channels unless it is removed chemically, and (2) that the oxide-coated metal forms the smoothest interfacial morphology in channels in which the oxide can form and adhere well during injection.

4.2 INTRODUCTION

This chapter provides evidence that injecting eutectic gallium indium (EGaIn) into microchannels results in a thin metal oxide layer between the liquid metal and the walls of the channels even if the walls of the channel are impermeable to air. EGaIn, like most alloys of Ga, has low viscosity, low toxicity, and metallic conductivity¹⁻⁴. Injecting the metal into microfluidic channels is a simple way to define the shape of the metal. During the filling process, the leading interface of the liquid metal is in contact with air and is therefore covered with a solid ‘cap’ of surface oxide. EGaIn reacts rapidly with oxygen to form a thin (1-3 nm thick) surface oxide composed of oxides of gallium⁵⁻⁷. Inducing the low viscosity metal to flow into microchannels requires applying modest pressure to yield this skin⁴. Once inside the channel, the thin oxide ‘cap’ that forms at both the inlet and outlet of the channel provides mechanical stability to the liquid metal despite the high surface tension of the fluid; that is, the oxide prevents the metal from withdrawing. This property enables the fabrication of stretchable wires⁸, antennas⁹⁻¹², sensors¹³⁻¹⁵, electrodes^{16,17}, self-healing circuits^{18,19}, thermocouples²⁰, and optical structures²¹.

We sought to understand if the oxide ‘skin’ exists at the interface between the metal and the walls of air impermeable microchannels. The liquid metal and the oxide have significantly different rheological, chemical, electrical, and wetting properties^{4,17,22-25} and thus the presence (or lack) of the oxide at that interface has implications for the mechanics of the flow of metal in and out of microchannels, as well as the morphology and physical properties of the metal at the interface. For example, oxide-free interfaces would allow a simple way to

make soft, metallic contacts that may be useful for probing the electrical properties of soft materials (e.g., self-assembled monolayers (SAMs)^{17,26}, biological species²⁷ and gels^{28,29}) without the need to deconvolve the influence of the oxide layer on sensitive measurements.

Here, we show that EGaIn injected into both air permeable (polydimethylsiloxane, PDMS) and air impermeable (glass and silicon nitride) microchannels, results in a thin oxide between the walls and the metal. We verify the presence of the oxide at the interface by using energy dispersive X-ray spectroscopy (EDS) and characterize the morphology under a scanning electron microscope (SEM). We also establish the importance of the chemistry and permeability of the walls of the microchannel in dictating the morphology of the metal at the interface formed via injection.

4.3 EXPERIMENTAL DESIGN

We sought to characterize the chemical composition of the metal (whether oxygen is present or not) at the interface with an air-impermeable wall. Previously, the chemical composition of the surface of gallium-based alloys has been studied by using different characterization techniques including EDS, X-ray photoelectron spectroscopy (XPS) and Auger spectroscopy⁴⁻⁷. The studies, however, focused on metal surfaces that were exposed to air, and thus, known to have the native surface oxide. One study suggests this oxide forms at oxygen levels as low as ppm.⁵

Probing the interface between the liquid metal and the wall is experimentally challenging. The measurement must be done without exposing the interface between the metal and the wall of the channel to ambient air after injection. Thus, the experiments require an air impermeable, oxygen-free, and optically and electron transparent substrate to enable interfacial characterization techniques such as microscopy and spectroscopy. The oxide, if present, is expected to be very thin (~1 nm) based on previous studies in oxygen^{5,6}; thus, any characterization technique must be surface sensitive. Considering these demanding requirements, we developed an experimental method to investigate the interface of the liquid metal with air-impermeable substrates by performing a series of experiments that involve EDS through silicon nitride “windows”.

The qualitative nature of EDS as a thin film characterization technique could be seen as a limitation in this study. Indeed, the e-beam of EDS generates a tear-drop shape of interaction volume in a specimen that probes beyond the surface. Moreover, the low energy X-rays from light elements such as nitrogen, carbon and oxygen are easily absorbed by the detector. Thus, it is difficult to analyze quantitatively ultra-thin layers composed of light elements. Despite these challenges and limitations (and the lack of alternatives), it represents the best characterization technique that meets all of the requirements for our analysis.

In our experiments, we choose to work with “windows” consisting of a thin film of Si_3N_4 on a Si substrate. Etching a hole through the backside of the Si substrate generates the silicon nitride window (Figure 1). The window provides an oxygen-impermeable interface that is

effectively transparent to electrons and photons (necessary for EDS and SEM measurements and optical inspection). Such silicon nitride windows have been used as the walls of a microfluidic channel to image liquid flow with a scanning transmission electron microscope³⁰, but not in the case of interfacial investigation of atomic composition. The Si_3N_4 films are available in various thicknesses; thin nitride windows are less mechanically stable, but provide more sensitive measurements since the e-beam involved in EDS experiments does not have to travel as far through the window. We used the thinnest window that is mechanically robust toward the liquid metal injection process (~50 nm).

Injecting the liquid metal into microchannels sealed against these nitride windows is information-limited and brings numerous experimental challenges: (i) preventing the PDMS channels from overlapping the windows, which would lead to unwanted detection of oxygen, (ii) establishing a mechanically stable contact between the channels and the nitride substrate, (iii) injecting the metal without rupturing the thin nitride windows, and (iv) preventing the disturbance of channels in vacuum during EDS measurements. To overcome those issues, we fabricated a 2 mm wide and 1 cm long channel and placed it on the silicon nitride such that it straddled the window (1 mm \times 1 mm). Injecting the metal into these wide channels requires low pressure, thus minimizing the stress on the thin nitride windows. We sealed the edges of the PDMS channel to the nitride substrate by using a silver paint adhesive (Figure 1). The presence of silver in the adhesive allowed us to confirm by EDS that no adhesive entered into proximity of the nitride window. We also prepared reference samples that are expected to

show an oxygen peak for EDS measurements by gently placing a drop of oxide-coated metal onto the nitride window in the presence of air.

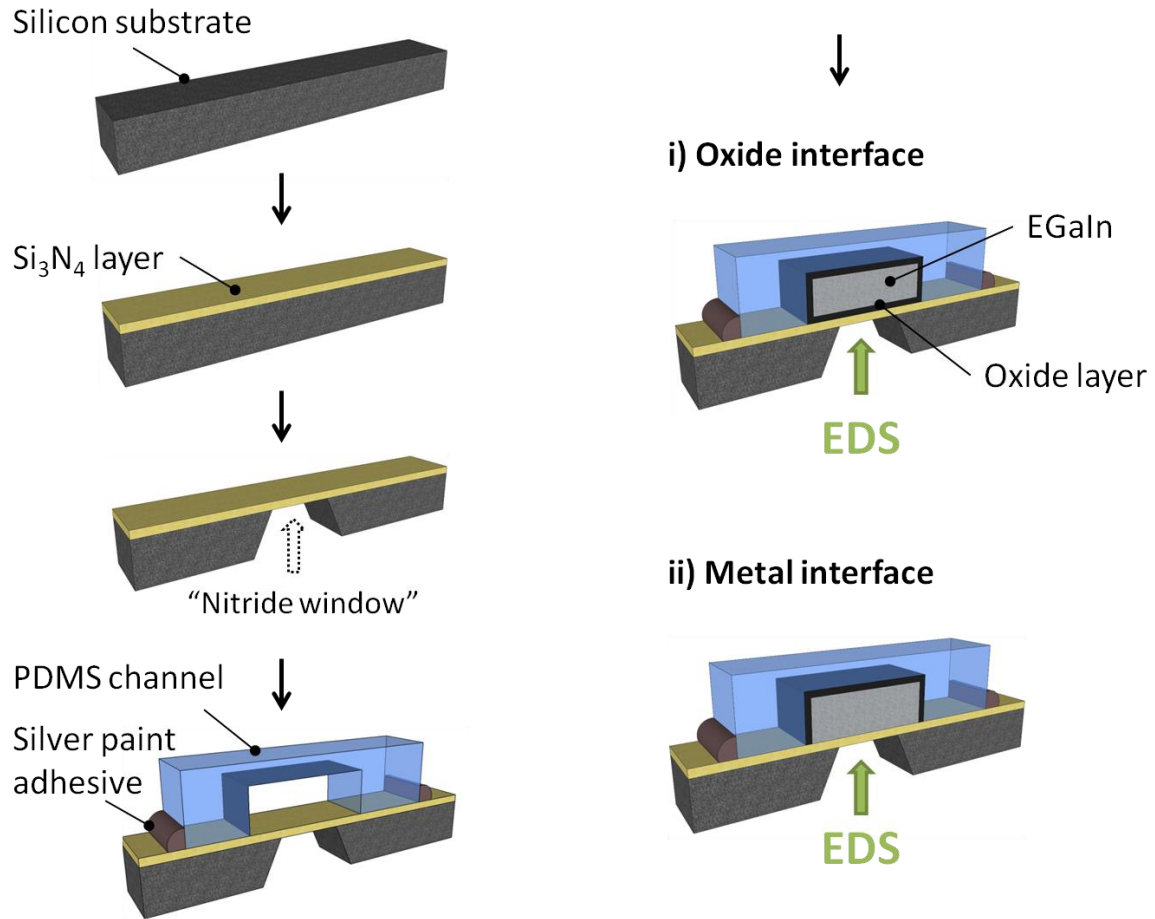


Figure 1. Experimental procedure for detecting the presence of oxide at the interface with an air-impermeable wall. Liquid metal is injected into a PDMS microfluidic channel on top of a silicon nitride window and examined by EDS through the window. We sought to study whether there is a metal oxide at the interface (i) or the interface is pure metal (ii).

4.4 RESULT AND DISCUSSION

We examined the interface of liquid metal in contact with the nitride window (Figure 2(a)). SEM images confirmed that the liquid metal maintained mechanical stability under the high vacuum state without flowing and disturbing the interface. The injected EGaIn formed a smooth interface with the nitride window (Figure 2 (b)), whereas the oxide-coated droplet of EGaIn had a wrinkled texture (Figure 2(c)). The amount of wrinkles on the surface of the droplet depended how gently it was handled during sample preparation.

We inspected the atomic composition of the interfaces by EDS. To determine the appropriate parameters for the EDS measurements, we used two EDS modeling software packages (Casino and Electron Flight Simulator). Results suggest that the electron beam used for EDS can penetrate the nitride window and the signal from the oxide layer will be distinct and detectable through the window. In the model, we varied the acceleration voltage (0 – 10 keV) and the thickness of the oxide (0 – 10 nm) through a 50 nm thick nitride window. At large accelerating voltages (> 5 keV), the model suggests that the beam penetrates too deep into the sample to distinguish the thin oxide layer from the large interaction volume of the e-beam. At small accelerating voltages (< 3 keV), the model suggests that the beam does not penetrate through the nitride window. Although these values can be considered estimates, they provided a guide for determining an appropriate range of accelerating voltages to probe the sample.

Based on the theoretical range of accelerating voltage, we performed EDS measurements on the reference samples of droplets and control samples of PDMS channels (Figure 3). EDS measurements performed on blank nitride windows contained no oxygen and no gallium in the spectra. Both reference and control samples had oxygen and gallium peaks at 4.5 and 5.0 keV, suggesting the presence of the oxide layer in both samples. The data in Figure 3 represent the average of six measurements performed by two different researchers. We also repeated this test four times where we first cleaned the Si_3N_4 surface with low pressure oxygen plasma prior to injection, but the plasma treatment did not change the result. Regardless of preparation, a small amount of adventitious carbon appeared in all the spectra.

Increasing the accelerating voltage increased the gallium to oxygen ratio (from 0.22 to 0.47 for the droplet samples and from 0.33 to 0.34 for the channel samples) since the beam probes deeper into the metal. Indium peaks ($M = 0.368$ keV, $L\alpha = 3.286$ keV) are barely detectable at accelerating voltages between 4-5 keV. This result is not surprising given the small gallium peaks (~1% of the signal), the lower population of M and L peaks relative to K peaks, and the possible overlap of the M peak with the large nitrogen peak ($K\alpha = 0.392$ keV) from the nitride windows. The lack of indium may also be indicative of enrichment in gallium at the interface based on previous studies.^{4,5,7} Nevertheless, the In peaks became apparent after increasing the accelerating voltage (e.g., 20keV) to probe deeper into the bulk of the metal.

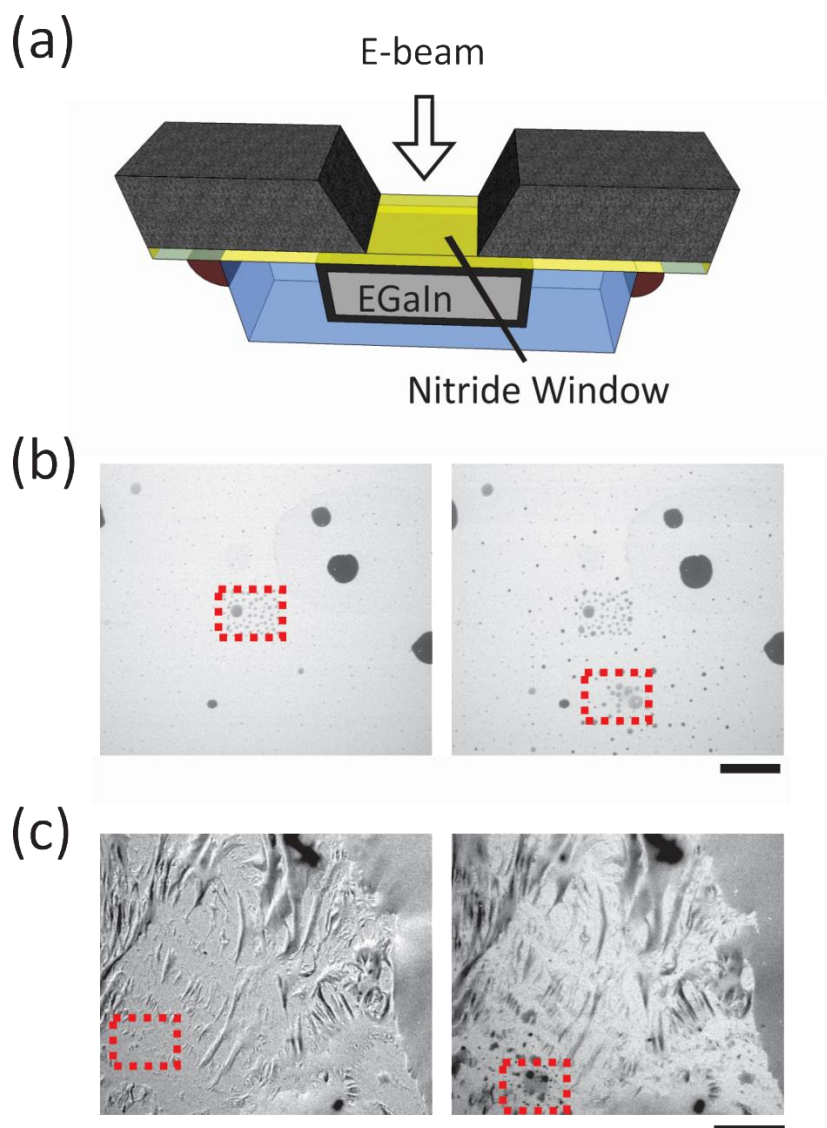


Figure 2. (a) A schematic diagram of the assembly of EGaIn and the nitride window for EDS measurement. (b) SEM images of EGaIn in a microchannel focused through the nitride window. The rectangles represent the probed area where the e-beam focused at the first (left) and second (right) EDS measurements. (c) SEM images of a droplet of EGaIn that was

exposed to air and gently placed on the nitride window before the measurement. The scale bars are 50 μm .

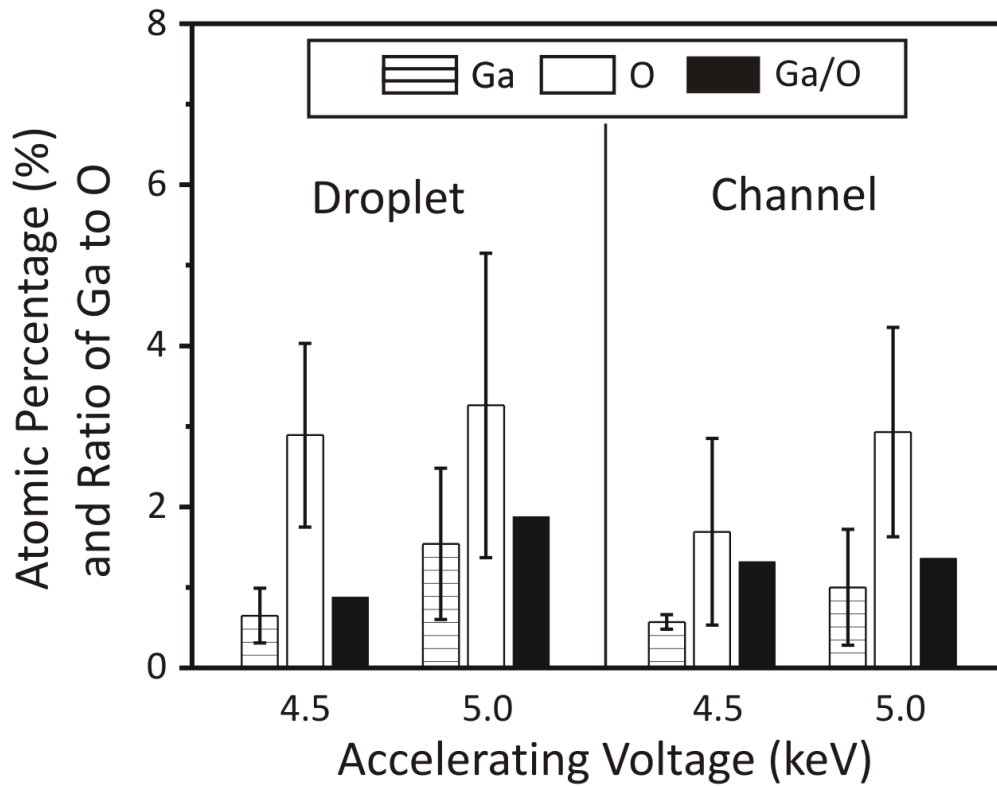


Figure 3. Atomic percentage of gallium and oxygen from EDS measurements on EGaIn-silicon nitride interfaces prepared by placing the droplet of EGaIn on the nitride substrate or injecting EGaIn into a channel with the nitride wall.

The thin silicon nitride windows are transparent for both optical and scanning electron microscopy. Microscopy suggests that immediately after injection the interface is smooth with a few ‘dimples’ (cf. Figure 2b). During SEM imaging, additional dimples formed upon exposing the smooth regions to the electron beam (marked by rectangles in Figure 2 (b) and (c)). These dimples expanded when irradiated with electrons, which suggested that gaseous species may exist at these dimples. The source of these dimples is unknown, but we speculate (based on subsequent experiments) that the poor wetting of the metal to the nitride may contribute to the formation of these dimples. . In presence of air, EGaIn can be physically spread on many substrates (e.g., PDMS, glass), yet it is hard to spread the metal onto silicon nitride substrates. In the absence of the oxide, the high surface tension of EGaIn renders it is impossible to spread on most surfaces (e.g., PDMS, silicon wafers, glass slides) including silicon nitride.

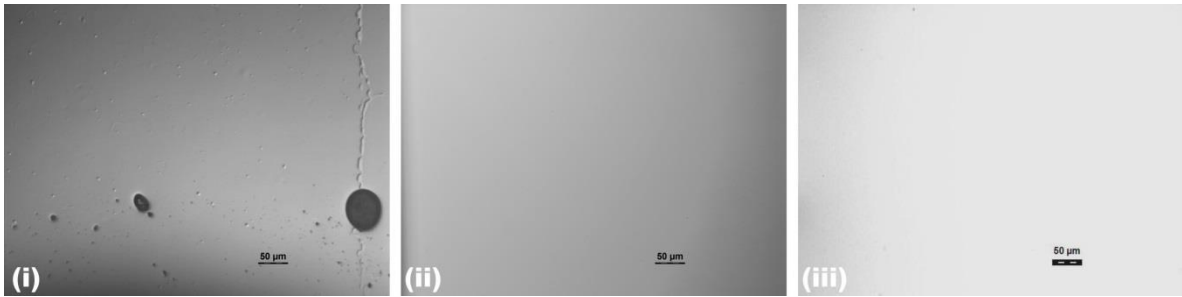


Figure 4. Interfacial morphology of EGaIn with pristine (a), oxygen plasma treated (b), or plasma treated and acid-treated (c) PDMS substrates.

We sought to gain a more complete understanding of the role of the channel walls on the interfacial morphology of EGaIn by imaging the metal / substrate interface formed by injecting metal into PDMS microchannels placed against substrates of various surface properties. In all cases, we chose optically transparent substrates to image the interface. We hypothesized that the interfacial morphology of the metal depends mainly on both the air permeability of the substrates and the adhesion of the surface oxide to the substrate. We first utilized PDMS substrates, which are known for being highly permeable to air. Injecting metal into microchannels placed on unmodified PDMS results in dimples and ripples, as shown in Figure 4a(i). Injecting the metal by applying a positive pressure to the inlet produced the same result as injecting the metal by applying vacuum to the outlet.

Unmodified PDMS is hydrophobic, but can be rendered hydrophilic by generating surface hydroxyl groups upon exposure to oxygen plasma. Injecting EGaIn into hydrophilic PDMS resulted in a smoother interfacial morphology (Figure 4a(ii)) than the unmodified PDMS substrate. These results suggest that the hydroxyl groups on the PDMS more favorably interact with the oxide on the EGaIn to create a more conformal interface. We speculate that the dimples that form on the nitride surfaces may form for the same reasons. Figure 4a(iii) shows the interface of the metal injected into a PDMS channel pre-treated with oxygen plasma and pre-filled with 1M HCl. The presence of the acid prevents the oxide on the metal from forming during injection, resulting in a smooth interface, as expected.

Unlike PDMS, nitride windows are air impermeable and mechanically rigid. To explore the effect of air-impermeability, we replaced the PDMS substrate with glass which has hydroxyl groups on the surface but is impermeable to air and mechanically rigid. The interface of EGaIn on a pristine glass substrate is shown in Figure 5 (a).

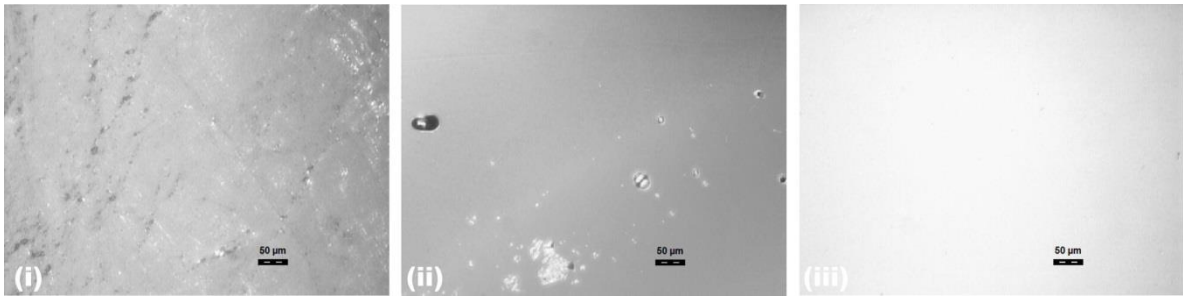


Figure 5. Interfacial morphology of EGaIn with pristine (a), oxygen-plasma treated (b), acid-treated (c) glass substrates.

Injecting EGaIn into a microchannel with an oxygen plasma treated glass substrate creates a smooth interfacial morphology (Figure 4b(ii)). There are a few dimples that are randomly distributed throughout the entire length of the microchannel. Relative to the smooth interface formed on plasma treated PDMS (Figure 4a(ii)), the generation of dimples may be due to the glass substrate being rigid or impermeable. Similar to Figure 4a(iii), the glass substrate treated with 1M HCl appeared smooth without the noticeable presence of the oxide, which suggests that the dimples on the other substrates are not due to particles.

To investigate the effect of the surface chemistry, we silanized the glass slides to render the surface hydrophobic. The interface of EGaIn with a glass substrate treated by fluorosilane shows very rough and patchy surface morphology (not shown here) which can be attributed to unfavorable interaction of oxide with the silanized surface of the glass. Taken in sum, these results suggest that both of the air-permeability and the presence of hydroxyl groups of substrates contribute to conformal formation and wetting of the oxide at the interface.

4.5 CONCLUSION

This chapter shows that there is oxide at the interface between EGaIn and air impermeable microchannel walls. The morphology of this interface depends on the composition of the channel walls. Dimples form on hydrophobic PDMS (i.e., an oxygen permeable substrate), but do not on hydrophilic PDMS. Dimples form on rigid glass (i.e., oxygen impermeable), but there are significantly fewer after the glass slide is treated with oxygen plasma. Treated (plasma or solvent) substrates directly affects the wetting or non-wetting properties of the oxide skin. This can be utilized as a direct evidence to study the presence of oxide as well as can be harnessed to form soft intermetallic contacts at room temperature. The ability to form well-defined, soft metallic contacts at room temperature may be useful for probing various electronic devices in a non-damaging, high throughput manner. Also we can further utilize this tool to study the importance of surface chemistry and roughness by placing films or self-assembled monolayers on the Si_3N_4 substrate prior to filling.

4.6 REFERENCES

- (1) French, S. J.; Saunders, D. J.; Ingle, G. W. The System Gallium-Indium. *J. Phys. Chem.* **2002**, *42*, 265–274.
- (2) Sheka, I. A.; Chaus, I. S.; Mitiureva, T. T. *The Chemistry of Gallium*; Elsevier: New York, 1966.
- (3) Zrnic, D.; Swatik, D. S. On the Resistivity and Surface Tension of the Eutectic Alloy of Gallium and Indium. *J. Common Met.* **1969**, *18*, 67–68.
- (4) Dickey, M. D.; Chiechi, R. C.; Larsen, R. J.; Weiss, E. A.; Weitz, D. A.; Whitesides, G. M. Eutectic Gallium-Indium (EGaIn): A Liquid Metal Alloy for the Formation of Stable Structures in Microchannels at Room Temperature. *Adv. Funct. Mater.* **2008**, *18*, 1097–1104.
- (5) Regan, M. J.; Tostmann, H.; Pershan, P. S.; Magnussen, O. M.; DiMasi, E.; Ocko, B. M.; Deutsch, M. X-Ray Study of the Oxidation of Liquid-Gallium Surfaces. *Phys. Rev. B Condens. Matter* **1997**, *55*, 10786–10790.
- (6) Regan, M. J.; Pershan, P. S.; Magnussen, O. M.; Ocko, B. M.; Deutsch, M.; Berman, L. E. X-Ray Reflectivity Studies of Liquid Metal and Alloy Surfaces. *Phys. Rev. B* **1997**, *55*, 15874–15884.
- (7) Cademartiri, L.; Thuo, M. M.; Nijhuis, C. A.; Reus, W. F.; Tricard, S.; Barber, J. R.; Sodhi, R. N. S.; Brodersen, P.; Kim, C.; Chiechi, R. C.; et al. Electrical Resistance of Ag-TS-S(CH₂)(n-1)CH₃//Ga₂O₃/EGaIn Tunneling Junctions. *J. Phys. Chem. C* **2012**, *116*, 10848–10860.

- (8) Zhu, S.; So, J.-H.; Mays, R.; Desai, S.; Barnes, W. R.; Pourdeyhimi, B.; Dickey, M. D. Ultrastretchable Fibers with Metallic Conductivity Using a Liquid Metal Alloy Core. *Adv. Funct. Mater.* **2013**, *23*, 2308–2314.
- (9) Cheng, S.; Rydberg, A.; Hjort, K.; Wu, Z. Liquid Metal Stretchable Unbalanced Loop Antenna. *Appl. Phys. Lett.* **2009**, *94*, 144103.
- (10) Khan, M. R.; Hayes, G. J.; So, J.-H.; Lazzi, G.; Dickey, M. D. A Frequency Shifting Liquid Metal Antenna with Pressure Responsiveness. *Appl. Phys. Lett.* **2011**, *99*, 013501.
- (11) Kubo, M.; Li, X.; Kim, C.; Hashimoto, M.; Wiley, B. J.; Ham, D.; Whitesides, G. M. Stretchable Microfluidic Radiofrequency Antennas. *Adv. Mater.* **2010**, *22*, 2749–2752.
- (12) So, J. H.; Thelen, J.; Qusba, A.; Hayes, G. J.; Lazzi, G.; Dickey, M. D. Reversibly Deformable and Mechanically Tunable Fluidic Antennas. *Adv. Funct. Mater.* **2009**, *19*, 3632–3637.
- (13) Kramer, R. K.; Majidi, C.; Sahai, R.; Wood, R. J. Soft Curvature Sensors for Joint Angle Proprioception. In *2011 IEEE/RSJ International Conference on Intelligent Robots and Systems (IROS)*; 2011; pp. 1919–1926.
- (14) Cheng, S.; Wu, Z. A Microfluidic, Reversibly Stretchable, Large-Area Wireless Strain Sensor. *Adv. Funct. Mater.* **2011**, *21*, 2282–2290.
- (15) Majidi, C.; Kramer, R.; Wood, R. J. A Non-Differential Elastomer Curvature Sensor for Softer-than-Skin Electronics. *Smart Mater. Struct.* **2011**, *20*, 105017.
- (16) So, J.-H.; Dickey, M. D. Inherently Aligned Microfluidic Electrodes Composed of Liquid Metal. *Lab Chip* **2011**, *11*, 905–911.

- (17) Chiechi, R. C.; Weiss, E. A.; Dickey, M. D.; Whitesides, G. M. Eutectic Gallium-Indium (EGaIn): A Moldable Liquid Metal for Electrical Characterization of Self-Assembled Monolayers. *Angew. Chem. Int. Ed.* **2008**, *47*, 142–144.
- (18) Palleau, E.; Reece, S.; Desai, S. C.; Smith, M. E.; Dickey, M. D. Self-Healing Stretchable Wires for Reconfigurable Circuit Wiring and 3D Microfluidics. *Adv. Mater.* **2013**, *25*, 1589–1592.
- (19) Blaiszik, B. J.; Kramer, S. L. B.; Grady, M. E.; McIlroy, D. A.; Moore, J. S.; Sottos, N. R.; White, S. R. Autonomic Restoration of Electrical Conductivity. *Adv. Mater.* **2012**, *24*, 398–401.
- (20) Dorozhkin, P. S.; Tovstonog, S. V.; Golberg, D.; Zhan, J. H.; Ishikawa, Y.; Shiozawa, M.; Nakanishi, H.; Nakata, K.; Bando, Y. A Liquid-Ga-Fitted Carbon Nanotube: A Miniaturized Temperature Sensor and Electrical Switch. *Small* **2005**, *1*, 1088–1093.
- (21) Mohammed, M. G.; Dickey, M. D. Strain-Controlled Diffraction of Light from Stretchable Liquid Metal Micro-Components. *Sens. Actuators Phys.* **2013**, *193*, 246–250.
- (22) Larsen, R. J.; Dickey, M. D.; Whitesides, G. M.; Weitz, D. A. Viscoelastic Properties of Oxide-Coated Liquid Metals. *J. Rheol.* **2009**, *53*, 1305–1326.
- (23) Xu, Q.; Qudalov, N.; Guo, Q.; Jaeger, H.; Brown, E. Effect of Oxidation on the Mechanical Properties of Liquid Gallium and Eutectic Gallium-Indium. *arXiv:1201.4828* **2012**.

- (24) Doudrick, K.; Liu, S.; Mutunga, E. M.; Klein, K. L.; Damle, V.; Varanasi, K. K.; Rykaczewski, K. Different Shades of Oxide: From Nanoscale Wetting Mechanisms to Contact Printing of Gallium-Based Liquid Metals. *Langmuir* **2014**, *30*, 6867–6877.
- (25) Kim, D.; Thissen, P.; Viner, G.; Lee, D.-W.; Choi, W.; Chabal, Y. J.; Lee, J.-B. (J. B. . Recovery of Nonwetting Characteristics by Surface Modification of Gallium-Based Liquid Metal Droplets Using Hydrochloric Acid Vapor. *ACS Appl. Mater. Interfaces* **2013**, *5*, 179–185.
- (26) Nijhuis, C. A.; Reus, W. F.; Barber, J. R.; Whitesides, G. M. Comparison of SAM-Based Junctions with Ga₂O₃/EGaIn Top Electrodes to Other Large-Area Tunneling Junctions. *J. Phys. Chem. C* **2012**, *116*, 14139–14150.
- (27) Hallfors, N.; Khan, A.; Dickey, M. D.; Taylor, A. M. Integration of Pre-Aligned Liquid Metal Electrodes for Neural Stimulation within a User-Friendly Microfluidic Platform. *Lab. Chip* **2013**, *13*, 522–526.
- (28) Koo, H.; So, J.; Dickey, M. D.; Velev, O. D. Towards All-Soft Matter Circuits: Prototypes of Quasi-Liquid Devices with Memristor Characteristics. *Adv. Mater.* **2011**, *23*, 3559–3564.
- (29) So, J.; Koo, H.; Dickey, M. D.; Velev, O. D. Ionic Current Rectification in Soft-Matter Diodes with Liquid-Metal Electrodes. *Adv. Funct. Mater.* **2012**, *22*, 625–631.
- (30) Ring, E. A.; de Jonge, N. Microfluidic System for Transmission Electron Microscopy. *Microsc. Microanal. Off. J. Microsc. Soc. Am. Microbeam Anal. Soc. Microsc. Soc. Can.* **2010**, *16*, 622–629.

Chapter 5

RECAPILLARITY: ELECTROCHEMICALLY CONTROLLED CAPILLARY WITHDRAWAL OF A LIQUID METAL ALLOY FROM MICROCHANNELS*

**This work has been published in Advanced Functional Materials. Contributor to this work:*

Chris Trlica.

5.1 ABSTRACT

This chapter describes the mechanistic details of an electrochemical method to control the withdrawal of a liquid metal alloy, eutectic gallium indium (EGaIn), from microfluidic channels. EGaIn is one of several alloys of gallium that are liquid at room temperature and form a thin (nm scale) surface oxide that stabilizes the shape of the metal in microchannels. Applying a reductive potential to the metal removes the oxide in the presence of electrolyte and induces capillary behavior; we call this behavior ‘recapillarity’ because of the importance of electrochemical reduction to the process. Recapillarity can repeatedly toggle on and off capillary behavior by applying voltage, which is useful for controlling the withdrawal of metal from microchannels. This chapter explores the mechanism of withdrawal and identifies the applied current as the key factor dictating the withdrawal velocity. Experimental observations suggest that this current may be necessary to reduce the oxide on the leading interface of the metal as well as the oxide sandwiched between the wall of the microchannel and the bulk liquid metal. The ability to control the shape and position of a metal using an applied voltage may prove useful for shape reconfigurable electronics, optics, transient circuits, and microfluidic components.

5.2 INTRODUCTION

The ability to accurately manipulate liquids on the sub-mm length scale is important for many applications including MEMS devices (e.g., sensors, actuators, and RF electronics), micro-total analysis systems, micropumps for mixing and analyses of fluids, reconfigurable electronics (antennas, interconnects, relays), and optics^{1–14}. Metals are particularly desirable for such applications because of their optical, thermal, and electrical properties. One material that holds promise for these applications is eutectic gallium indium (EGaIn), one of several alloys of gallium that are liquid metals at room temperature^{14,15}. EGaIn has a melting point of 15.7 °C¹⁶ and a liquid phase viscosity approximately twice that of water^{17,18}. It has metallic conductivity^{15,19} and low toxicity²⁰, making it an attractive alternative to mercury for many applications^{3,21–23}.

EGaIn spontaneously forms a thin and passivating surface oxide layer at room temperature in the presence of oxygen, even at ppm O₂ levels^{24,25}. Though this oxide has historically been considered a nuisance^{26,27}, it provides unique opportunities to control the shape of the metal²⁸. This oxide ‘skin’ envelops the liquid and provides mechanical stability that allows EGaIn to be molded into non-equilibrium shapes that would usually be disallowed by surface tension^{29,30}. The skin has been Supporting harnessed to print the metal in 3-D³⁰ and 2-D³¹ and to form stretchable interconnects³², wires³³, antennas^{13,29}, sensors^{34,35}, and plasmonic structures³⁶ fabricated by injecting the metal into microchannels.

Because EGaIn is a liquid, its shape and position can be controlled by inducing it to flow.

Injecting the metal into a microchannel is straightforward by using pressure differentials. This injection technique has been used to create shape-reconfigurable antennas and filters composed of alloys of gallium that change length in response to pressure^{37–39}.

Inducing the metal to flow out of a microchannel, however, is more challenging. The presence of the oxide skin can cause the metal to leave residue on the channel walls (Figure 1a), like wet paint flowing through a tube⁴⁰. It is possible to use Teflon-like surfaces or roughened surfaces^{40–43} to reduce the adhesion of the metal oxide, but these approaches limit the materials of construction and increase the complexity of fabrication. It is also possible to use acid or base to remove the oxide skin, but this approach lacks external control and involves the use of possibly hazardous or corrosive materials⁴⁴. For these reasons, most studies involving the actuation of liquid metals in microchannels focus on Hg despite its toxicity^{45–47}.

The Pourbaix diagram predicts that reductive electrochemical potentials can remove the oxide skin on gallium⁴⁸. Without the stabilizing presence of the skin, the metal undergoes capillary action to minimize its surface energy. Figure 1b illustrates this concept: A puddle of the metal beads up in response to a reductive potential. Although an applied bias likely lowers the interfacial tension of the metal (relative to bare metal) via electrocapillarity⁴⁹, the tension is still large enough to induce capillary phenomena. This phenomenon can be exploited to induce withdrawal of the metal in microchannels (Figure 1c) by capillary action toward a reservoir where the metal may lower its interfacial energy by adopting a larger

radius of curvature⁵⁰. Importantly, in the absence of applied potential, the skin rapidly reforms, allowing capillary flow to be stopped on demand. Controlling interfacial phenomena represents an attractive way to manipulate fluids since capillary forces dominate on the sub-mm length scale^{51,52}. Furthermore, the use of applied voltage is an ideal way to manipulate fluids because it is highly controllable, easily accessible, and does not require bulky or moving parts⁵³⁻⁵⁶.

We call the technique ‘recapillarity’ because it uses reduction to induce capillarity. The term also refers to the ability to repeatedly turn on and off the capillary behavior. Recapillarity is an attractive alternative to conventional electrohydrodynamic approaches for manipulating fluids (e.g., electroosmosis, electrowetting⁵⁷), which are difficult to implement with EGaIn for a number of reasons including the large yield stress of the oxide skin¹⁴. In contrast, recapillarity takes advantage of the skin by removing it on demand. Here, we describe the velocity of the withdrawal of EGaIn from microchannels induced by recapillarity, characterize the role various experimental parameters play on the withdrawal, and propose a mechanism to explain the withdrawal. The proposed mechanism implies that oxide is present between the metal and the walls of the channel, which is otherwise a difficult interface to probe.

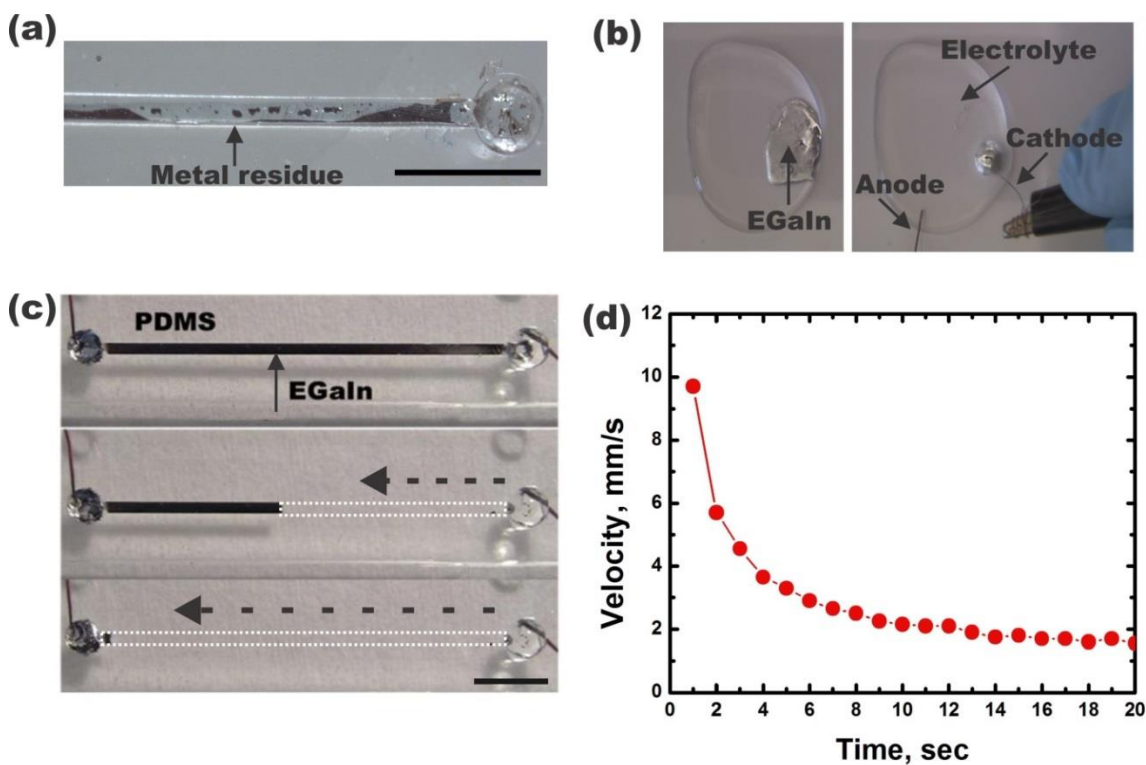


Figure 1. (a) Photograph of metal residue on the sidewalls of polydimethylsiloxane (PDMS) microchannels after attempting to withdraw EGaIn using pneumatics. (b) The oxide skin stabilizes the shape of a puddle of metal submerged in electrolyte. Application of a reductive potential to the metal removes the oxide and the high surface tension of the metal causes it to bead up. (c) An example of reduction-driven liquid metal withdrawal in a PDMS microchannel. The EGaIn cathode connects electrically to a counter electrode by a dilute salt solution (10mM NaF). A reductive potential (1 V) applied to the liquid metal causes it to withdraw from the microchannel toward a reservoir, leaving the capillary filled with electrolyte. (d) A characteristic plot of the velocity of liquid metal withdrawal over time. (Both scale bars are 5mm).

5.3 RESULTS AND DISCUSSION

To study withdrawal induced by recapillarity, we used an inert acrylic platform with two reservoirs for holding liquid, bridged by a glass capillary (depicted in Supplementary Information, Figure S1). Electrodes connected the fluid in each reservoir to a voltage source (Pine WaveNow AFTP1 potentiostat). An electrolyte (10 mM NaF) filled one reservoir and EGaIn filled the other. Capillaries pre-filled with liquid metal spanned the apparatus horizontally such that each end remained immersed in a reservoir, completing the circuit. Straight borosilicate capillaries (0.9 +/- 0.1 mm inner diameter, 70 mm long) are well-suited for these experiments because they are inexpensive, optically transparent, and oxygen impermeable. They also have round cross-sections and thus lack sharp corners that could create void space.

Upon applying a reductive potential, the liquid metal withdraws from microchannels at a velocity that decays over time, as shown in Figure 1d. Regardless of the absolute velocity, withdrawal velocities start high and then decay. This holds for all of the constant-voltage experimental conditions we explored, including a range of salt concentrations (1 μ M to 3 M), applied voltages (100 mV to 4 V), and capillary tube diameters (0.25 mm to 1 mm inner diameter). We sought to understand the behavior of this system by studying the parameters that could impact the rate of withdrawal.

Unless otherwise noted, 10 mM NaF served as the electrolyte (though all the electrolytes we tried produced similar results). More concentrated electrolytes result in withdrawal velocities

that are too fast to observe easily; remarkably, 1 M NaF at 1 V causes the metal to withdraw at a maximum velocity of ~10-30 cm/sec (Supplementary Information, Figure S2)..

There are a number of possible factors contributing to the decay in the withdrawal velocity. Since capillary forces are often important on the sub-mm length scale, we examined potential interfacial factors in addition to electrochemical factors. We examined: 1) the shape of the liquid metal meniscus as the metal retreats from the channel; 2) the size and shape of the metal in the reservoir; 3) possible ion gradients at the EGaIn/electrolyte interface; 4) effects of physical channel geometry such as length; and 5) electrical path length. After systematically studying each of these parameters, we show that the only variables significantly influencing withdrawal velocity are those affecting the applied current.

Meniscus Shape: At rest, the metal plug in the capillary adopts a hemispherical meniscus at the electrolyte interface, as shown in Figure 2a(i). However, during withdrawal, the meniscus flattens (cf., Figure 2a(ii)). We hypothesized that this change in the meniscus shape lowers the withdrawal velocity relative to a curved meniscus since a flat meniscus would have a lower capillary pressure and therefore a smaller driving force for withdrawal. To test this hypothesis, we used recapillarity to withdraw the liquid metal halfway along the length of the glass capillary. In the absence of potential, the metal stops moving and the meniscus equilibrates to a round shape within ~100 microseconds (Figure 2a(iii)). The round shape of the meniscus at equilibrium is similar to its shape prior to starting the experiment. Applying a reductive potential again [at 21 seconds in Figure 2b] causes the metal to begin

withdrawing again, continuing at a similar velocity as before the voltage ceased. Since the velocity did not increase after allowing the meniscus to re-equilibrate, we rejected this hypothesis. We will later show that the shape of the meniscus is a consequence of the withdrawal mechanism.

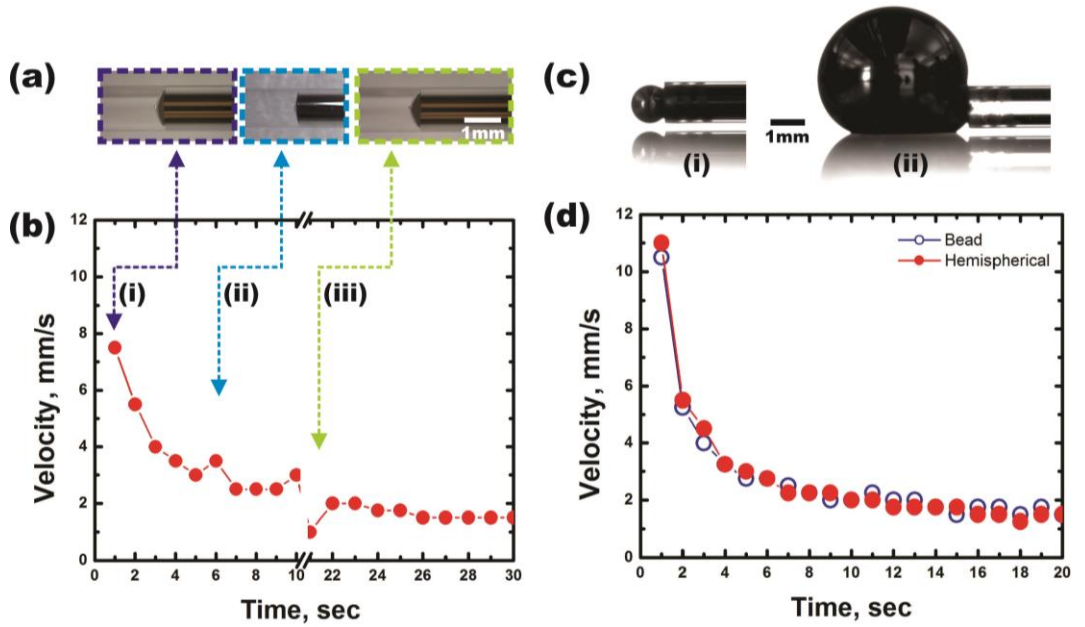


Figure 2. Effect of meniscus shape (a-b) and shape of the metal in the reservoir (c-d) on withdrawal velocity. (a) Top down photographs (i-iii) of liquid metal menisci. At the beginning of the experiment, (i) a hemispherical meniscus (ii) flattens out during recapillarity, and then (iii) returns to an equilibrium hemispherical shape in the absence of voltage. (b) Plot of velocity versus time to test the effect of meniscus shape. After 10 seconds, withdrawal stops when the applied voltage is zero. Ten seconds later, after the meniscus has re-equilibrated, withdrawal continues by re-application of the voltage with no appreciable change in velocity (at $t=22$ s). (c) Side view of two end reservoirs over time including one in the shape of (i) a small bead and (ii) a large hemisphere. (d) Plot of the

velocity with metal reservoirs of different shape and size, showing that geometry of the metal does not have a significant effect on metal withdrawal.

Shape of Metal Reservoir: As the metal flows out of the capillary into the reservoir, the reservoir increases in volume. We speculated that the capillary pressure at the receiving reservoir might affect the withdrawal velocity, although in principle, the pressure opposing recapillarity should decrease as the reservoir inflates with more metal and therefore allow the withdrawal velocity to increase with time. We varied the amount of metal at the reservoir to change its shape from a small bead (i.e., bead diameter approximately equal to tube diameter) to a much larger drop (i.e., diameter two or more times larger than the tube diameter), as shown in Figure 2c. The withdrawal velocities were nearly identical in both cases (Figure 2d), suggesting that withdrawal velocities are independent of reservoir size and shape for the range of length scales explored in the experiments described in this chapter. Later we show that electrochemical processes dictate the velocity of withdrawal.

Ion Gradients: Because electrochemical reactions drive the withdrawal process, we hypothesized that local changes in the concentration of ion species (e.g., Ga^{+3} , OH^- , H^+ , Na^+ , F^-) near the liquid metal interface may affect the withdrawal. After withdrawing the metal partially, we turned off the applied voltage. We waited for ~10-20 sec to let the meniscus recover its shape, i.e., a flat meniscus returns back to hemispherical shape (cf., Figure 2a). Then we refreshed the electrolyte / metal oxide interface by inserting a syringe needle (Figure S3a) into the capillary tube and gently flushing the interface with fresh electrolyte.

Figure S3b shows that after re-initiating withdrawal, there is no increase in velocity, suggesting that ion gradients do not significantly affect the withdrawal velocity.

Liquid Displacement: As metal withdraws from the capillary it simultaneously pulls electrolyte into the capillary. The viscosity of the electrolyte is lower than that of the metal, so it should not reduce the speed of withdrawal. Our results suggest a more dominant effect is the change in electrical resistance along the long axis of the tube. Electrolyte replaces the metal as it withdraws, lengthening the electrical path between the two electrodes. We therefore hypothesized that the increasing electrical distance between the liquid metal surface and the counter-electrode causes the decay in velocity. To test this hypothesis, we withdrew the metal halfway out of the capillary and then turned off the voltage. Inserting the counter-electrode into the capillary (Supporting Information, Figure S4) returned the electrode-electrode distance to a value similar to that at the beginning of the experiment. After reinitiating withdrawal by application of potential, the velocity began high and subsequently decayed, mimicking the decay observed during the first portion of the experiment, as seen in Figure 3a. This result supports the hypothesis that the electrical length causes the decay of the withdrawal velocity. As a complementary experiment, we reversed the direction of flow by using a syringe pump to physically force metal into an electrolyte-filled capillary while measuring the amperometric behavior. In principle, as the electrolyte gets displaced by metal, the electrical resistance should decrease through the capillary. Consistent with our hypothesis, the current increases as EGaIn displaces the solution (Supporting Information,

Figure S5). Likewise, physically obstructing the withdrawal during recapillarity results in constant current.

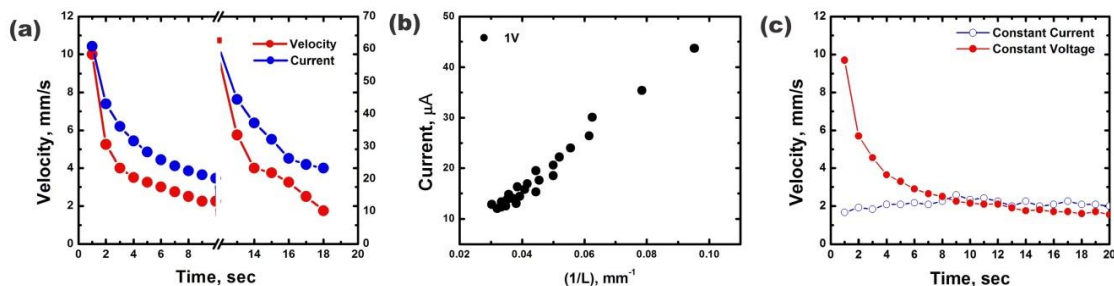


Figure 3. Effect of electrical length on the liquid metal withdrawal. **(a)** After withdrawing the metal for 10 s but before starting the second withdrawal, a copper wire (anode) inserted into the capillary shortens the electrical distance between the anode and the metal interface. We do not show the time spent inserting the electrode on the time axis. Restarting the withdrawal by application of a reductive potential ($t=13$ sec) to the liquid metal causes the velocity and current to mimic both the starting magnitude and decay profile of the initial withdrawal. **(b)** Plot of measured current versus inverse length of partially withdrawn metal yields a nearly linear relationship; linear best fit $R^2 = 0.97$. **(c)** A recapillarity experiment performed at constant current rather than constant voltage results in a nearly constant withdrawal velocity.

Given these results, we sought a mechanism to relate current to velocity. As the metal withdraws, the electrical length between the two electrodes increases and current decreases.

The current decreases proportional to velocity, as shown in Figure 3a. Figure 3b shows that current scales inversely with length (i.e., the length of the electrolyte in the capillary), as expected for a system following Ohm's law. Figure 3c shows that it is possible to attain constant withdrawal velocity by applying a constant current ($\sim 20\mu\text{A}$). These results illustrate the importance of current, but they do not explain why current is necessary.

Electro-osmotic Effects: First, electro-osmotic flow is a sensible consideration for fluid motion in a system driven by current. For several reasons, we reject electroosmosis as a primary driving force in this system. Appreciable electro-osmotic flow in DC systems usually requires high electric field strength; the electric field in this system is quite weak ($\sim 0.014\text{ V/mm}$) and increasing field strength does not proportionally increase flow velocity. The maximum demonstrated electro-osmotic flow rates are on the order of mm/s^{51} , whereas we observe velocities of tens of cm/s . Finally, electro-osmotic mobility declines with increasing electrolyte concentration and we observe greatly increased flow velocities at higher electrolyte concentrations (cf. Supporting Information Figure S2).

Electrochemical Effects and Meniscus Analysis: The dependence of withdrawal velocity on current is intuitive in the sense that the electrochemical reduction of the oxide necessitates current (i.e., Faradaic processes must occur), but it is less obvious why current must be

applied throughout the withdrawal. We initially expected that the current would remove the hemispherical oxide ‘cap’ that separates the metal and the solution, but in that case, the withdrawal should be approximately constant after an initial transient and show a dependence on the radii of curvature of both the meniscus and the reservoir. The need for continual current suggests that oxide must be removed continually.

The shape of the meniscus and velocity during the withdrawal provides some insight into the withdrawal mechanism. The four columns in Figure 4 represent different approaches for inducing withdrawal. All of the experiments begin with an empty capillary (Figure 4a-c) except those depicted in Figure 4d, which begin with a capillary prefilled with 1 M HCl. After injecting the metal into these capillaries, the metal assumes a hemispherical profile at rest (cf. Figure 2a). An oxide layer coats the hemispherical cap due to its contact with air. We also depict an oxide layer separating the metal from the capillary walls to help explain our interpretation of the withdrawal mechanism. Due to the presence of the oxide, the metal does not withdraw spontaneously from the capillaries. In contrast, Figure 4d shows that the presence of acid during injection keeps the metal oxide-free and the metal withdraws spontaneously and rapidly ($\sim 30\text{-}40$ cm/s) with a rounded meniscus the entire time.

Figure 4a shows the shape of the meniscus during recapillarity. The metal-electrolyte interface flattens (i.e., large radius of curvature), which is unexpected based on the large surface tension of the bare metal. We refer to the shape of the meniscus as flat but note that the opaque nature of the metal makes it difficult to determine the exact shape.

In a separate experiment, we blocked the outlet of the capillary to hinder the withdrawal (Figure 4b). The small pressure from injecting water via a syringe needle into the capillary causes the oxide-coated meniscus to artificially flatten prior to applying potential. This flattened meniscus is apparent at the onset of recapillarity. Upon application of a reductive potential, the metal does not withdraw because it is physically obstructed. The shape of the meniscus, however, slowly becomes more round, as shown in Figure 4b, which suggests the metal slowly pulls away from the wall over time and that reduction of oxide along the wall may be occurring.

We also observed a flat meniscus while inducing the withdrawal by the addition of 10mM acid after pre-filling an empty capillary with metal, as shown in Figure 4c. The acid causes the metal to withdraw in the absence of potential. If the oxide coated only the meniscus of the metal, then removing it via acid should cause rapid withdrawal. Instead, the withdrawal velocity is relatively slow (~ 3- 4 mm/min) compared to that obtained with a channel pre-filled with acid. The similarity of the shape of the menisci in Figure 4a and 4c suggests that electrocapillarity is not a primary cause of the shape of the meniscus observed during recapillarity⁴⁹.

These results, taken in sum, suggest that (1) there is oxide between the walls of the capillary and the metal, (2) upon removal of the oxide on the meniscus, the resulting bare metal wets the remaining oxide on the walls to create a non-hemispherical meniscus, and (3) the

reduction of the oxide on the walls limits the rate of withdrawal and may explain why the withdrawal velocity correlates only with applied current.

If there is an oxide between the metal and the walls of the capillary, then it likely forms during injection since the capillary walls are impermeable to oxygen. We speculate that the oxide layer on the leading meniscus of the metal adheres to the walls during injection and a new oxide reforms rapidly and repeatedly shears off as the metal fills the channel.

We performed an additional experiment to test for consistency of the presence of oxide between the metal and the walls of the channel. If this oxide layer exists, the withdrawal velocity during recapillarity should scale with radius rather than cross-sectional area of the capillary (for a given current) since the oxide surrounds the circumference of the metal plug. Using the conditions found in Figure 3c, we compared the withdrawal velocity at constant current (20 μA) for capillaries with small (260 μm) and large (1 mm) inner diameters, and found average withdrawal velocities of 3.8 mm/s and 2 mm/s, respectively, over a withdrawal distance of 4 cm. The ratio of withdrawal velocity (1:2) is much closer to scaling with perimeter (1:4) rather than cross sectional area (1:16). There are complications that come with such comparisons, however. First, a decrease in capillary diameter corresponds not only to a decrease in the circumferential length of the oxide but also to changes in viscous drag. Second, applying a constant current can also cause a fluctuation in voltage, which can lead to electrochemical reactions other than reduction of the oxide that contribute

to the current but do not influence the velocity. We are currently working to understand these subtleties.

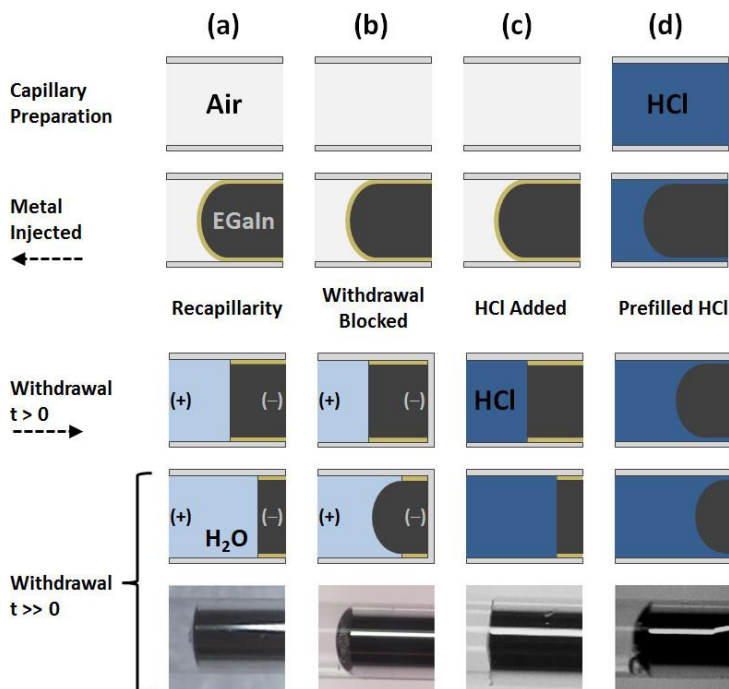


Figure 4. The shape of the meniscus during withdrawal provides mechanistic insight into recapillarity. The four columns correspond to four unique experiments. In columns (a-c) metal is injected right-to-left into an empty capillary tube, followed by addition of electrolyte. In column (d), the metal is injected into a capillary prefilled with 1 M HCl. In all cases, the meniscus is hemispherical after injection. (a) The meniscus is nearly flat during recapillarity (withdrawing left to right). (b) The capillary is physically blocked to keep the metal from withdrawing. Application of a reductive potential removes the oxide on the cap of the meniscus, and it begins to become round as the oxide is etched away from the wall. (c) The meniscus is also flat when withdrawal is induced by adding acid to the end of a capillary prefilled with metal (no voltage). (d) The meniscus is round when the metal withdraws spontaneously (no voltage) from a capillary prefilled with acid.

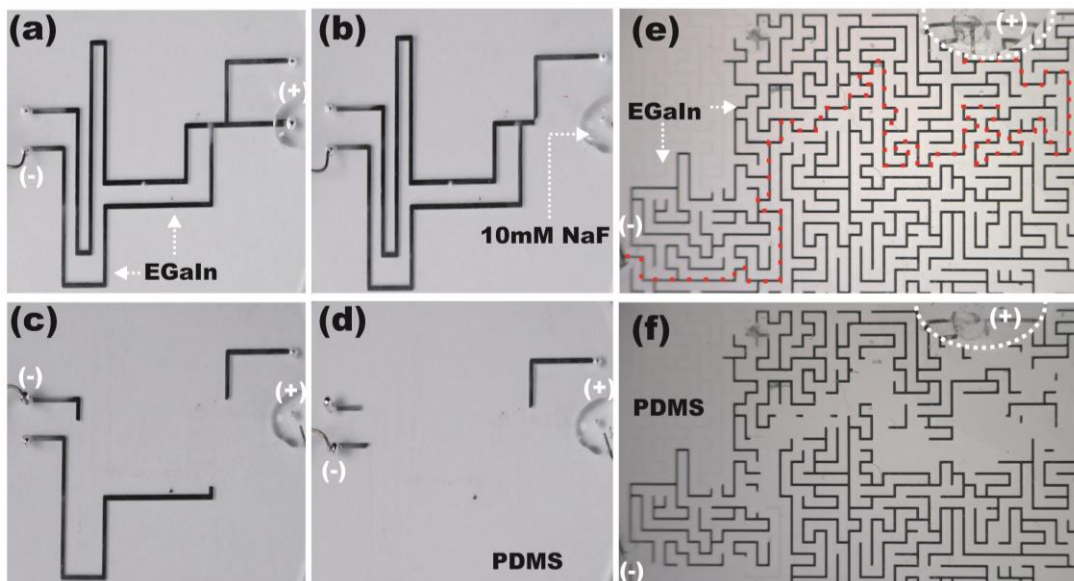


Figure 5. Two demonstrations of shape-reconfigurability of liquid metal microstructures by recapillarity. **(a)** A microfluidic channel of arbitrary shape is filled with liquid metal that is mechanically stabilized by its oxide skin. 10 mM NaF is added as working electrolyte and copper electrodes are attached to the inlet and outlet. **(b)** Applying $\sim 40 \mu\text{A}$ reductive current induces withdrawal. **(c-d)** Switching the position of the active electrode controls the withdrawal path. The withdrawal can be halted at any time by turning off the voltage. Only the metal in the electrical path withdraws when the voltage is turned on. **(e-f)** Withdrawal of liquid metal from a maze-shaped array of microchannels. The red dotted line as shown in **(e)** is the only electrically connected path through which the metal can be withdrawn. **(f)** Application of $40 \mu\text{A}$ induces withdrawal. Only the metal along the electrical path flows out of the device.

Demonstration: It is possible to use recapillarity to withdraw the metal along arbitrary paths by maintaining an electrically connected pathway. We created a complex metal shape to illustrate the ability to induce withdrawal of the metal along specific paths on demand. For example, Figure 5(a-d) shows that by arbitrarily switching the position of the electrodes, the directionality of withdrawal can be controlled to reconfigure the shape of the liquid metal. This concept can also be applied to a much more complicated microfluidic network of liquid metal microstructures as shown in Figure 5(e-f). The results of Figure 5f suggest that recapillarity enables fluids to ‘solve’ complex mazes by withdrawing along the shortest electrical path.

5.4 CONCLUSION

We demonstrate a simple approach to turn on and off capillary behavior of a liquid metal in microchannels, exploiting the reduction of a thin gallium oxide layer that forms spontaneously on EGaIn. Flow can be stopped or started arbitrarily using low voltages (~ 1 V), withdrawal speed can be controllably varied up to 30 cm/s, and the metal can withdraw selectively along complex paths with minimal disturbance to neighboring metal traces. Current-limiting effects, such as electrolyte concentration and electrical path length, are the most important factors governing the rate of withdrawal of the liquid metal. We speculate that this withdrawal requires current because of the need to continually reduce the thin oxide layer. The results suggest further that in addition to forming a cap on the meniscus of the metal, an oxide layer likely exists sandwiched between the bulk liquid metal and the sidewall

of the capillary, which may further explain why current is needed throughout the withdrawal process and why the meniscus flattens during withdrawal.

Recapillarity has several limitations. First, it requires electrolyte. Second, high withdrawal velocities require large applied currents, but large currents in dilute electrolytes may necessitate voltages exceeding the electrolysis voltage of water. Bubbles can disrupt the electrical circuit required to induce withdrawal of the metal; although this was not a serious issue for the conditions used in this chapter, it could pose problems for some applications. Finally, recapillarity induces capillary behavior, which implies that the metal will only flow in directions that lower the total interfacial energy.

Nevertheless, the ability to electrically control the position and velocity – and therefore the shape – of a liquid metal in microchannels is a promising development in the realization of a number of novel applications such as reconfigurable wires, antennas, sensors, actuators, soft robots, meta-materials, plasmonics, transient circuits, and micro pumps.

5.5 REFERENCES

- (1) Gravesen, P.; Branebjerg, J.; Jensen, O. S. Microfluidics-a Review. *J. Micromechanics Microengineering* **1993**, *3*, 168.
- (2) Zhao, B.; Moore, J. S.; Beebe, D. J. Surface-Directed Liquid Flow Inside Microchannels. *Science* **2001**, *291*, 1023–1026.
- (3) Sen, P.; Kim, C.-J. A Fast Liquid-Metal Droplet Microswitch Using EWOD-Driven Contact-Line Sliding. *J. Microelectromechanical Syst.* **2009**, *18*, 174–185.
- (4) Shabani, R.; Cho, H. J. Active Surface Tension Driven Micropump Using Droplet/meniscus Pressure Gradient. *Sens. Actuators B-Chem.* **2013**, *180*, 114–121.
- (5) Gallardo, B. S.; Gupta, V. K.; Eagerton, F. D.; Jong, L. I.; Craig, V. S.; Shah, R. R.; Abbott, N. L. Electrochemical Principles for Active Control of Liquids on Submillimeter Scales. *Science* **1999**, *283*, 57–60.
- (6) Stone, H. A.; Stroock, A. D.; Ajdari, A. Engineering Flows in Small Devices. *Annu. Rev. Fluid Mech.* **2004**, *36*, 381–411.
- (7) Zhang, C. S.; Xing, D.; Li, Y. Y. Micropumps, Microvalves, and Micromixers within PCR Microfluidic Chips: Advances and Trends. *Biotechnol. Adv.* **2007**, *25*, 483–514.
- (8) Sen, P.; Kim, C.-J. Microscale Liquid-Metal Switches -A Review. *IEEE Trans. Ind. Electron.* **2009**, *56*, 1314–1330.
- (9) Nie, Z.; Nijhuis, C. A.; Gong, J.; Chen, X.; Kumachev, A.; Martinez, A. W.; Narovlyansky, M.; Whitesides, G. M. Electrochemical Sensing in Chapter-Based Microfluidic Devices. *Lab. Chip* **2010**, *10*, 477–483.

- (10) Tang, S.-Y.; Sivan, V.; Khoshmanesh, K.; O'Mullane, A. P.; Tang, X.; Gol, B.; Eshtiaghi, N.; Lieder, F.; Petersen, P.; Mitchell, A.; et al. Electrochemically Induced Actuation of Liquid Metal Marbles. *Nanoscale* **2013**, *5*, 5949–5957.
- (11) Ho, C.-M.; Tai, Y.-C. Micro-Electro-Mechanical-Systems (mems) and Fluid Flows. *Annu. Rev. Fluid Mech.* **1998**, *30*, 579–612.
- (12) Hessel, V.; Löwe, H.; Schönfeld, F. Micromixers—a Review on Passive and Active Mixing Principles. *Chem. Eng. Sci.* **2005**, *60*, 2479–2501.
- (13) Cheng, S.; Wu, Z. Microfluidic Stretchable RF Electronics. *Lab. Chip* **2010**, *10*, 3227–3234.
- (14) Dickey, M. D.; Chiechi, R. C.; Larsen, R. J.; Weiss, E. A.; Weitz, D. A.; Whitesides, G. M. Eutectic Gallium-Indium (EGaIn): A Liquid Metal Alloy for the Formation of Stable Structures in Microchannels at Room Temperature. *Adv. Funct. Mater.* **2008**, *18*, 1097–1104.
- (15) Chiechi, R. C.; Weiss, E. A.; Dickey, M. D.; Whitesides, G. M. Eutectic Gallium-Indium (EGaIn): A Moldable Liquid Metal for Electrical Characterization of Self-Assembled Monolayers. *Angew. Chem. Int. Ed.* **2008**, *47*, 142–144.
- (16) French, S. J.; Saunders, D. J.; Ingle, G. W. The System Gallium-Indium. *J. Phys. Chem.* **2002**, *42*, 265–274.
- (17) Spells, K. E. Determination of the Viscosity of Liquid Gallium over an Extended Range of Temperature. *Proc. Phys. Soc. Lond.* **1936**, *48*, 299–311.
- (18) Koster, J. N. Directional Solidification and Melting of Eutectic GaIn. *Cryst. Res. Technol.* **1999**, *34*, 1129–1140.

- (19) Zrnic, D.; Swatik, D. S. Resistivity and Surface Tension of the Eutectic Alloy of Gallium and Indium. *J. -Common Met.* **1969**, *18*, 67–68.
- (20) *CRC Handbook of Chemistry and Physics, 92nd Edition - CRC Press Book.*
- (21) Yun, K.-S.; Cho, I.-J.; Bu, J.-U.; Kim, C.-J.; Yoon, E. A Surface-Tension Driven Micropump for Low-Voltage and Low-Power Operations. *J. Microelectromechanical Syst.* **2002**, *11*, 454 – 461.
- (22) Arscott, S.; Gaudet, M. Electrowetting at a Liquid Metal-Semiconductor Junction. *Appl. Phys. Lett.* **2013**, *103*, 074104.
- (23) Cumby, B. L.; Hayes, G. J.; Dickey, M. D.; Justice, R. S.; Tabor, C. E.; Heikenfeld, J. C. Reconfigurable Liquid Metal Circuits by Laplace Pressure Shaping. *Appl. Phys. Lett.* **2012**, *101*, 174102–174102–5.
- (24) Regan, M. J.; Tostmann, H.; Pershan, P. S.; Magnussen, O. M.; DiMasi, E.; Ocko, B. M.; Deutsch, M. X-Ray Study of the Oxidation of Liquid-Gallium Surfaces. *Phys. Rev. B Condens. Matter* **1997**, *55*, 10786–10790.
- (25) Cademartiri, L.; Thuo, M. M.; Nijhuis, C. A.; Reus, W. F.; Tricard, S.; Barber, J. R.; Sodhi, R. N. S.; Brodersen, P.; Kim, C.; Chiechi, R. C.; et al. Electrical Resistance of Ag-TS-S(CH₂)(n-1)CH₃//Ga₂O₃/EGaIn Tunneling Junctions. *J. Phys. Chem. C* **2012**, *116*, 10848–10860.
- (26) Giguere, P. A.; Lamontagne, D. Polarography with a Dropping Gallium Electrode. *Science* **1954**, *120*, 390–391.

- (27) Shen, W.; Edwards, R. T.; Kim, C.-J. Electrostatically Actuated Metal-Droplet Microswitches Integrated on CMOS Chip. *J. Microelectromechanical Syst.* **2006**, *15*, 879–889.
- (28) Dickey, M. D. Emerging Applications of Liquid Metals Featuring Surface Oxides. *ACS Appl. Mater. Interfaces* **2014**.
- (29) So, J. H.; Thelen, J.; Qusba, A.; Hayes, G. J.; Lazzi, G.; Dickey, M. D. Reversibly Deformable and Mechanically Tunable Fluidic Antennas. *Adv. Funct. Mater.* **2009**, *19*, 3632–3637.
- (30) Ladd, C.; So, J.-H.; Muth, J.; Dickey, M. D. 3D Printing of Free Standing Liquid Metal Microstructures. *Adv. Mater.* **2013**, *25*, 5081–5085.
- (31) Boley, J. W.; White, E. L.; Chiu, G. T.-C.; Kramer, R. K. Direct Writing of Gallium-Indium Alloy for Stretchable Electronics. *Adv. Funct. Mater.* **2014**, *24*, 3501–3507.
- (32) Kim, H.-J.; Son, C.; Ziaie, B. A Multiaxial Stretchable Interconnect Using Liquid-Alloy-Filled Elastomeric Microchannels. *Appl. Phys. Lett.* **2008**, *92*, 011904–011904–3.
- (33) Zhu, S.; So, J.-H.; Mays, R.; Desai, S.; Barnes, W. R.; Pourdeyhimi, B.; Dickey, M. D. Ultrastretchable Fibers with Metallic Conductivity Using a Liquid Metal Alloy Core. *Adv. Funct. Mater.* **2012**, n/a–n/a.
- (34) Majidi, C.; Kramer, R.; Wood, R. J. A Non-Differential Elastomer Curvature Sensor for Softer-than-Skin Electronics. *Smart Mater. Struct.* **2011**, *20*, 105017.

- (35) Majidi, C.; Wood, R. J. Tunable Elastic Stiffness with Microconfined Magnetorheological Domains at Low Magnetic Field. *Appl. Phys. Lett.* **2010**, *97*, 164104–164104–3.
- (36) Wang, J.; Liu, S.; Vardeny, Z. V.; Nahata, A. Liquid Metal-Based Plasmonics. *Opt. Express* **2012**, *20*, 2346–2353.
- (37) Khan, M. R.; Hayes, G. J.; So, J.-H.; Lazzi, G.; Dickey, M. D. A Frequency Shifting Liquid Metal Antenna with Pressure Responsiveness. *Appl. Phys. Lett.* **2011**, *99*, 013501–013503.
- (38) Khan, M. R.; Hayes, G. J.; Zhang, S.; Dickey, M. D.; Lazzi, G. A Pressure Responsive Fluidic Microstrip Open Stub Resonator Using a Liquid Metal Alloy. *IEEE Microw. Wirel. Compon. Lett.* **2012**, *22*, 577–579.
- (39) Wang, J.; Liu, S.; Guruswamy, S.; Nahata, A. Reconfigurable Liquid Metal Based Terahertz Metamaterials via Selective Erasure and Refilling to the Unit Cell Level. *Appl. Phys. Lett.* **2013**, *103*, 221116.
- (40) Kramer, R. K.; Boley, J. W.; Stone, H. A.; Weaver, J. C.; Wood, R. J. Effect of Microtextured Surface Topography on the Wetting Behavior of Eutectic Gallium-Indium Alloys. *Langmuir* **2013**.
- (41) Kim, D.; Lee, D.-W.; Choi, W.; Lee, J.-B. A Super-Lyophobic PDMS Micro-Tunnel as a Novel Microfluidic Platform for Oxidized Galinstan. In *2012 IEEE 25th International Conference on Micro Electro Mechanical Systems (MEMS)*; 2012; pp. 1005–1008.

- (42) Kim, D.; Jung, D.; Yoo, J. H.; Lee, Y.; Choi, W.; Lee, G. S.; Yoo, K.; Lee, J.-B. Stretchable and Bendable Carbon Nanotube on PDMS Super-Lyophobic Sheet for Liquid Metal Manipulation. *J. Micromechanics Microengineering* **2014**, *24*, 055018.
- (43) Doudrick, K.; Liu, S.; Mutunga, E. M.; Klein, K. L.; Damle, V.; Varanasi, K. K.; Rykaczewski, K. Different Shades of Oxide: From Nanoscale Wetting Mechanisms to Contact Printing of Gallium-Based Liquid Metals. *Langmuir* **2014**, *30*, 6867–6877.
- (44) Li, G.; Parmar, M.; Kim, D.; Lee, J.-B. (JB); Lee, D.-W. PDMS Based Coplanar Microfluidic Channels for the Surface Reduction of Oxidized Galinstan. *Lab. Chip* **2013**, *14*, 200–209.
- (45) Jackel, J. L.; Hackwood, S.; Beni, G. Electrowetting Optical Switch. *Appl. Phys. Lett.* **1982**, *40*, 4–5.
- (46) Maltezos, G.; Nortrup, R.; Jeon, S.; Zaumseil, J.; Rogers, J. A. Tunable Organic Transistors That Use Microfluidic Source and Drain Electrodes. *Appl. Phys. Lett.* **2003**, *83*, 2067–2069.
- (47) Rodrigo, D.; Jofre, L.; Cetiner, B. A. Circular Beam-Steering Reconfigurable Antenna With Liquid Metal Parasitics. *IEEE Trans. Antennas Propag.* **2012**, *60*, 1796–1802.
- (48) Pourbaix, M. *Atlas of Electrochemical Equilibria in Aqueous Solutions*; Second English Edition.; Natl Assn of Corrosion: TX, USA, 1974; Vol. 16.1.
- (49) Frumkin, A.; Polianovskaya, N.; Grigoryev, N.; Bagotskaya, I. Electrocapillary Phenomena on Gallium. *Electrochimica Acta* **1965**, *10*, 793–802.

- (50) Khan, M.; Eaker, C.; Bowden, E.; Dickey, M. Giant and Switchable Surface Activity of Liquid Metal via Surface Oxidation. *Proc. Natl. Acad. Sci.* **2014**, *111*, 14047–14051.
- (51) Castellanos, A. *Electrohydrodynamics*; Springer, 1998.
- (52) Tabeling, P. *Introduction to Microfluidics*; Reprint.; Oxford University Press, USA, 2010.
- (53) Mugele, F.; Baret, J.-C. Electrowetting: From Basics to Applications. *J. Phys. Condens. Matter* **2005**, *17*, R705–R774.
- (54) Sivan, V.; Tang, S.-Y.; O’Mullane, A. P.; Petersen, P.; Eshtiaghi, N.; Kalantar-zadeh, K.; Mitchell, A. Liquid Metal Marbles. *Adv. Funct. Mater.* **2013**, *23*, 144–152.
- (55) Tang, S.-Y.; Khoshmanesh, K.; Sivan, V.; Petersen, P.; O’Mullane, A. P.; Abbott, D.; Mitchell, A.; Kalantar-zadeh, K. Liquid Metal Enabled Pump. *Proc. Natl. Acad. Sci.* **2014**, *111*, 3304.
- (56) Tsai, J. T. H.; Ho, C.-M.; Wang, F.-C.; Liang, C.-T. Ultrahigh Contrast Light Valve Driven by Electrocapillarity of Liquid Gallium. *Appl. Phys. Lett.* **2009**, *95*, 251110.
- (57) Wan, Z.; Zeng, H.; Feinerman, A. Area-Tunable Micromirror Based on Electrowetting Actuation of Liquid-Metal Droplets. *Appl. Phys. Lett.* **2006**, *89*, 201107–201107–3.
- (58) Kramer, R. K.; Boley, J. W.; Stone, H. A.; Weaver, J. C.; Wood, R. J. Effect of Microtextured Surface Topography on the Wetting Behavior of Eutectic Gallium–Indium Alloys. *Langmuir* **2014**, *30*, 533–539.

CHAPTER 6

LOCALIZED INSTABILITIES OF LIQUID METAL

FILMS VIA IN-PLANE RECAPILLARITY*

**This work is in progress. Contributor to this work: J. Bell.*

6.1 ABSTRACT

This chapter describes a simple method to turn on or off instabilities in thin films of a liquid metal alloy (eutectic gallium indium, EGaIn) using low voltages. These instabilities can be localized to pattern films of the metal. The patterning process begins by spreading a film of the metal on a substrate. A thin oxide layer that forms spontaneously on the surface of the metal stabilizes the film despite the large surface tension and low viscosity of the metal. In the absence of the oxide, the metal film beads up to minimize interfacial energy. The localized electrochemical reduction of the oxide in the presence of electrolyte induces capillary withdrawal of the metal (so-called ‘recapillarity’). The withdrawal stops in the absence of potential due to the reformation of the oxide. The resulting patterns and shapes of the liquid metal can be controlled by the placement of the counter electrode with respect to the metal, as well as the duration of the applied current. This patterning method is similar in spirit to the Etch-a-Sketch™ toy, but is distinguished by the use of capillary withdrawal rather than physical scribing. An appeal of this approach is its simplicity: it is possible to carry out the patterning utilizing only AA batteries, salt water, and two wires as electrodes. A quantitative analysis of the system suggests that the withdrawal velocity of EGaIn relates directly to the current density. The dependence of velocity on current density, the shape of the withdrawing interface, and the independence of withdrawal rate on film thickness suggests the electrochemical reduction of the oxide layer between the substrate and metal dictate the rate of withdrawal. The technique may be useful for patterning the liquid into 2D shapes for soft, stretchable, or flexible micro-components composed of metal and represents a new way to induce thin film instabilities in a controlled manner.

6.2 INTRODUCTION

This chapter describes a simple method to control instabilities in thin films of liquid metal composed of eutectic gallium indium (EGaIn). These instabilities can be harnessed to pattern the metal. EGaIn – a low toxicity alternative to mercury - is one of several alloys of gallium that is liquid at room temperature with a low viscosity and low vapor pressure¹. Metals that are liquid at room temperature are interesting because they have metallic electrical properties, but can flow like liquids and can therefore be patterned and utilized in ways that are not possible with solid metals. The ability to control the shape of the metal is important for a variety of applications including soft electrodes²⁻⁴, microfluidic components^{5,6}, reconfigurable electronics^{7,8}, soft robotics⁹, stretchable wires and antennas¹⁰⁻¹⁴, self-healing circuits¹⁵, and interconnects^{16,17}.

There are a number of ways to pattern the metal including direct writing¹⁸, stencil lithography¹⁹⁻²¹, 3D printing^{19,22}, laser ablation²³, micro contact printing²⁴, injection²⁵, embossing and molding^{26,27}. The approach described in this chapter is one of the few ‘subtractive’ methods to pattern the metal, although unlike conventional ‘subtractive’ methods, the approach here maintains conservation of mass of metal on the substrate.

The method starts with a thin film of the metal produced by spreading a drop of EGaIn onto a glass slide. Fluids prefer to adopt shapes that minimize surface energy. However, the presence of a thin^{28,29} (<1 nm thick, according to x-ray studies²⁸) oxide skin that forms spontaneously on the surface of the liquid metal holds it in metastable shapes, such as the

thin films used here. The oxide also likely lowers the interfacial tension of the metal³⁰. We show it is possible to locally induce instabilities in the film by electrochemically removing the oxide using an electrode as a ‘scribe’ to pattern the metal. Unlike conventional scribes, which physically scratch away material, the ‘scribe’ described here never touches the film, but instead localizes electrochemical reactions that induce localized instabilities. Upon removal of the oxide from the surface, the exposed metal returns to a state of high interfacial energy and withdraws locally and spontaneously to minimize its surface energy, but stops flowing in the absence of a reducing potential due to the spontaneous reformation of the oxide. An appeal of this approach is its simplicity: it requires only a battery, salt water, and two wires. It is also appealing because the application of voltage can turn on or off the instability at any time and therefore may represent a new way to study thin film instabilities. Electrochemical processes can pattern solid metals and other surfaces in a process called electrochemical micromachining³¹. Electrochemical micromachining locally dissolves and shapes metals through an anodic reaction (i.e. oxidation). Scanning probe methods^{32,33} also remove materials to achieve surface modification³⁴ (i.e., subtractive methods). In contrast, our approach removes only the surface metal oxide via a localized cathodic reaction (i.e., reduction) and therefore results in minimal loss of material while allowing the metal to flow to a new location.

The patterning approach described here relates to the classical dewetting phenomena of polymeric films³⁵, which are typically trapped in an energetically unfavorable state (i.e., a film) until the temperature exceeds a sufficiently high value to enable flow of the polymer.

In contrast, the method presented here induces destabilization using electrochemistry. We call this technique ‘recapillarity’ because the reduction of the oxide induces capillary action.^{30,36} In addition to demonstrating recapillarity for patterning films, experimental evidence shows that the rate of withdrawal depends strongly on the current density, which provides insight into the chemical composition of the interface between the metal and substrate.

6.3 RESULTS

Figure 1 depicts the in-plane patterning of liquid metal using localized electrochemistry. To demonstrate the principle, we spread a drop of EGaIn (Figure 1(a)) on a glass slide to create a thin film (Figure 1(b)). The films are generally smooth but often have some pin holes. A copper wire contacts the edge of the film, thereby making the EGaIn the working cathode. On a separate copper wire, a small drop of electrolyte (i.e., water or salt solution) wet the tip of the wire after dipping it in a reservoir of electrolyte. Contacting the fluid on the tip of the wire with the film completes the electrochemical circuit as shown in Figure 1(c). Application of a reductive bias to the film removes locally the oxide skin, which causes capillary withdrawal of the metal. We draw the letters “NCSU” and a straight line in the film by guiding the tip across the surface by hand. We occasionally re-dip the tip into the electrolyte to replenish it (similar to an old fashioned ink-well pen) as shown in Figure 1(d).

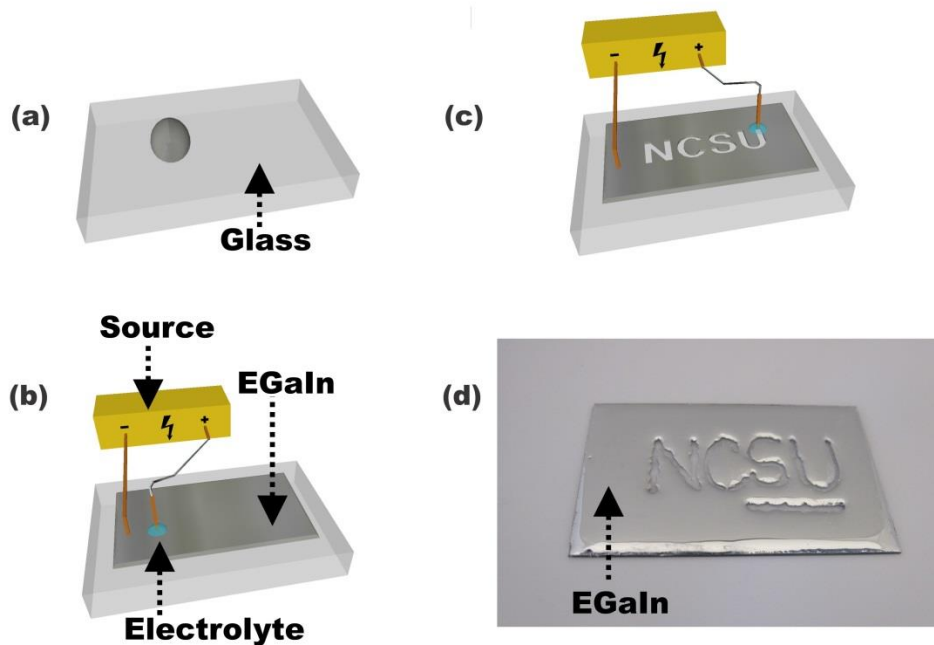


Figure 1. (a-c) Cartoon depiction of in-plane recapillarity. (a) A droplet of liquid metal is (b) smeared on a glass substrate. One of the two copper wires from a voltage source touches the metal film directly and the other one carries a drop of electrolyte on its tip that contacts the film to complete the circuit. While the voltage is on (d) patterning of “NCSU” is achieved by localized reduction of the oxide and capillary withdrawal of the metal. (b) Photograph of in-plane patterning on a 2 x 3” glass slide.

We sought to quantify and understand the primary variable(s) that control the velocity of withdrawal of the film during reduction. To improve repeatability, we built a spreader to smear drops of EGaIn (~0.3 ml) onto a glass slide cleaned with an oxygen plasma (cf., **Fig. 2a(i)**). The spreader consists of a glass tube ‘roller’ (diameter ~ 12mm) held by a Plexiglas[®] structure that sets the spacing between the glass slide and the roller to $\approx 90 \mu\text{m}$ (although the measured thickness of the film was found to be ~ 110 to 120 μm). After

spreading, we placed approximately 0.2 ml of 10 mM sodium fluoride (NaF) solution on the metal. This electrolyte formed a puddle covering the majority, but not the entire area of the EGaIn film (Figure 2a(ii)). The liquid metal served as the cathode by connecting one end of copper wire to the dry edge of the metal and the other end to a power supply. A 250- μ m-diameter copper wire touched the electrolyte to form the anode without making direct contact with the EGaIn. An applied bias induces withdrawal of the metal away from the anode, as depicted in Figure 2a(iii). Turning off the voltage stops the withdrawal.

A cathodic voltage of 1V proved to be sufficient to drive the electrochemical reduction of the oxide. The standard reduction potential of gallium is 0.52V vs. Ag/AgCl, which is lower than the standard reduction potential of water (1.23V vs. Ag/AgCl). We utilized a two electrode system in this study due to challenges of using a reference electrode with thin films of electrolyte. A two electrode system is also simpler and therefore more accessible to others who might use this method. Experiments performed with a reference electrode (i.e., three electrode system) did not cause significantly different behavior.

Application of a potential to a stationary counter electrode placed just above the film causes the metal to withdraw rapidly (1-10 mm/s) and radially away from the tip of the electrode to form a hole. We used a video camera to record the movement of the metal while a potentiostat simultaneously measured the electrochemical current. Figure 2b(i) shows four of the raw frames (on top) extracted from a video and processed (on bottom)

by an image processing software (ImageJ) that estimated the area of the expanding hole.

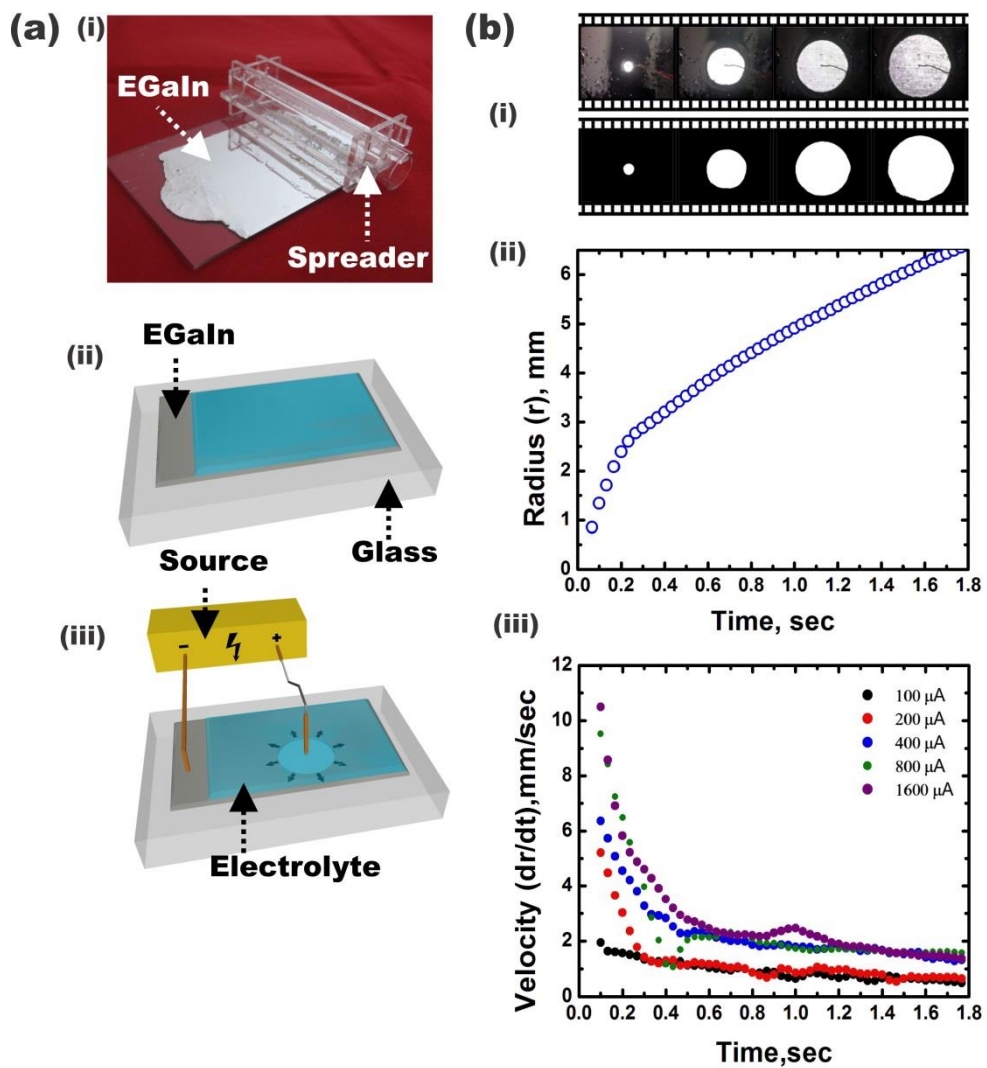


Figure 2. Photograph of the (a) EGaln spreader that can create a $\approx 120\mu\text{m}$ thin film. (ii) 10 mM NaF solution covers the majority of the film, except for (iii) only a small portion which serves as a contact point for a Cu wire. The film itself is the cathode and another

piece of Cu wire touches the electrolyte to serve as an anode. (b) Four frames from a typical withdrawal experiment at regular time intervals. Initial (i) raw frames are processed in ImageJ for analysis. (ii) Corresponding plot of radius (of the hole) vs. time, and (iii) Plots of velocity of withdrawal vs. time for different applied currents.

Figure 2b(ii) is a representative plot of the average radius of the circular hole versus time. It is apparent that the radius expands non-linearly with respect to time and that the velocity slows as the front moves away from the stationary counter electrode. Figure 2b(iii) plots the radial velocity of withdrawal versus time. The velocity of withdrawal is the instantaneous slope of the plot of radius versus time; that is, the radial rate of expansion.

Figure 2b(iii) shows that the velocity increases with current and decreases with time. The dependence on current is physically intuitive since the withdrawal occurs due to the removal of the oxide, which is a Faradaic process. The dependence on time suggests that the current density may be a more important factor since the circumference of the hole gets larger with time and therefore the current distributes over a larger circumference of the withdrawing metal rim. We therefore hypothesized that the rate of expansion of the hole depends primarily on the current *density*.

Figure 3(a) plots the velocity of withdrawal versus current density, which is calculated by normalizing the current by the product of the instantaneous circumference and the height of the film. The plot underscores the importance of current density across a range

of experimental conditions, including experiments with constant voltage and constant current.

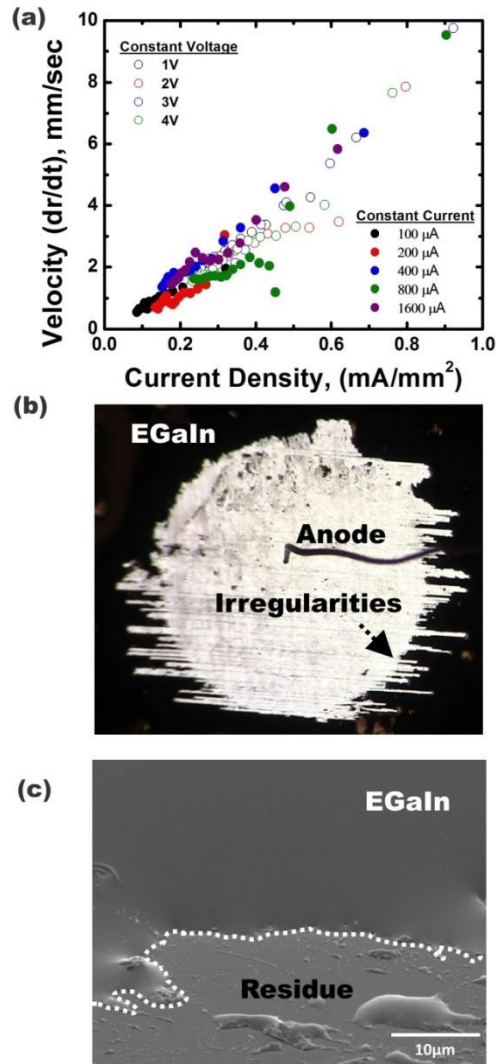


Figure 3: a) Plots of velocity of withdrawal (i.e., radial rate of expansion) vs. current density for different applied currents and applied voltages, showing linear correlation. b) A sample frame from the video of withdrawal, showing an extreme case of withdrawal

irregularities. c) Scanning-electron microscope (SEM) image of the leading edge of the EGaIn film after a partial withdrawal.

While measuring the withdrawal behavior, we made two unexpected observations: Firstly, the metal assumes a low (wetting) contact angle along the perimeter of the withdrawing circle. Although the angle is difficult to quantify, it is apparent from the scanning electron micrograph in Fig. 3c that the metal assumes a wetting contact angle ($<90^\circ$). This result is surprising because it is well known that in the complete absence of the oxide, the metal adopts a large contact angle on glass surfaces (~ 140 degrees³⁷). During the withdrawal, the metal should rapidly adopt a large contact angle in the absence of the oxide. The wetting contact angle suggests the metal may be resting primarily on its own oxide layer³⁸. Recent studies suggest the interfacial tension between the metal and the interior of its own oxide may be low³⁰, which could explain this wetting contact angle.

Secondly, the metal did not always withdraw in a perfect circle, as shown in Figure 3(b). This result is unexpected since a fluid with a large surface tension should adopt a shape that minimizes surface energy. The ‘fingers’ around the circumference of the metal are parallel to the direction of shear applied to form the film. It is apparent that these fingers arise from varying rates of withdrawal. We reasoned that regions that advance faster may be due to regions of thin oxide (or no oxide) and likewise, regions that advance slower rest on a layer of surface oxide. Others have shown that spreading metal on a

surface breaks the surface oxide, resulting in a non-uniform oxide layer between the metal and substrate³⁸.

We sought to understand the presence of these streaks lines by repeating the experiments on an oxygen permeable substrate (polydimethylsiloxane, PDMS; Sylgard-184). An oxygen permeable substrate ensures that the liquid metal is conformally covered with oxide. No streak lines occurred during withdrawal on PDMS, which suggests a conformal oxide layer between the metal and PDMS. We repeated this experiment at least 10 times. In contrast, irregularities (Figure 3b) occurred in approximately ~30% of the experiments performed on glass. Deviations of a few experimental data points (e.g., 800 μ A, 2V and 3V) in Figure 2a are attributed to this effect. The presence of residue on the substrate (apparent in both Fig 3c and Fig 2b(i)) is also consistent with the oxide being non-uniform below the metal.

Finally, we performed withdrawal experiments with varying amounts of liquid metal (from a volume of 0.25ml to 1.7ml) to vary the thickness of the metal while keeping all other parameters constant. The capillary forces in a thin film should be larger than a thick film. Yet, the velocity (~ 1.1 mm/s average) did not vary as a function of film thickness except for a very thick film (i.e., 1.7ml of metal) which behaved differently. This result, combined with (1) the dependency of the withdrawal velocity on current and (2) the wetting of the withdrawing interface to the substrate suggests that the removal of the oxide under the metal

dictates the rate of withdrawal. That is, the metal wets this oxide and only withdraws when the electrochemical reactions remove the underlying layer of oxide.

6.4 CONCLUSION

This chapter demonstrates a simple approach for patterning films of a liquid metal alloy by locally reducing the surface oxide of the metal. Removal of the oxide induces capillary withdrawal of the metal from the counter electrode until the voltage is turned off; we call this effect recapillarity because of the use of reduction reactions to induce capillary action. We show it is possible to use a ‘scribe’ – that is, a copper wire dipped in electrolyte—to locally reduce the film and induce withdrawal. We showed that the instantaneous rate of withdrawal of an EGaIn film is approximately proportional to the current density and can be controlled by applied voltage or current.

This method does not provide the precision or resolution of other patterning methods, but it does have the appeal of being simple. We created all the patterns and shapes in this study manually, i.e. the motion of the anode and the voltage applied were controlled by hand. The quality of the structures should improve with more precise control of the position of the anode and current. We only performed our experiments on glass slides and PDMS films, but we expect that the method could extend to other substrates onto which EGaIn films can be spread. In addition to patterning the metal, this method also provides a tool to study dewetting of films in a controlled manner at room temperature. Finally, the unusual dewetting observed in Figure 3b suggest that (1) there may be regions between the metal

and substrate that have oxide and some that do not, (2) chemically patterned substrates may seed secondary patterns by controlling the wetting (or dewetting) properties of the substrate, and (3) the rate of withdrawal is dictated by the reduction of the oxide between the metal and substrate.

6.5 REFERENCES

- (1) Dickey, M. D.; Chiechi, R. C.; Larsen, R. J.; Weiss, E. A.; Weitz, D. A.; Whitesides, G. M. Eutectic Gallium-Indium (EGaIn): A Liquid Metal Alloy for the Formation of Stable Structures in Microchannels at Room Temperature. *Adv. Funct. Mater.* **2008**, *18*, 1097–1104.
- (2) Chiechi, R. C.; Weiss, E. A.; Dickey, M. D.; Whitesides, G. M. Eutectic Gallium-Indium (EGaIn): A Moldable Liquid Metal for Electrical Characterization of Self-Assembled Monolayers. *Angew. Chem. Int. Ed.* **2008**, *47*, 142–144.
- (3) Wan, A.; Jiang, L.; Sangeeth, C. S. S.; Nijhuis, C. A. Reversible Soft Top-Contacts to Yield Molecular Junctions with Precise and Reproducible Electrical Characteristics. *Adv. Funct. Mater.* **2014**, *24*, 4442–4456.
- (4) Zhang, Y.; Zhao, Z.; Fracasso, D.; Chiechi, R. C. Bottom-Up Molecular Tunneling Junctions Formed by Self-Assembly. *Isr. J. Chem.* **2014**, *54*, 513–533.
- (5) So, J.-H.; Dickey, M. D. Inherently Aligned Microfluidic Electrodes Composed of Liquid Metal. *Lab Chip* **2011**, *11*, 905–911.
- (6) Cheng, S.; Wu, Z. Microfluidic Stretchable RF Electronics. *Lab. Chip* **2010**, *10*, 3227–3234.
- (7) Khan, M. R.; Hayes, G. J.; So, J.-H.; Lazzi, G.; Dickey, M. D. A Frequency Shifting Liquid Metal Antenna with Pressure Responsiveness. *Appl. Phys. Lett.* **2011**, *99*, 013501.

- (8) Khan, M. R.; Hayes, G. J.; Zhang, S.; Dickey, M. D.; Lazzi, G. A Pressure Responsive Fluidic Microstrip Open Stub Resonator Using a Liquid Metal Alloy. *IEEE Microw. Wirel. Compon. Lett.* **2012**, *22*, 577–579.
- (9) Majidi, C. Soft Robotics: A Perspective—Current Trends and Prospects for the Future. *Soft Robot.* **2013**, *1*, 5–11.
- (10) Zhu, S.; So, J.-H.; Mays, R.; Desai, S.; Barnes, W. R.; Pourdeyhimi, B.; Dickey, M. D. Ultrastretchable Fibers with Metallic Conductivity Using a Liquid Metal Alloy Core. *Adv. Funct. Mater.* **2013**, *23*, 2308–2314.
- (11) Mineart, K. P.; Lin, Y.; Desai, S. C.; Krishnan, A. S.; Spontak, R. J.; Dickey, M. D. Ultrastretchable, Cyclable and Recyclable 1- and 2-Dimensional Conductors Based on Physically Cross-Linked Thermoplastic Elastomer Gels. *Soft Matter* **2013**, *9*, 7695.
- (12) So, J. H.; Thelen, J.; Qusba, A.; Hayes, G. J.; Lazzi, G.; Dickey, M. D. Reversibly Deformable and Mechanically Tunable Fluidic Antennas. *Adv. Funct. Mater.* **2009**, *19*, 3632–3637.
- (13) Kubo, M.; Li, X.; Kim, C.; Hashimoto, M.; Wiley, B. J.; Ham, D.; Whitesides, G. M. Stretchable Microfluidic Radiofrequency Antennas. *Adv. Mater.* **2010**, *22*, 2749–2752.
- (14) Cheng, S.; Rydberg, A.; Hjort, K.; Wu, Z. Liquid Metal Stretchable Unbalanced Loop Antenna. *Appl. Phys. Lett.* **2009**, *94*, 144103–144103–3.
- (15) Palleau, E.; Reece, S.; Desai, S. C.; Smith, M. E.; Dickey, M. D. Self-Healing Stretchable Wires for Reconfigurable Circuit Wiring and 3D Microfluidics. *Adv. Mater.* **2013**, *25*, 1589–1592.

- (16) Zhang, B.; Dong, Q.; Korman, C. E.; Li, Z.; Zaghoul, M. E. Flexible Packaging of Solid-State Integrated Circuit Chips with Elastomeric Microfluidics. *Sci. Rep.* **2013**, *3*.
- (17) Kim, H.-J.; Son, C.; Ziaie, B. A Multiaxial Stretchable Interconnect Using Liquid-Alloy-Filled Elastomeric Microchannels. *Appl. Phys. Lett.* **2008**, *92*, 011904–011904–3.
- (18) Boley, J. W.; White, E. L.; Chiu, G. T.-C.; Kramer, R. K. Direct Writing of Gallium-Indium Alloy for Stretchable Electronics. *Adv. Funct. Mater.* **2014**, *24*, 3501–3507.
- (19) Jeong, S. H.; Hagman, A.; Hjort, K.; Jobs, M.; Sundqvist, J.; Wu, Z. Liquid Alloy Printing of Microfluidic Stretchable Electronics. *Lab. Chip* **2012**, *12*, 4657–4664.
- (20) Roberts, P.; Damian, D. D.; Shan, W.; Lu, T.; Majidi, C. Soft-Matter Capacitive Sensor for Measuring Shear and Pressure Deformation. In *2013 Ieee International Conference on Robotics and Automation (icra)*; Ieee: New York, 2013; pp. 3529–3534.
- (21) Kramer, R. K.; Majidi, C.; Wood, R. J. Masked Deposition of Gallium-Indium Alloys for Liquid-Embedded Elastomer Conductors. *Adv. Funct. Mater.* **2013**, *23*, 5292–5296.
- (22) Ladd, C.; So, J.-H.; Muth, J.; Dickey, M. D. 3D Printing of Free Standing Liquid Metal Microstructures. *Adv. Mater.* **2013**, *25*, 5081–5085.
- (23) Lu, T.; Finkenauer, L.; Wissman, J.; Majidi, C. Rapid Prototyping for Soft-Matter Electronics. *Adv. Funct. Mater.* **2014**, *24*, 3351–3356.
- (24) Tabatabai, A.; Fassler, A.; Usiak, C.; Majidi, C. Liquid-Phase Gallium–Indium Alloy Electronics with Microcontact Printing. *Langmuir* **2013**, *29*, 6194–6200.

- (25) Wang, J.; Liu, S.; Guruswamy, S.; Nahata, A. Reconfigurable Liquid Metal Based Terahertz Metamaterials via Selective Erasure and Refilling to the Unit Cell Level. *Appl. Phys. Lett.* **2013**, *103*, 221116.
- (26) Gozen, B. A.; Tabatabai, A.; Ozdoganlar, O. B.; Majidi, C. High-Density Soft-Matter Electronics with Micron-Scale Line Width. *Adv. Mater.* **2014**, n/a–n/a.
- (27) Fassler, A.; Majidi, C. 3D Structures of Liquid-Phase GaIn Alloy Embedded in PDMS with Freeze Casting. *Lab. Chip* **2013**, *13*, 4442–4450.
- (28) Regan, M. J.; Tostmann, H.; Pershan, P. S.; Magnussen, O. M.; DiMasi, E.; Ocko, B. M.; Deutsch, M. X-Ray Study of the Oxidation of Liquid-Gallium Surfaces. *Phys. Rev. B Condens. Matter* **1997**, *55*, 10786–10790.
- (29) Regan, M. J.; Pershan, P. S.; Magnussen, O. M.; Ocko, B. M.; Deutsch, M.; Berman, L. E. X-Ray Reflectivity Studies of Liquid Metal and Alloy Surfaces. *Phys. Rev. B* **1997**, *55*, 15874–15884.
- (30) Khan, M.; Eaker, C.; Bowden, E.; Dickey, M. Giant and Switchable Surface Activity of Liquid Metal via Surface Oxidation. *Proc. Natl. Acad. Sci.* **2014**, *111*, 14047–14051.
- (31) Schuster, R.; Kirchner, V.; Allongue, P.; Ertl, G. Electrochemical Micromachining. *Science* **2000**, *289*, 98–101.
- (32) Eigler, D. M.; Schweizer, E. K. Positioning Single Atoms with a Scanning Tunnelling Microscope. *Nature* **1990**, *344*, 524–526.
- (33) Salaita, K.; Wang, Y.; Mirkin, C. A. Applications of Dip-Pen Nanolithography. *Nat. Nanotechnol.* **2007**, *2*, 145–155.

- (34) Hüusser, O. E.; Craston, D. H.; Bard, A. J. Scanning Electrochemical Microscopy High-Resolution Deposition and Etching of Metals. *J. Electrochem. Soc.* **1989**, *136*, 3222–3229.
- (35) Reiter, G. Dewetting of Thin Polymer Films. *Phys. Rev. Lett.* **1992**, *68*, 75–78.
- (36) Khan, M.; Trlica, C.; Dikey, M. Recapillarity: Electrochemically Controlled Capillary Action of a Liquid Metal Alloy. *Prog.* **2014**.
- (37) Kim, D.; Thissen, P.; Viner, G.; Lee, D.-W.; Choi, W.; Chabal, Y. J.; Lee, J.-B. (J. B. . Recovery of Nonwetting Characteristics by Surface Modification of Gallium-Based Liquid Metal Droplets Using Hydrochloric Acid Vapor. *ACS Appl. Mater. Interfaces* **2013**, *5*, 179–185.
- (38) Doudrick, K.; Liu, S.; Mutunga, E. M.; Klein, K. L.; Damle, V.; Varanasi, K. K.; Rykaczewski, K. Different Shades of Oxide: From Nanoscale Wetting Mechanisms to Contact Printing of Gallium-Based Liquid Metals. *Langmuir* **2014**, *30*, 6867–6877.

CHAPTER 7

THE INFLUENCE OF WATER ON THE

INTERFACIAL BEHAVIOR OF GALLIUM LIQUID

METAL ALLOYS*

**This work has been published in Applied Physics Letters. Contributors to this work: Chris Trlica, Ju-Hee So, Michael Valeri,*

7.1 ABSTRACT

Eutectic gallium indium (EGaIn) is a promising liquid metal for a variety of electrical and optical applications that take advantage of its soft and fluid properties. The presence of a rapidly-forming oxide skin on the surface of the metal causes it to stick to many surfaces, which limits the ability to easily reconfigure its shape on demand. This paper shows that water can provide an interfacial slip layer between EGaIn and other surfaces, which allows the metal to flow smoothly through capillaries and across surfaces without sticking. Rheological and surface characterization shows that the presence of water also changes the chemical composition of the oxide skin and weakens its mechanical strength, although not enough to allow the metal to flow freely in microchannels without the slip layer. The slip layer provides new opportunities to control and actuate liquid metal plugs in microchannels—including the use of continuous electrowetting—enabling new possibilities for shape reconfigurable electronics, sensors, actuators and antennas.

7.2 INTRODUCTION

The ability to manipulate the shape and control the motion of liquid metals in microchannels holds great promise for many micro-device applications, such as valves, switches, pumps, sensors, actuators and electrodes¹⁻⁸. Mercury has most commonly been used for these applications, despite the danger it poses to human and environmental health⁹, because of nontrivial technical challenges associated with other room temperature liquid metals. Gallium is the leading alternative to mercury because of its low vapor pressure^{10,11}, low viscosity, low toxicity, and metallic electrical conductivity¹². However, gallium suffers from two challenges. The first challenge is that gallium is solid at room temperature (mp ~29.7 °C). Alloying gallium with certain metals addresses this problem; in this study we use eutectic gallium-indium (EGaIn), which remains liquid at room temperature¹².

The second challenge associated with the use of gallium and its alloys is the presence of a surface oxide composed primarily of oxides of gallium. This oxide is thin (1~3 nm)¹³⁻¹⁷, effectively passivating, and forms spontaneously and nearly instantaneously upon exposure to atmospheric oxygen¹⁸. The oxide sticks to most surfaces^{12,19-22} (with some notable exceptions^{23,24}), preventing the metal from flowing freely. The unique feature can provide opportunities for new applications since the oxide mechanically stabilizes the liquid metal in non-equilibrium shapes²⁵, which is useful for forming 2D²⁰ or 3D structures²⁶, antennas²⁷⁻²⁹, micro pumps³⁰, strain^{31,32} and curvature sensors^{33,34}, wires³⁵, interconnects³⁶, plasmonic structures³⁷ and frequency selective surfaces³⁸. The oxide, however, adheres to the walls of microchannels and thus excludes the use of gallium based alloys in applications requiring the

reversible control of microscale switches, pumps, optics, or shape reconfigurable electronics.³⁹

Contact with vapor or liquid of a strong acid or base (e.g., HCl) removes the oxide and can address this problem^{12,40,41}. However, the use of these harsh chemicals is undesirable for many practical implementations. It is also possible to modify the chemistry or roughness of the walls of microchannels to limit the wetting, but this approach limits the materials available for device construction, and it is not yet established how well it will work over many duty cycles^{19,23,42}. Electrochemistry can remove the oxide, but this approach requires a constant supply of energy to keep the metal oxide-free⁴³. For all of these reasons, most studies of liquid metal manipulation have used Hg.

Here, we show that simply pre-filling a channel with water prior to adding metal creates an interfacial slip layer between the surface of the metal plug and the walls of the microchannel that prevents the oxide from sticking to the walls. The presence of water also changes the composition of the oxide, decreases its modulus by nearly an order of magnitude, and makes it less passivating. The presence of water lowers the pressure required to inject the liquid metal into microchannels, even though water is ≈ 55 times more viscous than air. The aqueous slip layer allows continuous electrowetting (CEW) of the metal,^{44,45} enabling the use of voltage to control the movement of the metal in microchannels. The slip layer also allows the use of pressure to inject and withdraw the metal from microchannels without it adhering to the channel walls.

The changes to the oxide in the presence of water are particularly important for applications that use the metal in aqueous environments, such as metal-hydrogel contacts^{46,47}. This paper describes the use of water to provide new opportunities to modify and control the interfacial properties and microfluidic behavior of oxide-forming liquid metals.

7.3 EXPERIMENTAL SECTION

Eutectic gallium indium (EGaIn) was purchased from 5N Plus. Capillary tubes were obtained from Friedrich and Dimmock Incorporation. An AR-G2 rheometer (TA instruments) was used for rheology of the EGaIn. Pristine laboratory glass slides (75 mm x 50 mm x 1 mm) were obtained from Fischer Scientific and Corning Corporation. These slides were cleaned by rinsing with isopropanol and water, unless otherwise noted. “Wet” substrates were prepared by submerging these slides into DI water and removing excess water such that no water was visible. PDMS microchannels, as shown in Figure 6, were fabricated by using soft lithography and replica molding techniques.

7.4 RESULTS & DISCUSSION

1. Plug flow in water and in air: To investigate the difference in the behavior of the metal interfaced with air or water, we injected EGaIn into a dry capillary (borosilicate glass, 70 mm length, 0.9 mm inner diameter) and a capillary pre-filled with deionized water. It is straightforward to inject the metal by syringe into microfluidic channels or capillary tubes. The capillaries were initially oriented horizontally and we observed whether the metal flows out of the capillaries under gravity as we rotated them vertically. Metal injected into a dry,

empty capillary tube is stable since the oxide skin adheres the capillary wall and provides mechanical stability to the liquid metal, as shown in Figures. Repeating the experiment with a capillary tube pre-filled with water produces a different result (Figure 1b): in this case, tilting the tube beyond $\sim 50^\circ$ relative to the horizon causes the metal to flow out of the capillary due to gravity (Figure 1b(iii)).

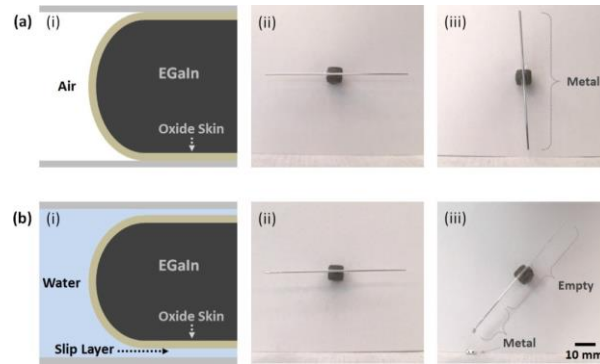


Figure 1. Contrasting the behavior of EGaIn in (a) a dry capillary, and (b) a capillary pre-filled with water. The capillaries are mounted on a wall using adhesive attached to a rotating holder. (a) (i, ii) When EGaIn is injected into a dry capillary, the oxide skin forms spontaneously and adheres to the capillary wall. (iii) When the capillary is rotated vertically (aligned with the force of gravity), the liquid metal does not flow out of the capillary. (b) (i) When a capillary tube pre-filled with water is injected with EGaIn, the oxide skin does not adhere to the capillary wall because of the presence of a thin aqueous layer between the metal plug and the capillary wall. (ii) In this case, the metal is stable horizontally, but (iii) flows out of the capillary when tilted due to gravity.

The oxide also forms in water because of the presence of dissolved oxygen, yet it does not provide mechanical stability in the capillary. Similar behavior was also observed when pre-filling the capillary with light mineral oil rather than water.

2. Rheology: There are two potential explanations of the behavior observed in Figure 1: (1) the presence of a slip layer between the metal plug and the walls of the capillary, and/or (2) the weakening of the oxide layer by water. We used rheological methods to determine the effect of water on the mechanical properties of the oxide that forms on EGaIn. With a rheometer (AR-G2, TA Instruments) configured with parallel plate geometry, we repeated previous rheological measurements^{12,48} of the mechanical properties of the oxide in air. The top plate rotates with a controllable angular frequency while the bottom plate remains stationary; these parallel plates (40 mm diameter) sandwich ~0.6 ml to 1 ml of EGaIn in a gap of ~1.2 to 1.6 mm. Because the bulk viscosity of the liquid is so low, the measurements provide information solely on the mechanical properties of the thin solid oxide skin that spans the top and bottom plates around the circumference of the metal. Small amplitude oscillatory stress sweeps provide information about the modulus (10 N/m) and the yield stress (~0.5 N/m) of the oxide in air as shown in Figure 2. The surface elastic modulus plateaus and dominates relative to the viscous modulus, as expected.

For the rheological measurements on the metal in water, we designed an acrylic reservoir which allows these measurements to also be made in a water environment. We filled the reservoir with deionized water, which brought water into direct contact with the oxide layer.

After exposing the oxide to water for ten minutes, we repeated the rheological measurements. The low viscosity of the surrounding water provides negligible resistance to the movement of the top plate and therefore any change in rheological properties are attributed to changes in the oxide itself.

We hypothesized that the surface elastic modulus and yield stress of the oxide skin in water would be similar to those in air because the oxide layer is considered passivating (in air). However, the surface elastic modulus decreases by an order of magnitude (~ 1 N/m) relative to that measured in air (~ 10 N/m). The yield stress of the oxide skin also shifts to a lower value in water compared to that in air from ~ 0.5 N/m in air to ~ 0.1 N/m in water. Thus, exposure to water represents a simple way to lower the elastic modulus and yield stress. These results suggest that when exposed to water, the oxide skin is either changing its composition or getting thinner. It is visually apparent that the oxide gets thicker after submerging the oxide-coated metal in water for long time period (e.g., weeks) and preliminary ellipsometry measurements (not reported here) also suggest the oxide gets slightly thicker on the time scales of our experiments here. These results suggest that chemical changes are responsible for the weakening of the oxide.

3. XPS: Inspired by these surprising rheological results, we sought to understand why water changes the mechanical properties of the oxide. An X-ray photoelectron spectroscopy (XPS) study of the surface of gallium as a dental amalgam suggests that the oxide changes its composition in the presence of water to a gelatinous complex of gallium oxide

monohydroxides (GaOOH)⁴⁹. This change in composition corresponds to a 0.5 to 0.7 eV shift in XPS data for the Ga ($2p_{3/2}$) and O (1s) peaks relative to their dry state. We carried out the same experiment and observed a similar 0.73 eV shift in the binding energies of Ga and O after exposing the oxide to water for ten minutes. In our control sample, binding energies of oxygen, O(1s) and gallium, Ga($2p_{3/2}$) peaks were found at 530.99eV and 1117.99eV respectively. Both of this spectra shifted by 0.73eV for the water-soaked sample, in which O(1s) was found at 530.26eV and Ga($2p_{3/2}$) was at 1117.26eV. These results suggest further that the changes in the mechanical properties of the oxide are likely associated with chemical changes.

We sought to understand whether the weakening of the oxide skin by exposure to water could explain the behavior in Figure 1b(iii). We filled a glass capillary with EGaIn (as shown in Figure 1a), oriented it vertically, and submerged it in water. If the weakened oxide was the only contributing factor to the mechanical instability of the metal in Figures 1b, then the metal should flow out of the capillaries within minutes. Instead, the metal is stable in the capillary throughout the duration of our experiment (several hours), which suggests that the order of injection of the fluids (i.e., pre-filled with water prior to injecting the metal) must be important and that the instability observed in Figure 1b is due to another mechanism.

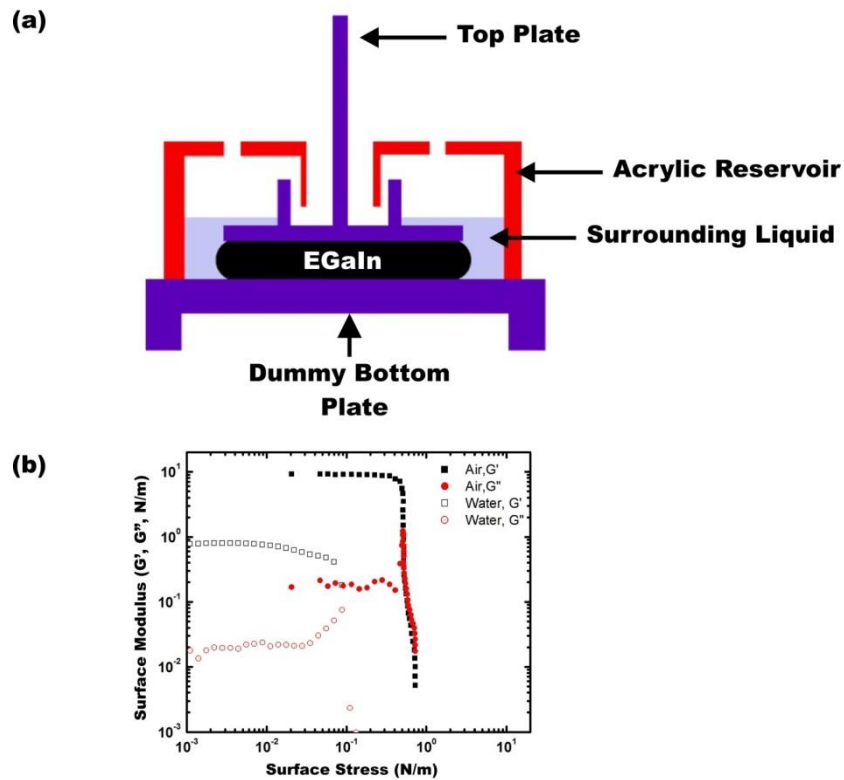


Figure 2. The effect of water exposure on the mechanical properties of the oxide skin that forms on EGaln. (a) A schematic of the experimental setup. EGaln is sandwiched between a top plate and the stationary bottom plate. To test EGaln in different environments, an acrylic reservoir fits firmly with the dummy bottom plate. The reservoir is filled with different liquids, which we call “surrounding liquids”, to see their effect on the mechanical properties of EGaln. (b) During a small amplitude oscillatory stress sweep in water, the elastic modulus G' plateaus near 1 N/m and yields at 0.1 N/m and dominates relative to the viscous modulus G'' . The elastic modulus decreases by an order of magnitude in water relative to the modulus in air. The yield stress is also reduced by approximately a factor of five.

4. Continuous Electrowetting: We hypothesized that a thin layer of water between the metal and the wall of a capillary explains the instability observed in Figure 1b. To test this hypothesis, we investigated whether a plug of the metal in a capillary pre-filled with water moved under an electric field by the mechanism of CEW. CEW relies on a potential drop across the interface of a metal plug and a thin electrolyte layer between the metal plug and the capillary sidewall. This potential drop varies along the length of the plug. Because of electrocapillarity, this potential gradient translates into a difference in interfacial tension, driving plug movement, which has been used previously to move plugs of liquid metal⁵⁰. Thus, movement of the metal plug in response to voltage provides evidence that there is a thin layer of water between the metal and the wall of the capillary.

To test the CEW effect, we injected aqueous electrolyte (0.01 M NaF) into a glass capillary, then subsequently injected a ~1 mm long plug of EGaIn into the capillary. The electrolyte provides a polarizable interface with the metal like a capacitor (i.e., minimal charge transfer) in the range of applied voltage used here. The capillary bridged two electrolyte-filled reservoirs in a plastic holder, forming an electrically continuous path. Copper electrodes inserted into each reservoir applied a 1 V AC voltage while sweeping the frequency. Figure 3 shows several frames from a video demonstrating the CEW effect.

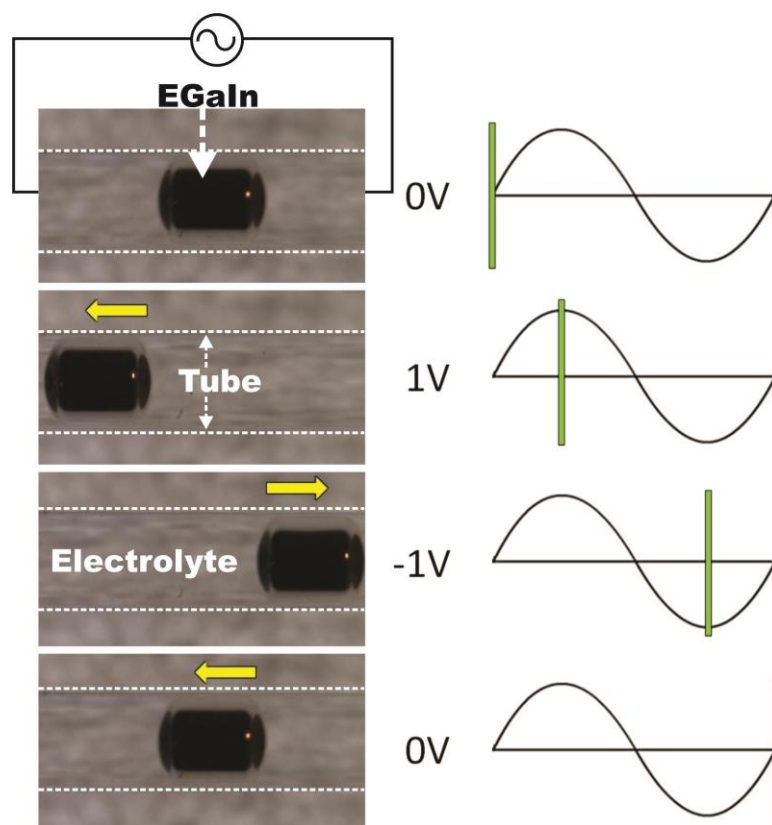


Figure 3. The presence of a thin slip layer of aqueous electrolyte between the capillary wall and a plug of liquid metal enables continuous electrowetting of the plug. Application of low-frequency AC bias (1 V) causes plug movement inside the capillary. As the potential oscillates from positive to negative, the plug displacement oscillates left and right.

The metal moves smoothly through the tube without leaving any residue on the walls of the capillary. The plugs oscillate in response to voltage and frequency using 1 V over frequencies spanning from DC to ~70 Hz. The observation of the movement of the metal

plug by CEW, confirms that there is a layer of water between the metal and the capillary wall.

We speculated that hydrophobic channels might prevent the slip layer from forming. While the system is seemingly more responsive in hydrophilic channels such as glass capillaries, CEW actuation occurred in hydrophobic channels, such as perfluoroalkoxy (PFA) tubing (Omegaflex TYTP-116132). This results suggests that the electrolyte solution wets the oxide skin during injection of the metal, forming a sheath over the metal plug. This sheath functions as a slip layer between the plug and the channel wall.

Notably, plugs of metal do not move under these same conditions if the metal plug is injected before the water. When there is a slip layer of water between the metal plug and the walls of the channel, ions can travel freely from end-to-end of the capillary and CEW occurs. However, in the absence of the slip layer, the ions in the electrolyte have to convert to electrons via electrochemical reactions at the interface to travel from the electrodes placed at each end of the capillary. In this case, application of higher voltage AC bias causes the electrolyte solution to slowly infiltrate from the ends of the plug towards the center of the plug, enabling plug oscillation only to the point at which water has maximally infiltrated. When the infiltration fronts from each end of the plug meet, the entire plug begins to move in a manner identical to that seen during CEW of a metal plug injected into a water-filled capillary. The infiltration of water is therefore likely due to the electrochemical reduction of the surface oxide that coats the metal and adheres to the walls of the capillary (cf., Figure 1a).

5. Slip layer: The presence of a slip layer also has implications outside of microchannels. We observed the behavior of droplets of metal placed on dry substrates and compared them to the same substrates exposed to water. As a control sample, we placed a drop of EGaIn on a pristine glass substrate cleaned by oxygen plasma (Figure 4a).

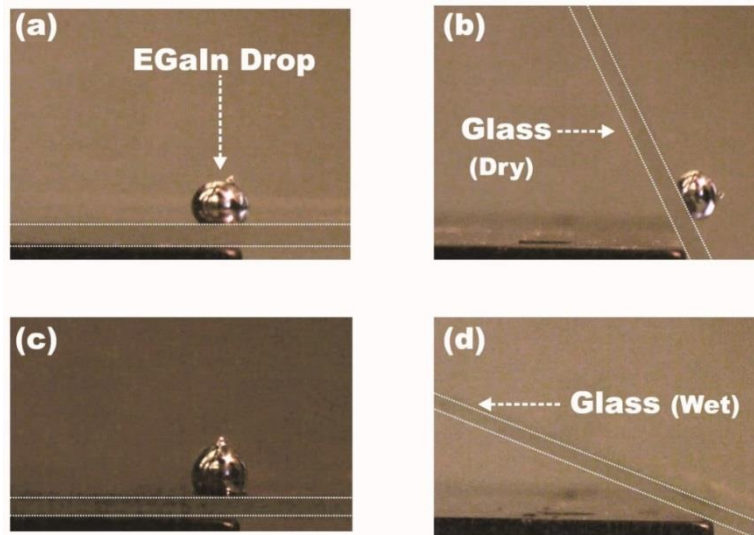


Figure 4. Evidence of a water slip layer in an open system. (a) An EGaIn drop is placed on a dry glass slide. (b) The glass slide is tilted to 90° yet the droplet does not slide off the surface. (c) An EGaIn drop placed on a glass slide dipped briefly in water. (d) When tilted, the drop slides off at a small angle (30° to 40°). For scale, the glass slides are 1mm thick.

We refer to these substrates as ‘dry’, although we made no additional efforts to remove surface-bound water to represent normal laboratory conditions. The drop stayed on the surface even after tilting the substrate to 90°(Figure 4b), as expected since the oxide skin

adheres to the substrate¹⁹. In contrast, after pre-exposing the glass surface to water (dipped in DI water), the drop of EGaIn slid off, as shown in Figure 4d. This result further supports the hypothesis that water acts as a slip layer. Notably, water was not visible on the surface of the glass when we placed the EGaIn drop onto it, which suggests that the water layer is thin. We repeated these experiments multiple times and observed the same result each time.

We speculated that substrates dipped in water would start to behave like a dry substrate as the trace amount of water on the surface evaporates. We brought droplets of the liquid metal hanging at the end of a needle into contact with glass slides. The droplets stick to dry substrates and break away from the needle as it is pulled away from the substrate. However, the droplets did not stick to glass slides pre-submerged in a DI water bath (Figure 5a), which further illustrates the importance of water as a non-stick layer. After ~8-9 minutes of drying (Figure 5b), the drop begins to stick to the substrate. After ~10-12 minutes (Figure 5c), the droplets fully adhere to the substrate. These results suggest that dipping substrates in water represents a temporary way to prevent adhesion of the oxide to the substrate. This may inspire new approaches for designing substrates that do not adhere to the metal, approaches such as liquid-infused surfaces⁵¹⁻⁵³, which mimic lubricating structures found in *Nepenthes* pitcher plants.

Prior work suggests that droplets of EGaIn only adhere to glass surfaces when the droplet volume increases while in direct contact with the glass¹⁹. Figure 5c suggests that droplets

adhere to the glass without expanding or significantly distorting the droplet. We repeated the experiments depicted in Figure 5 ten times.

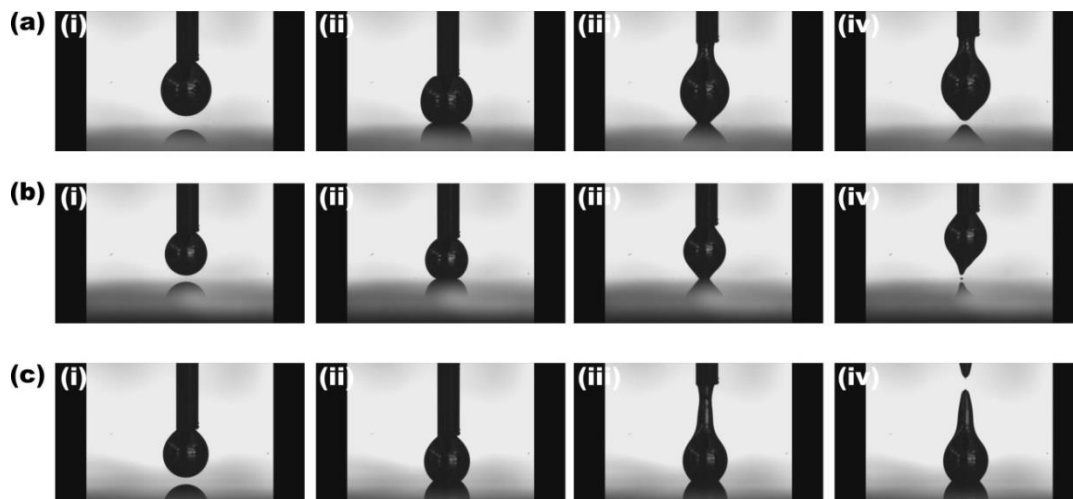


Figure 5. ‘Wet’ to ‘dry’ transition of a glass substrate. In each row, the metal is brought into contact with a substrate (i-ii) and then removed (iii-iv). (a) On a glass slide exposed to moisture (immediately after dipping in a water bath), the metal does not stick to the surface. (b) After 8-9 minutes of drying in air, the metal begins to stick and leaves some residue on the substrate. (c) After ~10 minutes, the metal sticks to the surface in a manner identical to adhesion on a dry glass substrate.

We also measured the adhesion of droplets to nominally dry glass slides (i.e., those without exposure to water immediately before measuring) after cleaning them separately with (1) water followed by a rinse with isopropanol, (2) water followed by a rinse with acetone, (3)

acetone followed by a rinse with water, (4) isopropanol only, (5) acetone only, (6) oxygen plasma, and (7) heating at 70 °C for an hour to drive off water. In all cases—which were each repeated at least ten times—the EGaIn droplets adhered to the glass in a manner similar to that shown in Figure 5c. However, the drops did not adhere to the glass after washing with soap and rinsing with isopropanol and acetone, which suggests that the method of preparation affects wetting. Nevertheless, the increased adhesion with time shown in Figure 5 suggests that the surface dries over time. |

6. Implications of slip layer and a demonstrative device

The presence of water has implications for injecting the metal into microchannels because (1) water weakens the oxide and (2) the slip layer prevents the oxide from sticking to the walls of the channel. We measured the pressure required to inject the metal into dry versus water-filled microchannels composed of polydimethylsiloxane (length 65 mm, width 1 mm, height 0.05 mm) and fabricated using standard replica molding techniques. We placed a drop of metal at the inlet to these channels and measured the pneumatic pressure required to inject the metal. The average pressure required to partially fill a microchannel pre-filled with water was ~40% lower than that needed to fill a dry microfluidic channel. We repeated these measurements more than twenty times and always found the pressure to be lower in wet channels. We are currently working to understand the competing influences of water during injection including the need to displace the fluid in the capillary (pressure increases due to the larger viscosity of water relative to air), rupture the oxide (pressure decreases due to water weakening the oxide), slip along the walls (only possible with water), and overcome

any effects of interfacial tension. Nevertheless, the presence of water provides a simple and non-intuitive way to lower the pressure required for injection of gallium alloys into microchannels.

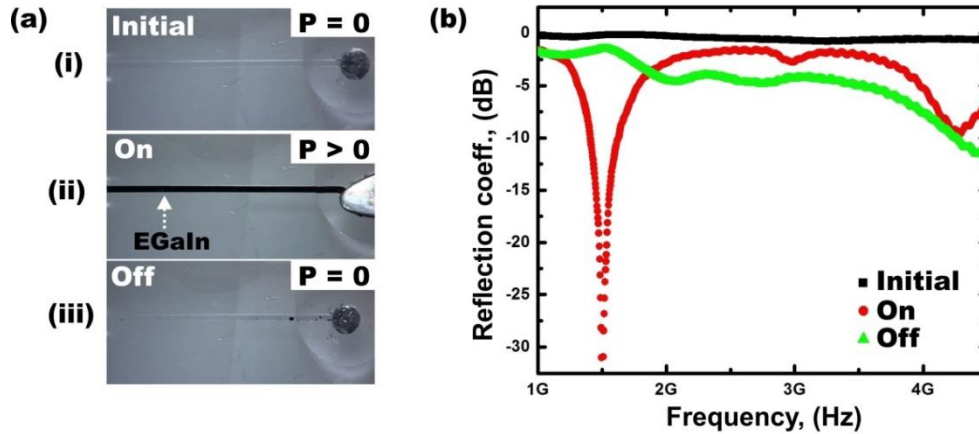


Figure 6: Demonstration of a reconfigurable antenna that can be injected and withdrawn from microchannels due to a water slip layer. (a) Initially (i), water fills the channel and a drop of metal rests in a reservoir at one end of the channel, capped by a hemisphere of PDMS. Pressing the reservoir with the tip of a spatula (ii) pushes the metal into the channel. Removing the pressure causes the metal to spontaneously withdraw back into the reservoir. (b) The spectral response of the device in all three states. For scale, the width of the microchannel is 1mm wide.

The presence of the slip layer offers an opportunity to push metal in and out of microchannels without adhesion to the channel walls. This capability is particularly

compelling for antennas since the frequency of an antenna depends on its shape. We utilized the slip layer to fabricate and characterize a reconfigurable antenna that can be activated or deactivated by hand. This antenna, depicted in Figure 6, is comprised of a reservoir of EGaIn connected to a water-filled PDMS microchannel. When confined to the reservoir, as shown in Figure 6a(i), the liquid metal has no resonant frequency because its negligible length – it is therefore in the ‘off’ state. To activate the antenna, we pressed the reservoir manually, forcing the metal into the microchannel, as shown in Figure 6a(ii). In this ‘on’ state, the antenna has a resonant frequency corresponding to the length of the microchannel, as expected. After releasing the applied pressure, the metal withdraws back into the reservoir, transitioning the antenna back to the ‘off’ state, as shown in Figure 6a(iii). A thin, dome-shaped membrane of PDMS caps the reservoir and deforms when depressed. Upon releasing the applied pressure, the dome returns back to a hemi-spherical shape and helps pull the metal back into the reservoir. The spectral responses of these three different states are shown in Figure 6b. The ‘off’ and ‘initial’ states are slightly different due to challenges connecting the antenna to the network analyzer in this prototype device.

7.5 CONCLUSION

This paper describes the effects of water on the oxide skin of EGaIn, and discusses the implications of these effects in the context of liquid metal microsystems. Water changes the chemical composition of the oxide and weakens its critical yield stress by a factor of five. Water can also create a slip layer between plugs of metal and the walls of microchannel by placing water in the microchannels prior to injecting the metal. We focus on water and

aqueous solutions in this paper, but other fluids appear to create slip layers too, including mineral oil. In the future it may be possible to use functional slip layers for active control over the metal⁵⁴. An aqueous slip layer enables controlled actuation of liquid metal plugs inside microchannels via continuous electrowetting and prevents the metal from sticking to wet surfaces, addressing one of the major practical issues in the use of gallium alloys. We utilize the slip layer to demonstrate a shape reconfigurable antenna based on EGaIn that reversibly changes its spectral properties by pushing metal in and out of microchannels. The presence of a slip layer thus provides a route to avoid Hg in devices and experiments that depend on liquid metals, but does have the drawback of requiring the presence of an additional fluid (and notably, water appears to cause the oxide to get thicker over long time scales). Remarkably, the presence of water also reduces the pressure necessary to inject the metal into microchannels relative to dry microchannels, which warrants further investigation.

This work is a step toward enabling the actuation of low toxicity liquid metals that have surface oxides. Although we focus on EGaIn, other alloys of gallium support a surface oxide of similar composition and thus, the conclusions can likely be extended to these metals. The ability to reversibly actuate liquid metal plugs by CEW or pneumatics may help facilitate the development of shape shifting devices and reconfigurable antennas, sensors, actuators, meta-materials, circuits and passive elements.

7.6 REFERENCES

- (1) Thorsen, T.; Maerkl, S. J.; Quake, S. R. Microfluidic Large-Scale Integration. *Science* **2002**, *298*, 580–584.
- (2) Sen, P.; Kim, C.-J. Microscale Liquid-Metal Switches -A Review. *IEEE Trans. Ind. Electron.* **2009**, *56*, 1314 –1330.
- (3) Lyshevski, S. E. *MEMS and NEMS: Systems, Devices, and Structures*; CRC Press: Boca Raton, FL, USA, 2002.
- (4) Unger, M. A.; Chou, H.-P.; Thorsen, T.; Scherer, A.; Quake, S. R. Monolithic Microfabricated Valves and Pumps by Multilayer Soft Lithography. *Science* **2000**, *288*, 113–116.
- (5) Zhang, C. S.; Xing, D.; Li, Y. Y. Micropumps, Microvalves, and Micromixers within PCR Microfluidic Chips: Advances and Trends. *Biotechnol. Adv.* **2007**, *25*, 483–514.
- (6) Yun, K.-S.; Cho, I.-J.; Bu, J.-U.; Kim, C.-J.; Yoon, E. A Surface-Tension Driven Micropump for Low-Voltage and Low-Power Operations. *J. Microelectromech. Syst.* **2002**, *11*, 454 – 461.
- (7) Ni J.; Coldiron S.J.; Zhong C.-J.; Porter M.D. Electrochemically-Actuated Mercury Valve for Flow Rate and Direction Control: Design, Characterization, and Applications. *J. Electroanal. Chem.* **2001**, *504*, 166–174.
- (8) Jackel, J. L.; Hackwood, S.; Beni, G. Electrowetting Optical Switch. *Appl. Phys. Lett.* **1982**, *40*, 4–5.
- (9) Clarkson, T. W.; Magos, L.; Myers, G. J. The Toxicology of Mercury--Current Exposures and Clinical Manifestations. *N. Engl. J. Med.* **2003**, *349*, 1731–1737.

- (10) Sheka, I. A.; Chaus, I. S.; Mitiureva, T. T. *The Chemistry of Gallium*; Elsevier: New York, 1966.
- (11) Morley, N. B.; Burris, J.; Cadwallader, L. C.; Nornberg, M. D. GaInSn Usage in the Research Laboratory. *Rev. Sci. Instrum.* **2008**, *79*, 056107.
- (12) Dickey, M. D.; Chiechi, R. C.; Larsen, R. J.; Weiss, E. A.; Weitz, D. A.; Whitesides, G. M. Eutectic Gallium-Indium (EGaIn): A Liquid Metal Alloy for the Formation of Stable Structures in Microchannels at Room Temperature. *Adv. Funct. Mater.* **2008**, *18*, 1097–1104.
- (13) Scharmann, F.; Cherkashinin, G.; Breternitz, V.; Knedlik, C.; Hartung, G.; Weber, T.; Schaefer, J. A. Viscosity Effect on GaInSn Studied by XPS. *Surf. Interface Anal.* **2004**, *36*, 981–985.
- (14) Regan, M. J.; Tostmann, H.; Pershan, P. S.; Magnussen, O. M.; DiMasi, E.; Ocko, B. M.; Deutsch, M. X-Ray Study of the Oxidation of Liquid-Gallium Surfaces. *Phys. Rev. B: Condens. Matter Mater. Phys.* **1997**, *55*, 10786–10790.
- (15) Regan, M. J.; Pershan, P. S.; Magnussen, O. M.; Ocko, B. M.; Deutsch, M.; Berman, L. E. X-Ray Reflectivity Studies of Liquid Metal and Alloy Surfaces. *Phys. Rev. B: Condens. Matter Mater. Phys.* **1997**, *55*, 15874–15884.
- (16) Cademartiri, L.; Thuo, M. M.; Nijhuis, C. A.; Reus, W. F.; Tricard, S.; Barber, J. R.; Sodhi, R. N. S.; Brodersen, P.; Kim, C.; Chiechi, R. C.; Whitesides, G. M. Electrical Resistance of Ag-TS-S(CH₂)(n-1)CH₃//Ga₂O₃/EGaIn Tunneling Junctions. *J. Phys. Chem. C* **2012**, *116*, 10848–10860.

- (17) Dumke, M.; Tombrello, T.; Weller, R.; Housley, R.; Cirlin, E. Sputtering of the Gallium-Indium Eutectic Alloy in the Liquid-Phase. *Surf. Sci.* **1983**, *124*, 407–422.
- (18) Downs, A. J. *Chemistry of Aluminium, Gallium, Indium, and Thallium*; Blackie Academic & Professional: London, 1993; Vol. 1st.
- (19) Doudrick, K.; Liu, S.; Mutunga, E. M.; Klein, K. L.; Damle, V.; Varanasi, K. K.; Rykaczewski, K. Different Shades of Oxide: From Nanoscale Wetting Mechanisms to Contact Printing of Gallium-Based Liquid Metals. *Langmuir* **2014**, *30*, 6867–6877.
- (20) Boley, J. W.; White, E. L.; Chiu, G. T.-C.; Kramer, R. K. Direct Writing of Gallium-Indium Alloy for Stretchable Electronics. *Adv. Funct. Mater.* **2014**, *24*, 3501–3507.
- (21) Li, G.; Parmar, M.; Kim, D.; Lee, J.-B. (JB); Lee, D.-W. PDMS Based Coplanar Microfluidic Channels for the Surface Reduction of Oxidized Galinstan. *Lab. Chip* **2013**, *14*, 200–209.
- (22) Khan, M.; Trlica, C.; Dickey, M. Recapillarity: Electrochemically Controlled Capillary Withdrawal of a Liquid Metal Alloy From Microchannels. *Adv. Funct. Mater. In press*.
- (23) Kim, D.; Lee, D.-W.; Choi, W.; Lee, J.-B. A Super-Lyophobic PDMS Micro-Tunnel as a Novel Microfluidic Platform for Oxidized Galinstan. In *2012 IEEE 25th International Conference on Micro Electro Mechanical Systems (MEMS)*; 2012; pp. 1005–1008.
- (24) Kramer, R. K.; Boley, J. W.; Stone, H. A.; Weaver, J. C.; Wood, R. J. Effect of Microtextured Surface Topography on the Wetting Behavior of Eutectic Gallium-Indium Alloys. *Langmuir* **2013**, *30*, 533-539.

- (25) Chiechi, R. C.; Weiss, E. A.; Dickey, M. D.; Whitesides, G. M. Eutectic Gallium-Indium (EGaIn): A Moldable Liquid Metal for Electrical Characterization of Self-Assembled Monolayers. *Angew. Chem. Int. Ed.* **2008**, *47*, 142–144.
- (26) Ladd, C.; So, J.-H.; Muth, J.; Dickey, M. D. 3D Printing of Free Standing Liquid Metal Microstructures. *Adv. Mater.* **2013**, *25*, 5081–5085.
- (27) So, J. H.; Thelen, J.; Qusba, A.; Hayes, G. J.; Lazzi, G.; Dickey, M. D. Reversibly Deformable and Mechanically Tunable Fluidic Antennas. *Adv. Funct. Mater.* **2009**, *19*, 3632–3637.
- (28) Khan, M. R.; Hayes, G. J.; So, J.-H.; Lazzi, G.; Dickey, M. D. A Frequency Shifting Liquid Metal Antenna with Pressure Responsiveness. *Appl. Phys. Lett.* **2011**, *99*, 013501–013503.
- (29) Cheng, S.; Rydberg, A.; Hjort, K.; Wu, Z. Liquid Metal Stretchable Unbalanced Loop Antenna. *Appl. Phys. Lett.* **2009**, *94*, 144103–144103–3.
- (30) Tang, S.-Y.; Khoshmanesh, K.; Sivan, V.; Petersen, P.; O’Mullane, A. P.; Abbott, D.; Mitchell, A.; Kalantar-zadeh, K. Liquid Metal Enabled Pump. *Proc. Natl. Acad. Sci.* **2014**, *111*, 3304.
- (31) Cumby, B. L.; Hayes, G. J.; Dickey, M. D.; Justice, R. S.; Tabor, C. E.; Heikenfeld, J. C. Reconfigurable Liquid Metal Circuits by Laplace Pressure Shaping. *Appl. Phys. Lett.* **2012**, *101*, 174102.
- (32) Ponce Wong, R. D.; Posner, J. D.; Santos, V. J. Flexible Microfluidic Normal Force Sensor Skin for Tactile Feedback. *Sens. Actuators Phys.* **2012**, *179*, 62–69.

- (33) Kramer, R. K.; Majidi, C.; Sahai, R.; Wood, R. J. Soft Curvature Sensors for Joint Angle Proprioception. In *2011 IEEE/RSJ International Conference on Intelligent Robots and Systems (IROS)*; 2011; pp. 1919–1926.
- (34) Majidi, C.; Kramer, R.; Wood, R. J. A Non-Differential Elastomer Curvature Sensor for Softer-than-Skin Electronics. *Smart Mater. Struct.* **2011**, *20*, 105017.
- (35) Zhu, S.; So, J.-H.; Mays, R.; Desai, S.; Barnes, W. R.; Pourdeyhimi, B.; Dickey, M. D. Ultrastretchable Fibers with Metallic Conductivity Using a Liquid Metal Alloy Core. *Adv. Funct. Mater.* **2013**, *23*, 2308–2314.
- (36) Kim, H.-J.; Son, C.; Ziaie, B. A Multiaxial Stretchable Interconnect Using Liquid-Alloy-Filled Elastomeric Microchannels. *Appl. Phys. Lett.* **2008**, *92*, 011904–011904–3.
- (37) Wang, J.; Liu, S.; Vardeny, Z. V.; Nahata, A. Liquid Metal-Based Plasmonics. *Opt. Express* **2012**, *20*, 2346–2353.
- (38) Khan, M. R.; Hayes, G. J.; Zhang, S.; Dickey, M. D.; Lazzi, G. A Pressure Responsive Fluidic Microstrip Open Stub Resonator Using a Liquid Metal Alloy. *IEEE Microw. Wirel. Compon. Lett.* **2012**, *22*, 577–579.
- (39) Giguere, P. A.; Lamontagne, D. Polarography with a Dropping Gallium Electrode. *Science* **1954**, *120*, 390–391.
- (40) Kim, D.; Thissen, P.; Viner, G.; Lee, D.-W.; Choi, W.; Chabal, Y. J.; Lee, J.-B. (J. B. . Recovery of Nonwetting Characteristics by Surface Modification of Gallium-Based Liquid Metal Droplets Using Hydrochloric Acid Vapor. *ACS Appl. Mater. Interfaces* **2013**, *5*, 179–185.

- (41) Kim, D.; Lee, Y.; Lee, D.; Choi, W.; Lee, J.-B. J. B. Hydrochloric Acid-Impregnated Paper for Liquid Metal Microfluidics. In *2013 Transducers Eurosensors XXVII: The 17th International Conference on Solid-State Sensors, Actuators and Microsystems (TRANSDUCERS EUROSENSORS XXVII)*; 2013; pp. 2620–2623.
- (42) Kim, D.; Jung, D.; Yoo, J. H.; Lee, Y.; Choi, W.; Lee, G. S.; Yoo, K.; Lee, J.-B. Stretchable and Bendable Carbon Nanotube on PDMS Super-Lyophobic Sheet for Liquid Metal Manipulation. *J. Micromech. Microeng.* **2014**, *24*, 055018.
- (43) Khan, M.; Eaker, C.; Bowden, E.; Dickey, M. Giant and Switchable Surface Activity of Liquid Metal via Surface Oxidation. *Proc. Natl. Acad. Sci.* **2014**, *111*, 14047–14051.
- (44) Beni, G.; Hackwood, S.; Jackel, J. L. Continuous Electrowetting Effect. *Appl. Phys. Lett.* **1982**, *40*, 912–914.
- (45) Gough, R.; Morishita, A.; Dang, J.; Hu, W.; Shiroma, W.; Ohta, A. Continuous Electrowetting of Non-Toxic Liquid Metal for RF Applications. *IEEE Access* **2014**, *Early Access Online*.
- (46) Koo, H.; So, J.; Dickey, M. D.; Velev, O. D. Towards All-Soft Matter Circuits: Prototypes of Quasi-Liquid Devices with Memristor Characteristics. *Adv. Mater.* **2011**, *23*, 3559–3564.
- (47) So, J.; Koo, H.; Dickey, M. D.; Velev, O. D. Ionic Current Rectification in Soft-Matter Diodes with Liquid-Metal Electrodes. *Adv. Funct. Mater.* **2012**, *22*, 625–631.
- (48) Larsen, R. J.; Dickey, M. D.; Whitesides, G. M.; Weitz, D. A. Viscoelastic Properties of Oxide-Coated Liquid Metals. *J. Rheol.* **2009**, *53*, 1305–1326.

- (49) Horasawa, N.; Takahashi, S.; Marek, M. Electrochemical Behavior of Amalgams and a Gallium Alloy in Two Electrolytes. *J Dent Res* **1997**, *76*, 1481–1481.
- (50) Lee, H. J.; Kim, C.-J. Surface-Tension-Driven Microactuation Based on Continuous Electrowetting. *J. Microelectromech. Syst.* **2000**, *9*, 171–180.
- (51) Wong, T.-S.; Kang, S. H.; Tang, S. K. Y.; Smythe, E. J.; Hatton, B. D.; Grinthal, A.; Aizenberg, J. Bioinspired Self-Repairing Slippery Surfaces with Pressure-Stable Omniphobicity. *Nature* **2011**, *477*, 443–447.
- (52) Lafuma, A.; Quere, D. Slippery Pre-Suffused Surfaces. *Europhys. Lett.* **2011**, *96*, 560001.
- (53) Chen, J.; Dou, R.; Cui, D.; Zhang, Q.; Zhang, Y.; Xu, F.; Zhou, X.; Wang, J.; Song, Y.; Jiang, L. Robust Prototypical Anti-Icing Coatings with a Self-Lubricating Liquid Water Layer between Ice and Substrate. *ACS Appl. Mater. Interfaces* **2013**, *5*, 4026–4030.
- (54) Khalil, K. S.; Mahmoudi, S. R.; Abu-dheir Numan; Varanasi, K. K. Active Surfaces: Ferrofluid-Impregnated Surfaces for Active Manipulation of Droplets. *Appl. Phys. Lett.* **2014**, *105*, 041604.

APPENDICES

Appendix A

SUPPORTING INFORMATION

CHAPTER 5

**RECAPILLARITY: ELECTROCHEMICALLY CONTROLLED
CAPILLARY WITHDRAWAL OF A LIQUID METAL ALLOY
FROM MICROCHANNELS**

Experimental Setup

To maintain consistency between experiments, we fabricated an acrylic plate to hold the liquid reservoirs, electrodes, and borosilicate capillaries.

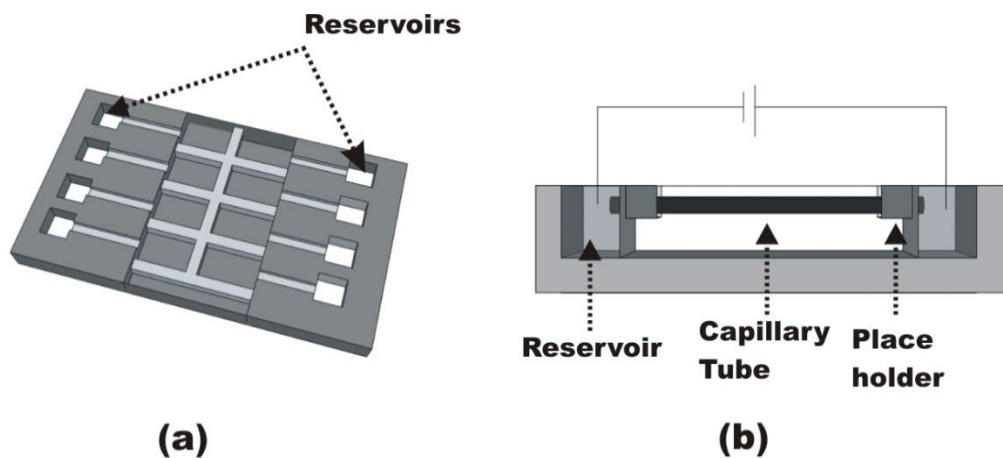


Figure S1. (a) Isometric view of the acrylic substrate used to perform recapillarity experiments in glass capillaries. (b) Side view of a typical setup using an acrylic substrate and a glass capillary. Reservoirs measure 4 mm x 4 mm x 2 mm.

Velocity Measurements

Results were recorded with a HD camcorder (Canon VIXIA HF S20) mounted on a stereoscope. We used video processing software (Avidemux) to extract frames from the video. Each frame contained time and position information, from which withdrawal velocity was calculated.

Effect of Electrolyte Concentrations

We used 70 mm long borosilicate glass capillaries (0.9 mm +/- 0.1 mm ID) and a range of different concentrations of NaF solution to quantify the effect of electrolyte concentration on recapillarity. At constant applied voltage, withdrawal velocities increase with increasing salt concentration, as illustrated in Figure S2. For a particular salt concentration and fixed bias, we also found that the withdrawal velocity is higher for capillaries with larger diameters.

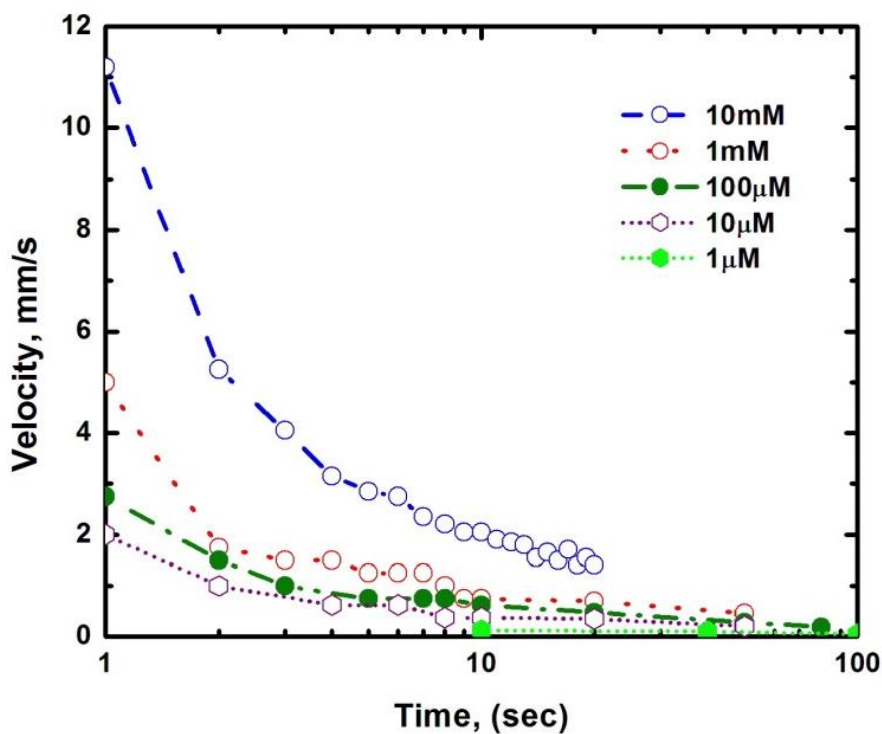


Figure S2. Effect of electrolyte concentration on withdrawal speed of EGaIn. For a given voltage, more concentrated electrolytes enable faster withdrawal due to increased current.

Effect of Ion Gradients

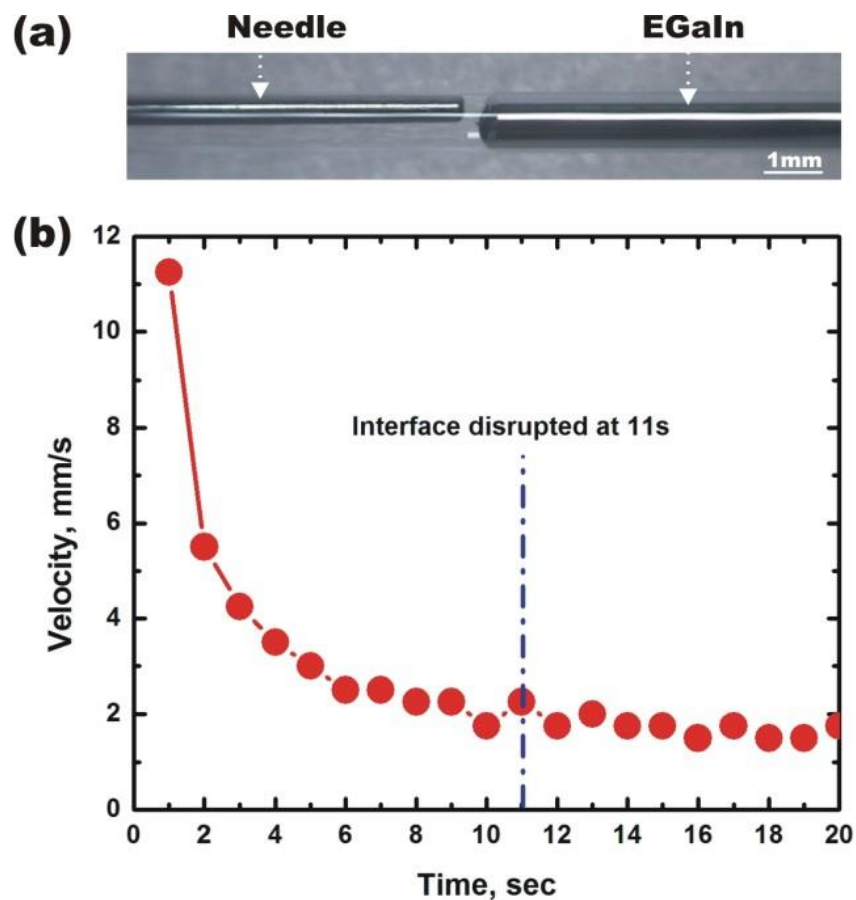


Figure S3. Effect of interfacial ion gradients on the withdrawal velocity. **(a)** After 11 sec of withdrawal, the voltage was turned off and a syringe needle was inserted into the capillary to flush the interface with fresh electrolyte before withdrawal was resumed. **(b)** The withdrawal velocity does not show any velocity increase after flushing the interface and turning the voltage back on after the 11 sec mark on the plot. A plot of current (not shown) also indicates insignificant changes after flushing.

Effect of Electrical Length



Figure S4. Effect of electrical length on withdrawal velocity. A copper wire (anode) was inserted into the capillary to shorten the electrical distance between the anode and the metal interface. Shortening the distance increases the velocity for a given voltage.

Physically Opposing Recapillarity

During a typical recapillarity experiment, the metal withdraws toward a reservoir in response to voltage. In this opposing recapillarity experiment, we physically blocked the outlet of the capillary (i.e., obstructing the withdrawal) by using tubing attached to a syringe secured in a syringe pump. From 0 to 5 s, the metal could not withdraw and therefore the current (at 1 V) is constant during this time frame. At $t=5$ s, we pumped the metal at a rate of $50\mu\text{L}/\text{min}$ into the electrolyte-filled capillary. Figure S5 shows that current increases as EGaIn displaces the electrolyte and the electrical length between the leading interface of the liquid metal and the anode shorten.

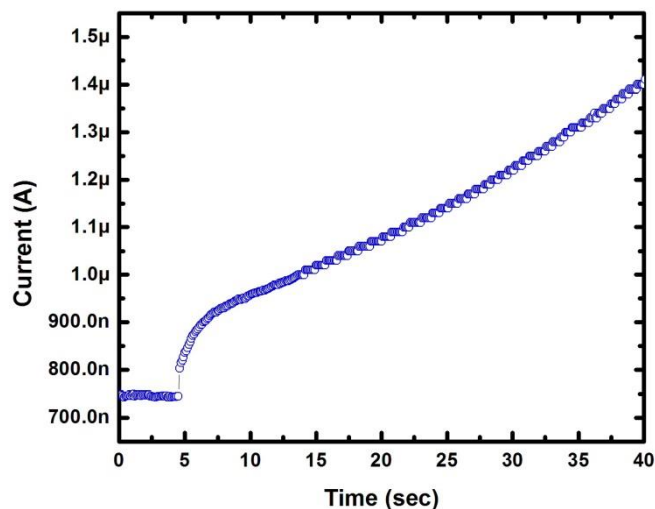


Figure S5. A plot of current vs. time as EGaIn is injected into a capillary toward the counter electrode. The pump injected EGaIn at $t=5$ sec and continued until $t=40$ sec. As EGaIn displaces electrolyte, current increases.

Liquid Metal Withdrawal from a Complex Microfluidic Network

The complex PDMS microfluidic channel network was fabricated using soft lithography and replica molding techniques. EGaIn was injected into the channels manually using a syringe. 10 mM NaF was added to one of the outlets and 40 μ A current was applied to induce withdrawal. The velocity of withdrawal is nearly constant due to the use of constant current. The metal followed the most direct electrical path. Formation of a bubble following the path of withdrawal was also observed. Movement of metal segments perpendicular to the electrical path suggests that there were some voids in the microchannels left unfilled during the EGaIn injection process.